TPF 5(230): Evaluation of Plant Produced RAP Mixtures in the Northeast

Phase III Report

Jo Sias Daniel, Ph.D., P.E.
Professor
Department of Civil and Environmental Engineering
University of New Hampshire, Durham, NH 03824
Tel: (603) 862-3277; Email: jo.daniel@unh.edu

Tom Bennert, Ph.D.
Research Professor
Center for Advanced Infrastructure and Transportation (CAIT)
Rutgers University, 100 Brett Road, Piscataway, NJ 08854
Tel: (609) 213-3312; Email: bennert@rci.rutgers.edu

Y. Richard Kim, Ph.D., P.E., F.ASCE
Distinguished University Professor
Department of Civil, Construction and Environmental Engineering
North Carolina State University, Raleigh, NC 27695-7908
Tel: (919) 515-7758; Fax: (919) 515-7908; Email: kim@ncsu.edu

Walaa Mogawer, Ph.D.
Professor
Department of Civil and Environmental Engineering
Director, Highway Sustainability Research Center
University of Massachusetts Dartmouth
151 Martine Street, Fall River, MA 02723
Tel: (508) 910 -9824; Fax: (508) 999 -9120; Email: wmogawer@umassd.edu

David Mensching
Mohammdreza Sabouri
Graduate Research Assistants

November 2015

Table of Contents

List of Figures

List of Tables

EXECUTIVE SUMMARY

This report summarizes findings from Phase III of a study that is funded through the Transportation Pooled Fund (TPF) Project 5(230): Evaluation of Plant Produced RAP Mixtures in the Northeast. The overall objectives of this research project were to: (1) evaluate the performance in terms of low temperature cracking, fatigue cracking, and moisture sensitivity of plant produced RAP mixtures in the laboratory and field; (2) establish guidelines on when it is necessary to bump binder grades with RAP mixtures; and (3) provide further understanding of the blending that occurs between RAP and virgin binder in plant-produced mixtures. Phase I included testing on 18 plant-produced mixtures with RAP contents from 0% to 40% by total weight of mixture, Phase II of the project included testing on 10 plant-produced mixtures with RAP contents of 0% to 40%, Phase III was a controlled laboratory study of nine mixtures, and there was an additional task that evaluated two sets of mixtures stored in a silo for various time periods. The findings from each phase are summarized in separate reports. The mixtures in Phase III included a partial factorial of two binder grades (PG 58-28 and PG 64-28), three RAP contents (0, 20, and 40% by total weight) and three asphalt contents (optimum and optimum ±0.5%). Binders were extracted and recovered from the laboratory produced mixtures for testing. Binder testing included PG grading, G* master curves and analysis of rheological parameters, and MSCR testing. Mixture testing included dynamic modulus, uniaxial tensile fatigue, triaxial stress sweeps, overlay tester, and thermal stress restrained specimen test. Pavement evaluations were conducted using a layered viscoelastic analysis.

The results from both the binder and mixture testing show that, in general, all the factors that improved the fatigue resistance deteriorated the rutting resistance of the asphalt mixture. Nevertheless, the results show that it is still possible to balance all the different factors to produce a material that performs well and is economical. The use of a soft binder is effective for this set of materials, as the predictions from the pavement evaluation showed a noticeable improvement in fatigue resistance of the mixture, whereas the permanent deformation test data suggested that rutting resistance would not worsen significantly. The predictions on fatigue cracking performance for thin and thick pavements clearly showed that high percentages of RAP can be tolerated easily once the layer thickness increases. Also, the optimum binder content was, not surprisingly, found to be the best, because increasing the asphalt binder above the optimum level resulted in higher levels of rutting even at a high percentage of RAP, and below the optimum level caused a noticeable decrease in fatigue resistance. The impact of the softer base binder and changing the binder content was observed to be greater for the 40% RAP mixtures than the 20% RAP mixtures. Therefore, the best strategies for incorporating high percentages of RAP in the mixtures evaluate in this Phase seem to be using soft base binder and maintaining the optimum asphalt binder content and/or increasing the asphalt layer thickness. However, these trends need to be confirmed with material produced in a plant.

CHAPTER 1 INTRODUCTION

1.1 Background

Production of HMA mixtures with higher percentages of RAP is gaining more attention as a way to save money and more efficiently utilize existing resources. Many state agencies and contractors are very comfortable using RAP percentages up to 20% by total weight of mixture. However, questions about low temperature and fatigue performance and the need to bump binder grades limit the amount of HMA that is produced with greater than 15-20% RAP in many areas of the northeast US. Possible increased moisture susceptibility is also an issue in some regions. In the winter of 2009, the New Hampshire Department of Transportation (NHDOT) and Pike Industries, Inc. (PII) collaborated to perform an evaluation of extracted binder properties for various batch plant produced HMA mixtures containing 0-25% RAP. The results of that study were published in the Transportation Research Record in 2010 and were also presented at the 2009 North Eastern States Materials Engineers' Association (NESMEA) meeting. The general conclusion was that binder bumping was not necessary at the 20% RAP level for the mixtures evaluated.

The purpose of this pooled fund study is to expand on the initial work by PII and NHDOT by including higher RAP percentages, drum and batch plants, and mixture testing. The previous study was limited to testing of recovered binder properties which represent the fully blended condition between the RAP and virgin binder. Testing of plant-produced mixtures allows for evaluation of blending and the impact of higher RAP percentages on material properties and performance with respect to low temperature and fatigue cracking as well as moisture susceptibility of the mixtures containing RAP.

The overall objectives of this research project are to:

1. evaluate the performance in terms of low temperature cracking, fatigue cracking, and moisture sensitivity of plant produced RAP mixtures in the laboratory and field
2. establish guidelines on when it is necessary to bump binder grades with RAP mixtures
3. provide further understanding of the blending that occurs between RAP and virgin binder in plant-produced mixtures

The project was broken down into three phases:

1. Phase I included 18 mixtures obtained from three different plants (NH, NY & VT) during the 2010 construction season and the primary variables were the percentage of RAP in the mixture and the virgin binder PG grade. The results of this work are summarized in the Phase I report.
2. Phase II included 10 mixtures obtained from two plants (NH & VA) during the 2011 construction season with varying RAP percentage and virgin PG grade. The results of this work are summarized in the Phase II report. Phase II also included the beginning of the Silo Storage Study; the results of the study are presented in a separate report.

3. Phase III was a controlled laboratory study conducted to evaluate the impact of RAP percentage, virgin PG grade, and asphalt content without the confounding effects of uncontrolled plant production variables. The results of this work, which also include pavement analysis, are summarized in this Phase III report.

The results of this project add to the body of knowledge and types of RAP mixtures that have been evaluated in other research projects across the country. Ultimately, the industry needs to understand how RAP interacts with the virgin materials in a mixture so that the proper techniques and procedures can be developed and used to design and construct RAP mixtures that have equal or better performance than virgin mixtures.

1.2 Objectives and Scope of Phase III Report

Phase III of the project was conducted on laboratory mixtures that were produced during 2013. The controlled laboratory study was selected for the final phase of the project to isolate mixture variables without the confounding effects of plant production variables that the research team is not able to control. The NH Phase I mixture was chosen for this evaluation. The objective was to evaluate the impact of virgin binder PG grade and total asphalt content on mixtures with 0%, 20%, and 40% RAP. Table 1.1 below presents a summary of the nine mixtures that were evaluated as part of Phase III of the project. This report presents the results of the testing conducted on these Phase III mixtures.

Table 1.1 Phase III mixtures

Mixture	**Asphalt content**	**RAP Content (total weight)**		
		0	**20**	**40**
NH Phase I	-0.5%	PG 64-28	PG 64-28 PG 58-28	PG 64-28 PG 58-28
	optimum	PG 64-28	PG 64-28	PG 64-28
	+0.5%	-	-	PG 64-28

Testing and Analysis of Asphalt Binders and Mixtures

Binder Testing
Binders from the various RAP mixtures were extracted and recovered. Testing was done to determine the PG grading, including the critical cracking temperature determination, and partial binder master curve of the fully blended material. Testing was also done on the virgin binder and the recovered RAP binder.

Mixture Testing
All specimens were fabricated in a single laboratory for consistency. Mixture testing included dynamic modulus (AASHTO TP 79), push-pull SVECD fatigue (AASHTO TP 107), triaxial stress sweep (TSS) to evaluate rutting performance, and the Thermal Stress Restrained Specimen Test (TSRST) to evaluate low temperature cracking. Mixture testing allowed for the characterization of mixture properties and provided inputs for pavement analysis that was performed using the Linear Viscoelastic Continuum Damage (LVECD)

approach being developed by North Carolina State University (NCSU) under the Federal Highway Agency (FHWA) Performance Related Specification (PRS) project.

The report is organized to present a description of the testing performed in Chapter 2, Chapter 3 describes the mixtures and materials, followed by the results in Chapter 4 and Chapter 5 presents a summary of the results and conclusions.

1.3 Research Team

This project was conducted by the University of New Hampshire, Rutgers University, University of Massachusetts at Dartmouth, and North Carolina State University. Dr. Jo Sias Daniel at UNH served as the Principal Investigator overseeing the research, performing data analysis, preparing reports, and presenting the findings. UNH fabricated all of the test specimens for this study. Dr. Richard Kim at North Carolina State University served as a co-PI on this project and was responsible for the dynamic modulus, S-VECD fatigue, and TSS testing as well as the LVECD pavement analysis. Dr. Tom Bennert at Rutgers served as a co-PI and was responsible for the extraction and recovery of the binders and binder testing. Dr. Walaa Mogawer at UMass Dartmouth served as a co-PI and was responsible for the TSRST testing.

1.4 Participating States and Technical Committee

The New Hampshire Department of Transportation is the lead agency for this project. Additional states that are participating in this study include: Maryland, New York, New Jersey, Pennsylvania, Rhode Island and Virginia. The Federal Highway Agency has also contributed funds to this project. The technical committee consists of representatives of each participating agency, as shown in Table 1.2.

Table 1.2 Technical committee members

Name	**Agency**
Nelson Gibson	FHWA
Denis Boisvert	NH DOT
Matt Courser	NH DOT
Zoeb Zavery	NYS DOT
Russell Thielke	NYS DOT
Eileen Sheehy	NJ DOT
Stacey Diefenderfer	VA DOT
Bob Voelkel	MD SHA
Timothy L. Ramirez	PA DOT
Mike Byrne	RI DOT

CHAPTER 2 TESTING AND ANALYSIS METHODS

The laboratory testing conducted during the study comprised of asphalt mixture and binder testing. The asphalt mixture testing was conducted on test specimens prepared in the laboratory. The asphalt binder testing was conducted on both tank stored and asphalt binder extracted and recovered using solvent extraction procedures.

2.1 Binder Tests

The asphalt binder sampled from the storage tank at the asphalt binder plant was performance graded for Original, Rolling Thin Film Oven (RTFO), and Pressure Aging Vessel (PAV) aged conditions. The asphalt binders were extracted and recovered from specimens that had been mixed and compacted in the laboratory in accordance with AASHTO T164, *Procedure for Asphalt Extraction and Recovery Process* and ASTM D5404, *Recovery of Asphalt from Solution from Solution Using the Rotatory Evaporator*, using tri-chlorethylene (TCE) as the extracting solvent (Figure 2.1). The recovered asphalt binder was treated as an RTFO-aged asphalt binder, assuming that the aging that occurred during specimen fabrication was equivalent to what occurs during RTFO aging. During the extraction and recovery process, the asphalt binder content was determined in accordance with AASHTO T164, *Procedure for Asphalt Extraction and Recovery Process.* All asphalt binders were performance graded (PG) in accordance with AASHTO M320, *Standard Specification for Performance-Graded Asphalt Binder*.

Figure 2.1 Rotatory evaporator system at Rutgers University for asphalt binder recovery

2.1.1 *Critical Cracking Temperature*

The low temperature critical cracking temperature was determined using the TSAR™ software developed by Abatech Consulting Engineers and conforming to AASHTO R49, *Determination of Low-Temperature Performance Grade (PG) of Asphalt Binders.* The analysis procedure utilizes the test data from the Bending Beam Rheometer (BBR) and Direct Tension Test (DTT). The BBR data is used to compute the thermal stress in the pavement using user-specified cooling rates and other material parameters, such as coefficient of linear expansion. The plot of thermal stress vs. temperature is then developed. Also plotted on the graph is the DTT failure stress vs. temperature. The location at which these two graphs intersect (BBR thermal stress and DTT failure stress) is noted as the low temperature critical cracking temperature. An example of this is shown in Figure 2.2.

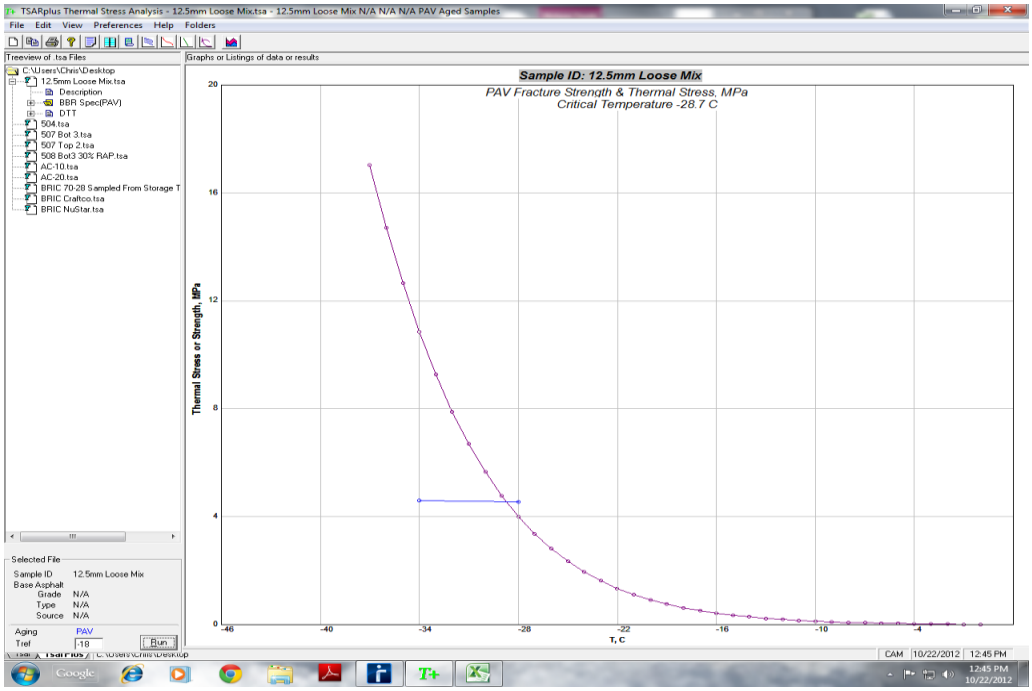

Figure 2.2 Screenshot from TSAR™ program calculating low temperature critical cracking temperature in accordance with AASHTO R49

AASHTO R49 recommends the analysis to be conducted using a cooling rate of 1°C/hr with a starting temperature of 0°C. However, these parameters are generalized and may not actually represent true field conditions. In fact, most surface temperature measurements indicate two distinct cooling rates with their own respective starting temperature. Figure 2.3 shows the two cooling rates and respective starting temperatures for a surface temperature profile in Augusta, Maine. The upper part of the curve has a cooling rate of -2.8°C/hr with a starting temperature of 5.5°C. Meanwhile, the lower part of the curve indicates a cooling rate of -0.51°C/hr with a starting temperature of -3.8°C. This indicates that a cooling event having two separate cooling rates/starting temperatures that may affect the low temperature critical cracking temperature differently.

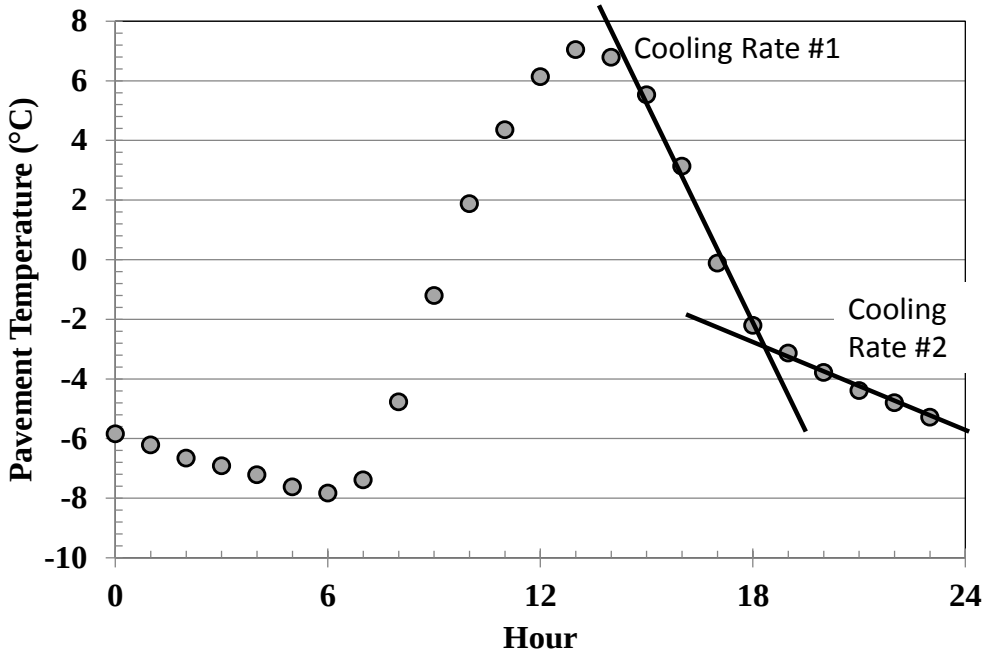

Figure 2.3 Field cooling rate at pavement surface (Augusta, Maine)

The analysis methodology described in AASHTO R49 allows for the determination of the low temperature critical cracking temperature at a multitude of cooling rate and starting temperature combinations, as long as there is enough test data to allow for the BBR thermal stress curve and DTT fracture stress curves to intersect. A parametric study of different starting temperatures and cooling rates was conducted for each mixture. The cooling rate was found to be the more significant factor with respect to low temperature critical cracking temperatures.

2.1.2 *Master Stiffness Curves (G*)*

The master stiffness curves were also determined for these materials. The asphalt binder master curves are constructed by collecting the dynamic complex modulus (G*) and phase angle (δ) over a wide range of temperatures and loading frequencies. The master curve is

then generated using the time-temperature superposition principle. A reference temperature, often 25°C, is used for which all of test data is shifted with respect to (Christensen and Anderson, 1992). For this study, the master curves were constructed using the RHEA software (Abatech, 2011).

In this study, the 4 mm geometry configuration (Figure 2.4) was used to measure the G* and δ of the extracted/recovered asphalt binder for some of the mixtures (Sui et al, 2010). The advantage of using the 4 mm geometry is that a much smaller amount of material is required for testing over the range of required temperatures. Typically, data from the BBR is necessary to provide the low temperature mechanical information needed to construct the master curve. However, the 4 mm geometry eliminates this need.

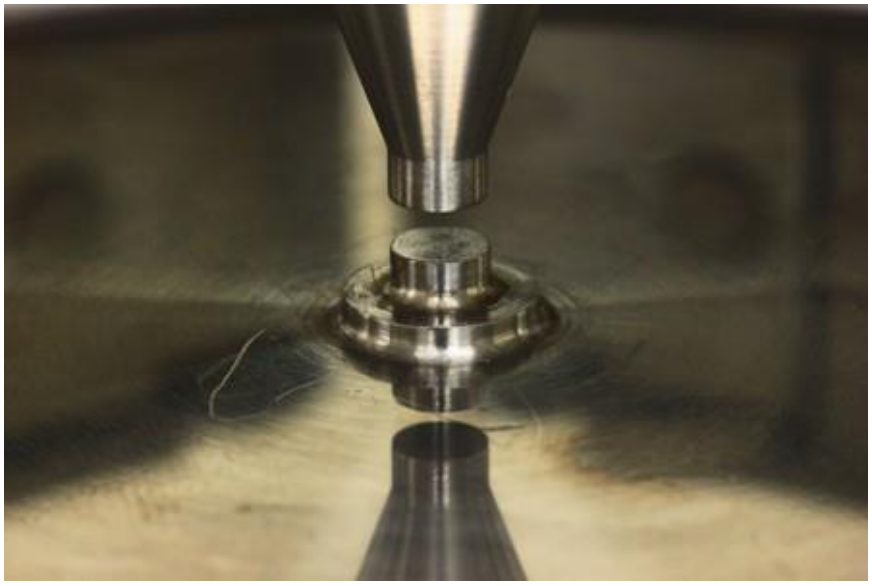

Figure 2.4 4 mm geometry for the dynamic shear rheometer

The form or shape of the G* master curve provides an indication of the "aging" characteristics of the asphalt binder. Figure 2.5 and Figure 2.6 show G* master curves for a PG 64-22 and PG 76-22 asphalt binder, respectively, that had undergone various levels of laboratory aging; RTFO, 20, 40, and 60 hours in the PAV. The constructed master curves shown in Figure 2.5 and Figure 2.6 clearly indicate that as the level of aging increases, the shape of the master curves become flatter and the magnitude of the shear modulus stiffer.

The same phenomena was originally noted by Christensen and Anderson (2002), who developed a model (Christensen-Anderson Model) that described shape parameters to define the master curves. Rheological Index (R) and Crossover Frequency (ω_o), are shape parameters within the model used to described the general slope and inflection point of the G* master curve (Figure 2.7). Therefore, as an asphalt binder undergoes different levels of aging, or rejuvenating, the shape parameters should change. Figure 2.8 shows how the Rheological Index and Crossover Frequency changes due to increased aging using the G* data shown in Figure 2.5 and Figure 2.6. As the respective asphalt binder ages, the shape

parameters move from the upper left quadrant of the R – ω_o space to the lower right quadrant. Therefore, by utilizing this methodology, one should be able to determine whether or not an asphalt binder has undergone a degree of aging, although an exact magnitude would not be able to be determined.

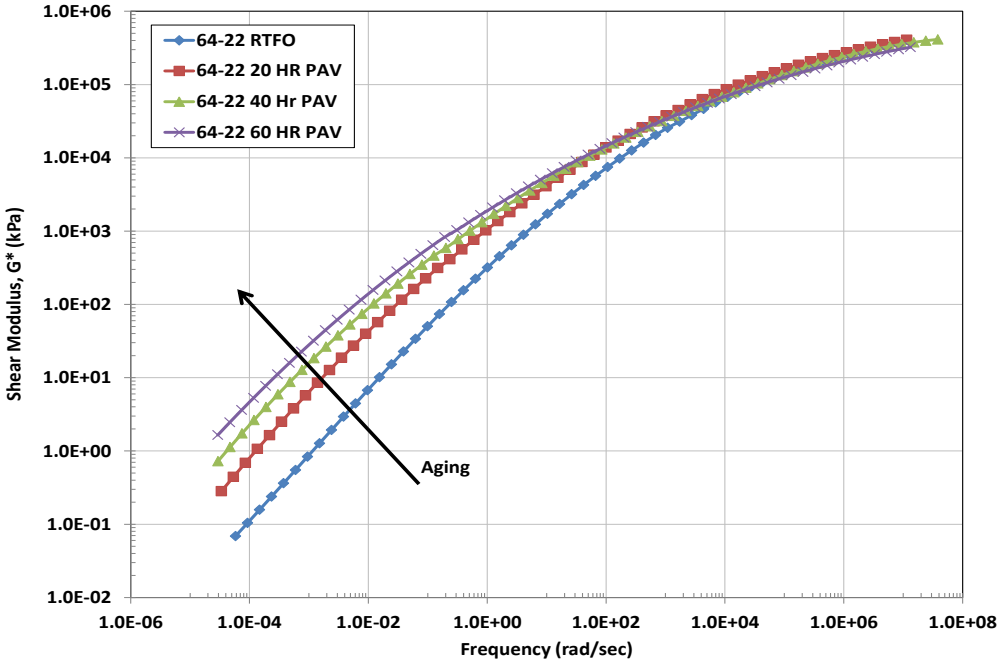

Figure 2.5 Shear modulus (G*) master curves for PG 64-22 asphalt binder

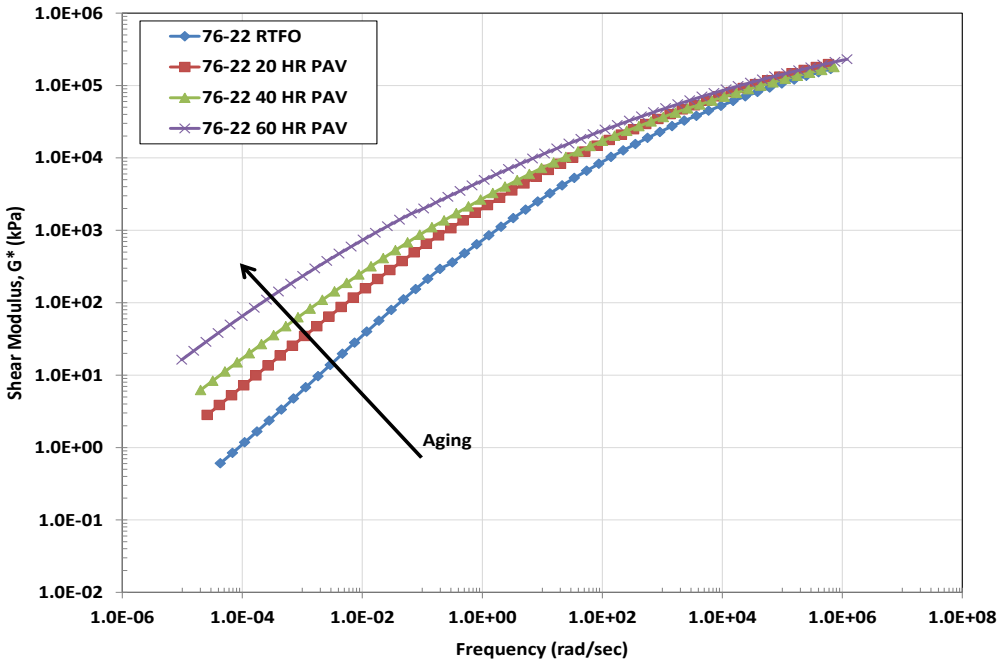

Figure 2.6 Shear modulus (G*) master curves for PG 76-22 asphalt binder

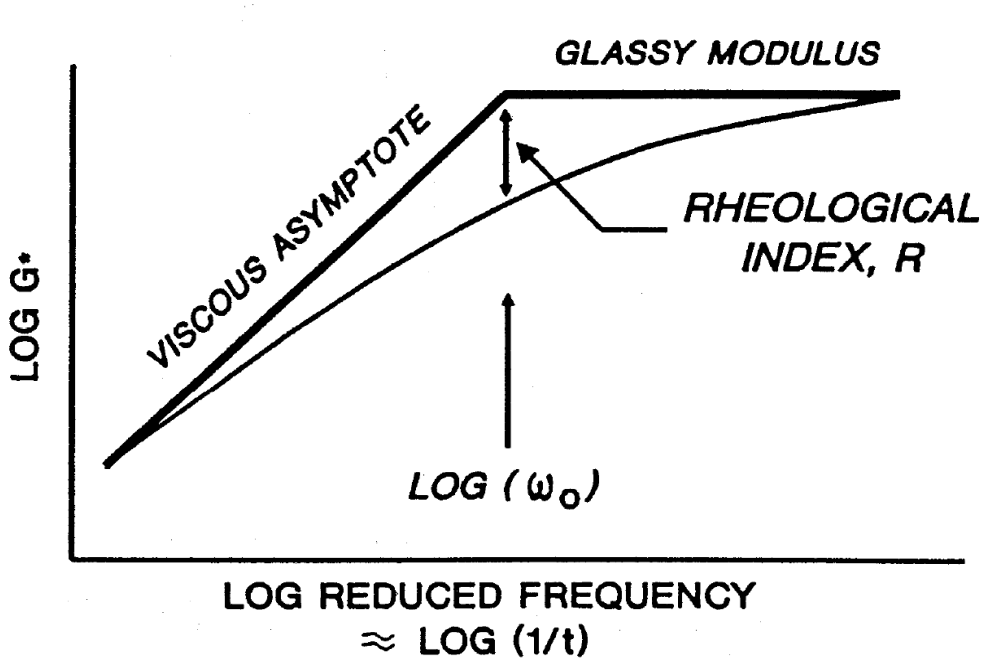

Figure 2.7 Christensen-Anderson model shape parameters

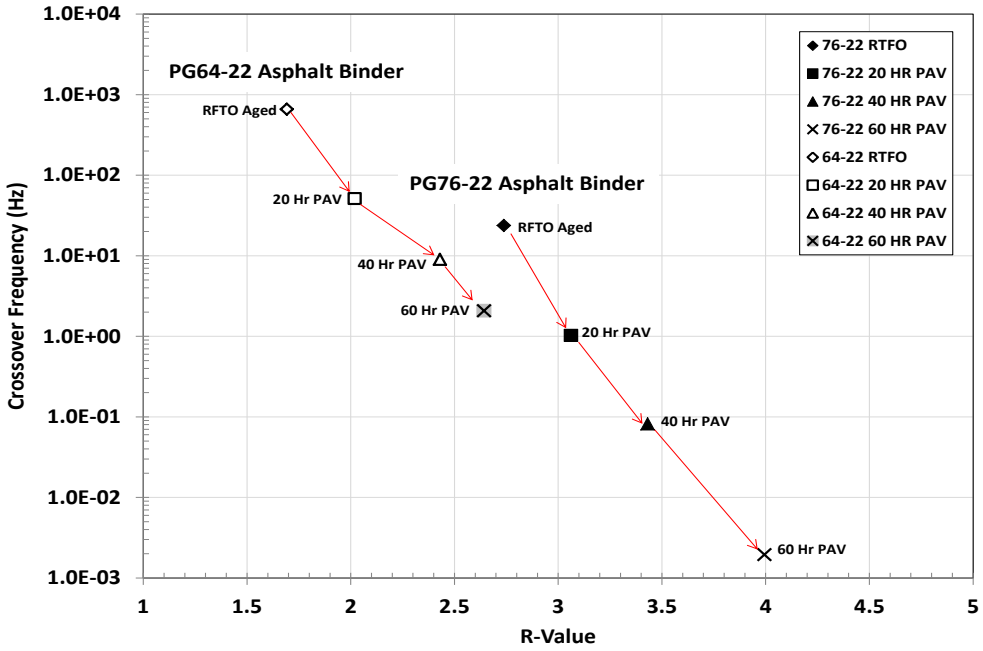

Figure 2.8 Christensen-Anderson model shape parameter changes due to different levels of aging

Along with a general trend of aging, the master curve analysis can also be utilized to evaluate the non-load associated cracking potential based on the work by Glover et al., (2005), Anderson et al. (2011), and Rowe (2011). Based on the original work of Glover et al. (2005), Rowe proposed to evaluate the following parameter, using master curve analysis, at a temperature of 15°C and loading frequency of 0.005 rad/sec.

$$\frac{G^*(\cos\delta)^2}{sin\delta} \qquad 2\text{-}1$$

When expressed in this manner, the limiting value of 9E-04 MPa at 0.005 rad/sec proposed by Glover et al. (2005) becomes $G^*(\cos\delta)^2/(\sin\delta) < 180$ kPa. The master curve information can then be expressed within Black Space (G* vs phase angle). Rowe's Black Space provides a means of assessing an asphalt binder and pre-screening it to determine if it is susceptible to cracking, using the same principles initially proposed by Glover et al. (2005).

Utilizing the same PG 64-22 and PG 76-22 asphalt binder samples shown earlier, Figure 2.9 shows that when plotted in Rowe's Black Space, as the degree of aging increases, the asphalt binders move from the lower right (passing) side of the proposed criteria to the upper left side (failing) side of the proposed criteria. The migration of test results is intuitive as one would expect asphalt binders to be more susceptible to cracking as the degree of aging increases.

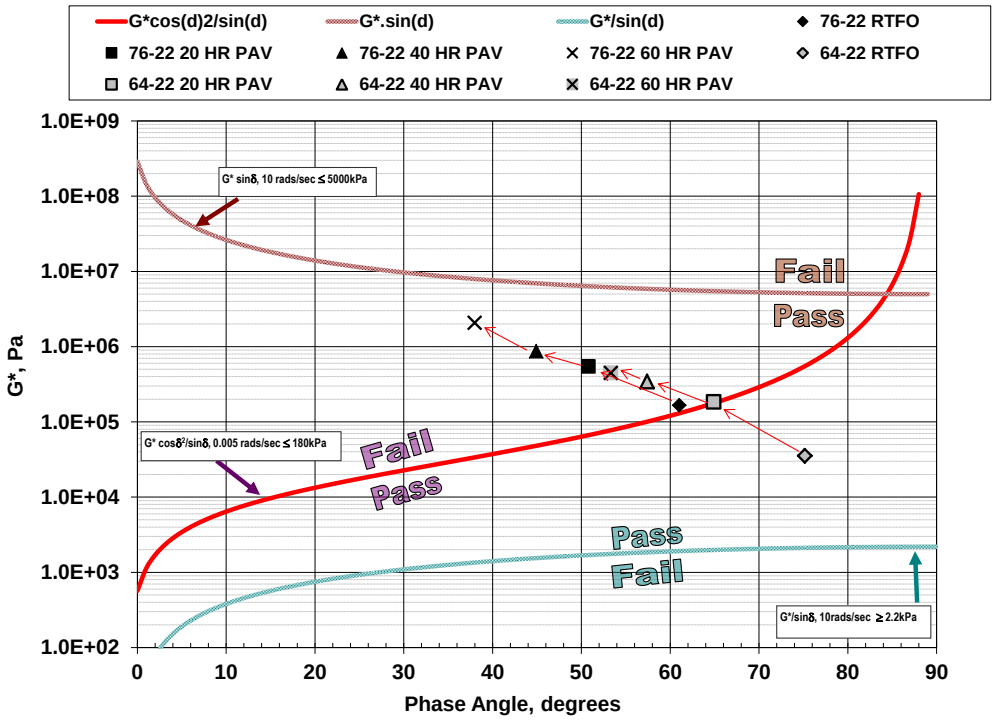

Figure 2.9 Rowe's (2011) black space analysis for non-load associated cracking potential

2.1.3 *Multiple Stress Creep and Recovery*

The Multiple Stress Creep and Recovery (MSCR) testing was performed on the recovered binders in accordance with AASHTO T340.

2.2 Mixture Tests

2.2.1 *Dynamic Modulus*

The AMPT (Asphalt Mixture Performance Tester) machine was used for the dynamic modulus testing in this study. The temperature control systems in the AMPT can achieve the required testing temperatures, ranging from 4°C to 54°C. In order to save time, specimen temperature conditioning was conducted in a support chamber outside the AMPT, and then the specimens were moved to the AMPT chamber. A temperature study was conducted to determine the temperatures at which the supporting temperature chamber and AMPT chamber should be set in order to achieve the target test temperatures for the shortest conditioning time. Table 2.1 summarizes the results of the temperature study for the dynamic modulus testing. The temperatures shown in Table 2.1 are the optimal temperatures determined from the lengthy temperature study. According to these results, the dynamic modulus test can start 30 minutes after the specimen is set in the AMPT chamber.

Table 2.1 AMPT temperature study results for dynamic modulus testing

Target Temperature, °C	Environmental Chamber Setting, °C	AMPT Setting, °C	Waiting Time, min.
4	2	2.5	30
19.5	19	19	30
40	40	40	30
54	56	55	30

Dynamic modulus testing was performed in load-controlled mode in axial compression following the protocol given in AASHTO TP 79. Tests were completed for all mixtures at 4°C, 20°C, 40°C, and 54°C and at frequencies of 25, 10, 5, 1, 0.5, and 0.1 Hz. Load levels were determined by a trial and error process so that the resulting strain amplitudes were between 50 and 75 microstrains. The testing order was from low to high temperatures and from high to low frequencies in order to minimize damage to the specimens. The complex modulus values were obtained from the final six cycles of each loading series, i.e., when the material reached the steady state. The dynamic modulus (|E*|) values were fitted for the coefficients of the sigmoidal function and time-temperature shift factors by optimizing the dynamic modulus mastercurve. After determining the shift factors, the dynamic modulus was converted to the relaxation modulus, E(t), of the Prony series form to obtain a constitutive relationship between strain and stress in the time domain. Finally, a power term, alpha (α), used in viscoelastic continuum damage (VECD) theory, was calculated from the maximum log-log slope, m, of the relaxation modulus and time using the relationship, $\alpha = 1 + 1/m$.

2.2.2 *Fatigue: Simplified Viscoelastic Continuum Damage (S-VECD)*

Simplified VECD (S-VECD) model is a mode-of-loading independent, mechanistic model that allows the prediction of fatigue cracking performance under various stress/strain amplitudes at different temperatures from only a few tests. The S-VECD model is composed of two material properties, that is, the damage characteristic curve that defines how fatigue damage evolves in a mixture and the energy-based failure criterion.

The S-VECD test method employs the controlled-crosshead direct tension cyclic test on 100 mm diameter, 130 mm tall cylindrical specimens cut and cored from 150 mm diameter, 178 mm tall gyratory specimens. Details of the test method can be found in AASHTO TP 107 *Determining the Damage Characteristic Curve of Asphalt Concrete from Direct Tension Cyclic Fatigue Tests*. Since the S-VECD test ends with the complete failure of the specimen, the properties measured from this test reflect the fatigue cracking resistance of asphalt mixture in both crack initiation and propagation stages.

The S-VECD testing was conducted using both the AMPT machine as well as a MTS 810 closed loop servo-hydraulic machine in this study. A temperature study similar to that conducted for dynamic modulus testing also was conducted for S-VECD fatigue testing; Table 2.2 shows the results. According to these results, cyclic testing can begin 60 minutes after the specimen is set in the AMPT chamber. The waiting time for cyclic testing is longer than in dynamic modulus testing because it takes more time to set up the specimen in the AMPT chamber for cyclic testing (end plates need to be screwed to the AMPT).

Table 2.2 AMPT temperature study results for S-VECD Fatigue testing

Target Temperature, °C	Environmental Chamber Setting, °C	AMPT Setting, °C	Waiting Time, min.
13	8	11.5	60
20	18	19	60
27	27	26.5	60

The remaining fatigue tests were conducted using the MTS 810 machine. This machine is capable of applying loads up to 20 kips, from 0.01 Hz to 25 Hz. The temperature control systems in the MTS can achieve the required testing temperatures, ranging from -10°C to 54°C. An asphalt concrete dummy specimen with a temperature probe placed in the middle of the specimen was placed inside the chamber in order to monitor the actual temperature of the specimen during testing.

The data acquisition system used for both the AMPT and MTS machine also is fully computer-controlled and is capable of measuring and recording data from several channels simultaneously. Six channels were used for this testing: four for the vertical linear variable differential transducers (LVDTs), one for the load cell, and one for the actuator. The data acquisition programs were prepared using LabView software for data collection and analysis.

Vertical deformations were measured using four loose-core, CD-type LVDTs at 90° radial intervals with a gauge length of 70 mm. Targets were glued to the specimen face, and the LVDTs were mounted to the targets to measure the deformation in the middle part of the specimen. For consistency in the measurements, a gluing device was used to maintain consistent spacing between the LVDT targets. Figure 2.10 shows the test specimens with the LVDTs mounted on their sides. DEVCON® steel putty was used to glue the steel end plates and targets for the LVDTs that were used for testing the specimens.

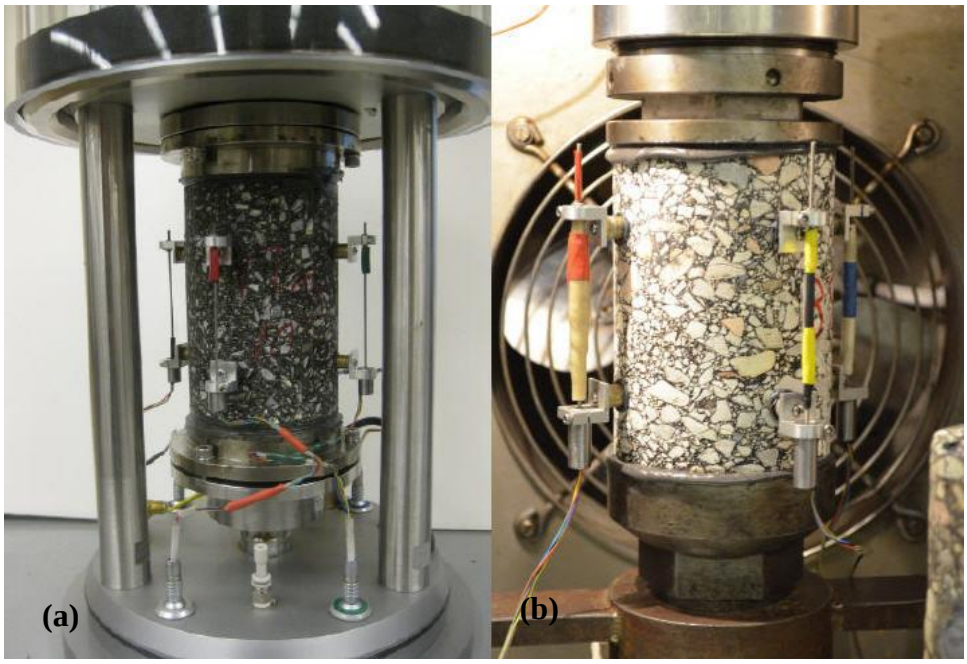

Figure 2.10 LVDT mounting and spacing: (a) AMPT and (b) MTS 810

Cyclic testing was conducted in crosshead-controlled mode. Fingerprint dynamic modulus tests were conducted by determining the dynamic modulus ratio (DMR) to check the variability of the test specimens before running the direct tension cyclic tests. A DMR in the range of 0.9 to 1.1 guarantees that the linear viscoelastic properties obtained from the dynamic modulus tests can be used properly in the S-VECD analysis.

All cyclic tests were performed at four to six different amplitudes to cover a range (from 1,000 to 100,000) of numbers of cycles to failure (N_f). Once the fatigue tests are conducted, the damage characteristic curves are developed by calculating the secant pseudo stiffness (S) and the damage parameter (S) at each cycle of loading. These values are cross-plotted to form the damage characteristic curve. An example of characteristic curves from fatigue tests conducted a different strain amplitudes is shown in Figure 2.11 for a VT mix. For all the mixtures, the exponential form shown in Equation 2-2 was used to fit the C versus S characteristic curves.

$$C(S) = e^{aS^b} \qquad 2\text{-}2$$

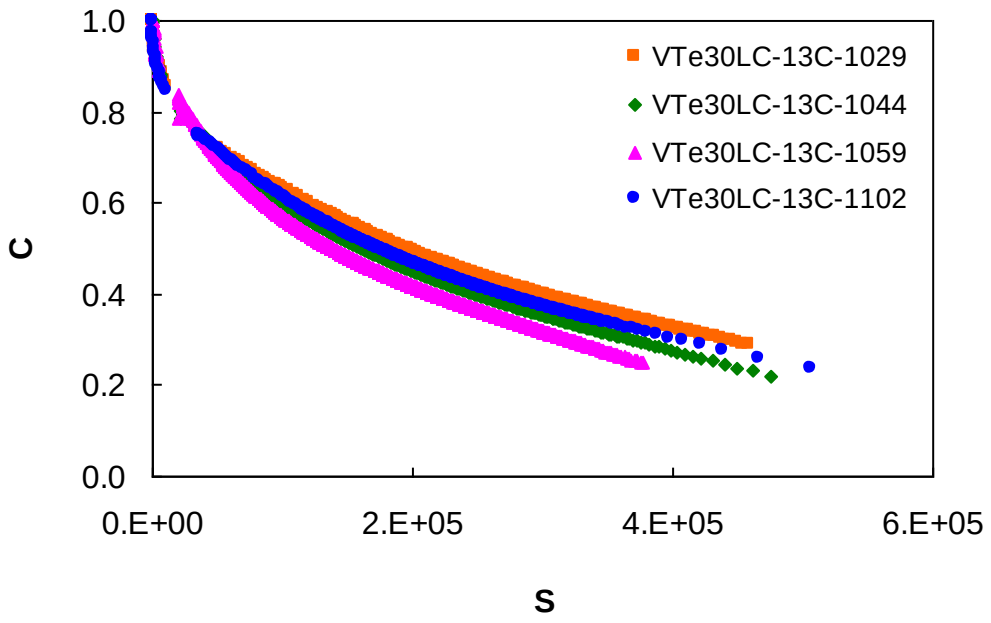

Figure 2.11 Individual results for fatigue testing for VT PG 64-28 30% RAP mixture at 13°C

The S-VECD fatigue failure criterion, called the G^R method, involves the released pseudo strain energy. This released pseudo strain energy concept focuses on the dissipated energy that is related to energy release due to damage evolution only and is fully compatible and predictable using the S-VECD model. G^R method development details are discussed in detail in Appendix A of the Phase I report. A characteristic relationship, which is found to exist in both recycled asphalt pavement (RAP) and non-RAP mixtures, can be derived between the rate of change of the averaged released pseudo strain energy during fatigue testing (G^R) and the final fatigue life (N_f). Figure 2.12 shows this relationship for the VT PG 64-28 30% RAP mixture as an example.

The G^R failure criterion combines the advantages of the VECD model and this characteristic relationship, which both originate from fundamental mixture properties. This method is able to predict the fatigue life of asphalt concrete mixtures across different modes of loading, temperatures, and strain amplitudes within a typical range of sample-to-sample variability that is observed in fatigue testing. Using the derived relationship and the S-VECD model, the fatigue life of asphalt concrete under different modes of loading and at different temperatures and strain amplitudes can be predicted from dynamic modulus tests and cyclic direct tension tests at three to four strain amplitudes.

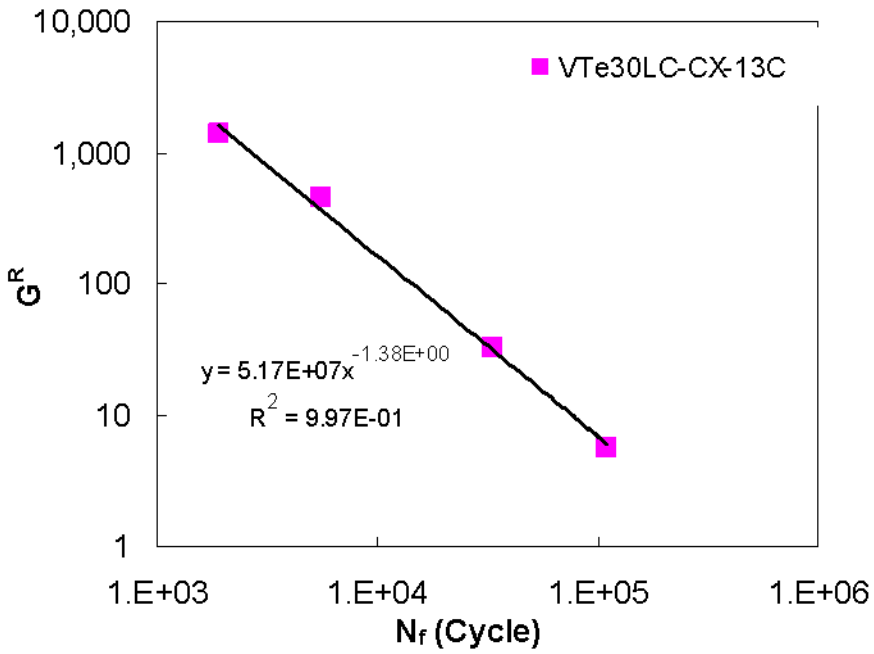

Figure 2.12 Relationship between G^R and N_f for VT PG 64-28 30% RAP mixture at 13°C

2.2.3 *Permanent Deformation: Triaxial Stress Sweep Testing*

The flow number test, as described in AASHTO TP 79, is composed of a 0.1-second haversine shape pulse and 0.9-second rest period and typically is used to assess the rutting resistance of asphalt materials. However, this specification does not refer to detailed test conditions, such as deviatoric stress and confining pressure. NCHRP 9-30A (NCHRP Report 719) recommends that the stress conditions for rutting tests should be 70 psi (490 kPa) for the deviatoric stress and 10 psi for the confining pressure. The deficiency of this test method is that it can only provide rutting resistance information in terms of ranking; that is, it cannot evaluate rutting performance in terms of the various loading conditions that are found in actual field loading scenarios.

Choi and Kim (2013) developed a permanent deformation model, the so-called *shift model*, which is based on two superposition principles: time-temperature (t-T) and time-stress (t-S). The triaxial sweep (TSS) test also was developed to provide a simple method to calibrate the shift model. Figure 2.13 illustrates that the TSS test is composed of two types of testing: first, a reference test at the high temperature (T_H) is conducted, and then, three (multiple stress sweep) MSS tests at three different temperatures of low, intermediate, and high (T_L, T_I, and T_H, respectively) are conducted. The reference test is a type of triaxial repeated load permanent deformation (TRLPD) test that uses a 0.4-second haversine pulse with a 10-second rest period. This test provides the permanent strain mastercurve by fitting the incremental model. The incremental model is expressed in Equation 2-3. The MSS test consists of three loading blocks. The deviatoric stress increases in each loading block while

the other loading conditions remain constant. The deviatoric stress begins at 70 psi and then increases to 100 psi and 130 psi in the second and third loading blocks, respectively. The shift factors are obtained by shifting the permanent strain of each individual loading block toward the permanent strain mastercurve that is obtained from the reference test. The reduced load time shift factors and deviatoric stress shift factors are shown in Equation 2-4. All the coefficients in Equation 2-3 and Equation 2-4 are used as inputs for linear viscoelastic continuum damage (LVECD) simulations to evaluate the rut depth of the asphalt pavement. Also, Equation 2-3 and Equation 2-4 include the shift model. The physical number of cycles is converted to a reduced number of cycles by using the total shift factor, which is the sum of the deviatoric stress shift factor and the reduced load time shift factor. These two shift functions utilize temperature, load time, and deviatoric stress to calculate the shift factors.

$$\varepsilon_{vp} = \frac{\varepsilon_0 \cdot N_{red}}{\left(N_I + N_{red}\right)^{\beta}}, \tag{2-3}$$

$$\begin{aligned} a_{\xi_p} &= p_1 \xi_p^{\,p_2} + p_3, \\ a_{\sigma_d} &= d_1 (\sigma_d / P_a)^{d_2} + d_3. \end{aligned} \tag{2-4}$$

where

N_{red} = reduced number of cycles at reference loading conditions,
p_1, p_2, p_3 = coefficients of reduced load time shift function,
d_1, d_2, d_3 = coefficients of deviatoric stress shift function, and
P_a = atmospheric pressure to normalize stress.

The calibration tests can be performed in the asphalt material performance tester (AMPT). Based on AASHTO TP 79-10, the test procedure is composed of six steps. Table 2.3 shows these steps and their descriptions. They are as follows: (1) specimen preparation, (2) temperature conditioning in a separate environmental chamber, (3) installation of the specimen in the AMPT, (4) pressurizing and additional temperature conditioning, (5) fingerprint testing, and (6) main protocol testing. Steps 1 and 2 are preparatory steps for the testing and take place separately. During Step 4 (pressurizing and additional temperature conditioning), the sample should reach a stabilized state in terms of pressure and temperature. The time that is needed to reach this stabilized state is then investigated.

Table 2.3 Procedure for Protocol Tests

Step	**Procedure**	**Description**	**Time**
1	Specimen preparation	Membrane, targets, LVDTs	-
2	Temperature conditioning	Outside oven	-
3	Specimen installation	AMPT chamber	< 5 min
4	Pressurizing and additional temperature conditioning	Application of contact force and confining pressure	> 1hr
5	Fingerprint testing	10 Hz, 20 cycles	5 min
6	Main testing	Multiple stress tests (@T_H, T_I, T_L); reference test (@T_H)	1.8 hr (T_H) 0.7 hr (T_I, T_L)

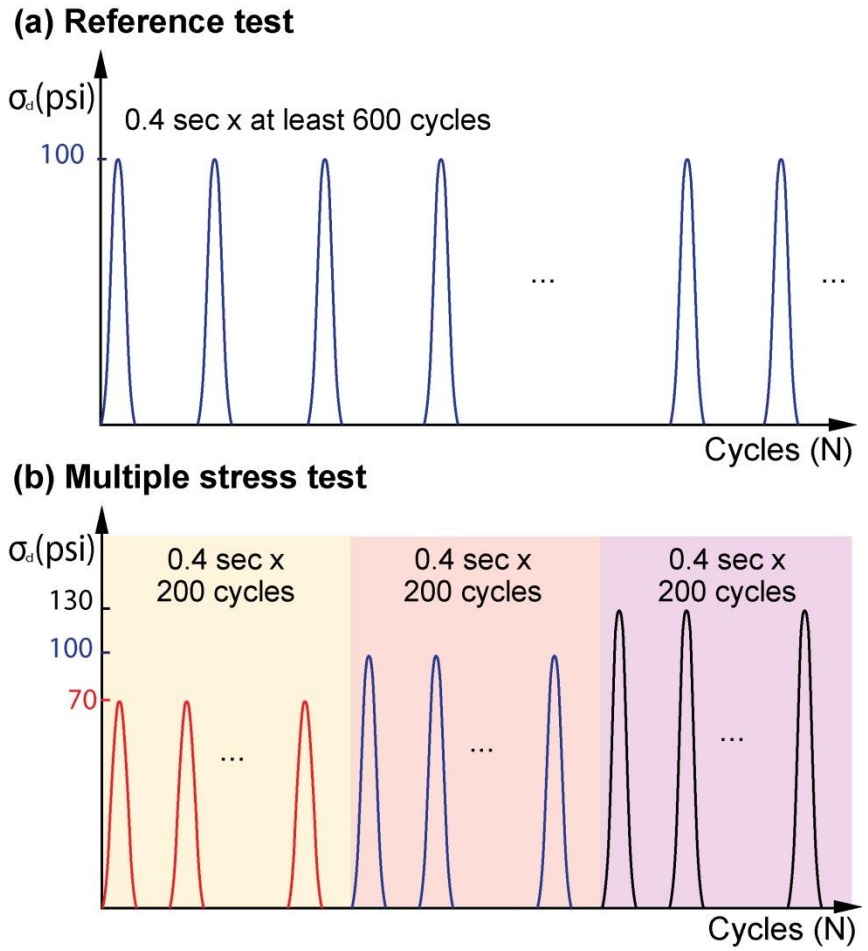

Figure 2.13 Schematic diagram of test protocols for shift model: (a) reference test at T_H and (b) multiple stress tests at T_L, T_I, and T_H (Choi and Kim 2013)

Taking all the aforementioned test conditions into consideration, the total test time becomes 2.9 hours for the high temperature test in which the rest period is 10 seconds, and 1.5 hours for the low and intermediate temperature tests in which the rest period is 1.6 seconds. Thus, completing one set of calibration tests takes about a day (total 9 hours for 4 tests). So, within only two to three days of testing, the calibrated shift model is able to predict the permanent strain growth in asphalt concrete for different temperatures, load times, and deviatoric stress levels.

According to the TSS test protocol, the enhanced integrated climate model (EICM), which is implemented in the MEPDG (2004), can be used to find the test temperatures (i.e., T_L, T_I, and T_H). The EICM is a one-dimensional coupled heat and moisture flow model that has been improved and integrated using other climate models. The EICM generates pavement temperatures with respect to pavement depth every hour. Because asphalt concrete is very sensitive to temperature, the distribution of temperature within a pavement structure is critical information. Moreover, the number of occurrences of the temperature in question is an important factor for rut depth calculation, too. Although low temperatures produce very small strain levels, they occur more frequently, so the cumulative strain due

to a low temperature may be significant. In that sense, both the distribution and the number of occurrences of temperatures should be considered at the same time.

In the approach suggested by Choi and Kim (2013), a cumulative density graph can be created by accumulating permanent strain with respect to pavement temperature, as shown in Figure 2.14. In order to select the test temperatures, the temperature that corresponds to the 10th percentile is chosen as the low temperature (T_L). For the high temperature, because it induces significant permanent deformation, the 100th percentile is chosen (T_H), which is the highest temperature that the pavement experiences during the analysis period. For the same reason, a temperature corresponding to the 60th ~ 80th percentile range is recommended as the intermediate temperature (T_I), so the 70th percentile temperature is chosen as the intermediate temperature.

In cases where the 100th percentile temperature (T_{100}) is higher than 54°C, the high temperature (T_H) is fixed at 54°C, and then the load time is increased by applying the t-TS principle in order to obtain the same reduced load time. The reason for having this maximum test temperature is that the AMPT cannot operate at higher temperatures. Also, at very high temperatures the samples can become too soft and difficult to handle.

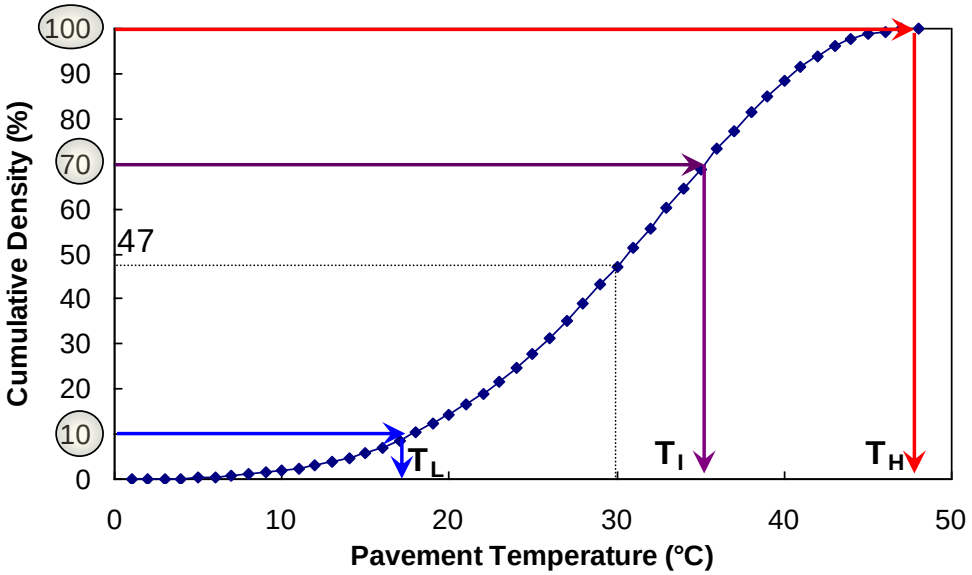

Figure 2.14 Example of cumulative density function of permanent strain for pavement structures in Angelica, NY (Choi and Kim 2013)

2.2.4 *Low Temperature: Thermal Stress Restrained Specimen Test*

In order to assess low temperature cracking of the mixtures, each mixture was tested in the thermal stress restrained specimen test (TSRST) device in accordance with AASHTO TP10-93. In the TSRST test, the asphalt specimen is cooled at a constant rate (-10ºC/hour) while its original length is held constant by the TSRST device. As the specimen becomes colder, it is restrained from contracting, resulting in the accumulation of thermal stress. Eventually, the thermal stress exceeds the tensile strength of the specimen, resulting in fracture (cracking). The temperature at which this fracture occurs is recorded and noted as the low cracking temperature of the mixture.

A minimum of three replicate gyratory specimens 185 mm (7.3 in.) tall by 150 mm (5.9 in.) in diameter were fabricated for each mixture. The TSRST specimens were then cored and cut to a final height of 160 mm tall (6.3 in.) by 54 mm (2.1 in.) in diameter. The air void content of the final cut specimens was 6 ±1 percent.

2.2.5 *Overlay Tester*

The Overlay Tester evaluates the asphalt mixture's ability to resist or retard crack propagation. Specimen preparation and test parameters used in this study followed that of TxDOT Tex-248-F testing specifications. These include:

- 25ºC (77ºF) test temperature;
- Opening width of 0.025 inches;
- Cycle time of 10 seconds (5 seconds loading, 5 seconds unloading); and
- Specimen failure defined as 93% reduction in initial load

Five replicate specimens were tested for each mixture. The low and high values were discarded and the remaining three were used to calculate the average value and standard deviation.

CHAPTER 3 MATERIALS AND MIXTURES

3.1 Mixture Design Information

The mixture designs from the NH Phase I 12.5 mm mixtures (50 gyration Superpave design) were used for this phase of the project. Nine mixtures were produced in the laboratory with varying RAP content and total asphalt content, as shown in Table 3.1. The asphalt content ranges were chosen to cover typical allowable production tolerances. The aggregate gradations for these mixtures are shown in Table 3.2. The RAP materials used in these mixtures had an average asphalt content of 4.3% and a grade of a continuous PG grade of PG 86.6-18.2.

Table 3.1 Phase III mixtures

Mixture	**Asphalt content**	**RAP Content (total weight)**		
		0	**20**	**40**
NH Phase I	5.2 (opt-0.5%)	PG 64-28	PG 64-28 PG 58-28	PG 64-28 PG 58-28
	5.7 (optimum)	PG 64-28	PG 64-28	PG 64-28
	6.2 (opt+0.5%)	-	-	PG 64-28

Table 3.2 Mixture gradations

Mix	**Mixture Gradation**								
	12.5	**9.5**	**#4**	**#8**	**#16**	**#30**	**#50**	**#100**	**#200**
NH 0 % RAP	98.6	85.8	58.3	42.5	32.0	24.7	15.5	7.2	3.58
NH 20 % RAP	98.7	86.5	57.5	42.4	33.0	25.5	15.8	7.0	3.60
NH 40 % RAP	98.7	86.4	55.5	41.2	33.0	24.8	15.0	6.1	2.65

The asphalt binders from the laboratory produced mixtures were extracted and recovered for additional testing (Chapter 4). During this process, the actual asphalt contents of each mixture were measured and are summarized in

Table 3.3. Variability in the asphalt content of the RAP material that could not be controlled in the laboratory created variation in the measured asphalt contents by several tenths in some cases.

Table 3.3 Measured Asphalt Contents

Base Binder Grade	Sample Name	AC% Condition	RAP Content (%)	Measured AC Content (%)
PG58-28	NH5820-opt	Opt-0.5%	20%	5.20
	NH5840-opt		40%	5.44
PG64-28	NH6400-opt	Opt-0.5%	0%	5.80
	NH6420-opt		20%	5.36
	NH6440-opt		40%	5.19
	NH6400opt	Opt	0%	5.80
	NH6420opt		20%	5.89
	NH6440opt		40%	5.90
	NH6440+opt	Opt+0.5%	40%	5.91

3.2 Specimen Preparation

Aggregate stockpiles were first dried and sieved into individual portions for batching individual specimen sizes. The aggregate particles were then heated to the mixing temperature of 165°C for at least four hours prior to mixing. The RAP was air-dried on a flat sheet for 24 hours prior to mixing and was heated to 60ºC for two hours prior to being mixed with the virgin aggregate and asphalt binder. The RAP, virgin aggregate, and asphalt binder were mixed together for three minutes using a bucket mixer. After that, the mixtures were short-term oven-aged for two hours at the compaction temperature of 145°C. Then, the mixtures were compacted to create specimens of appropriate geometry and air void content. All specimens were compacted to a height of 178 mm and a diameter of 150 mm using the Superpave gyratory compactor. To obtain specimens of uniform air void distribution, these samples were cored to a diameter of 100 mm and cut to height of 150 mm for dynamic modulus and TSS testing, and to 130 mm for tension testing. Prior to testing, the air void ratios were measured using the CoreLok method for each specimen for quality control. All the test specimens used in this study had an air void ratio within the range of 6.0% ± 0.5 percent.

3.3 Volumetric Analysis

Specimens for each RAP content were compacted to the design number of gyrations (50 gyration design) at different asphalt contents to evaluate the impact of asphalt content on the volumetric properties of the mixtures. The results, in Figure 3.1 through Figure 3.5 below, show the expected trends for the different mixtures, with a vertical shift with RAP content.

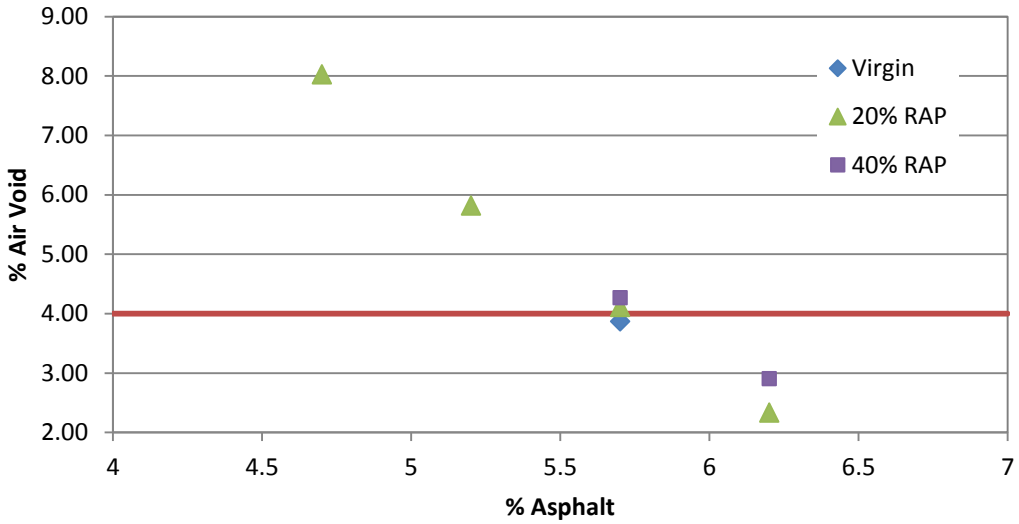

Figure 3.1 Air Void Content versus Asphalt Content for Mix Design Specimens

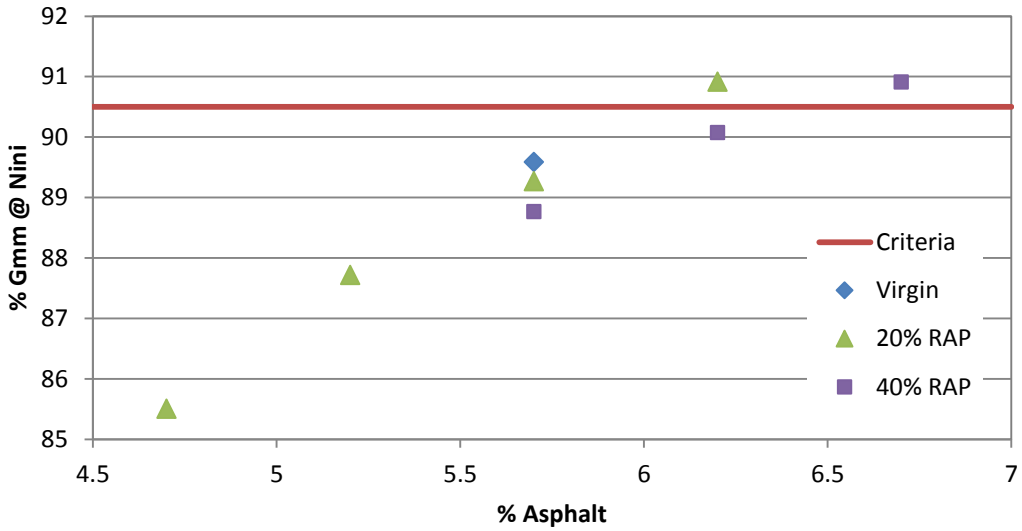

Figure 3.2 Percent Gmm at Nini versus Asphalt Content for Mix Design Specimens

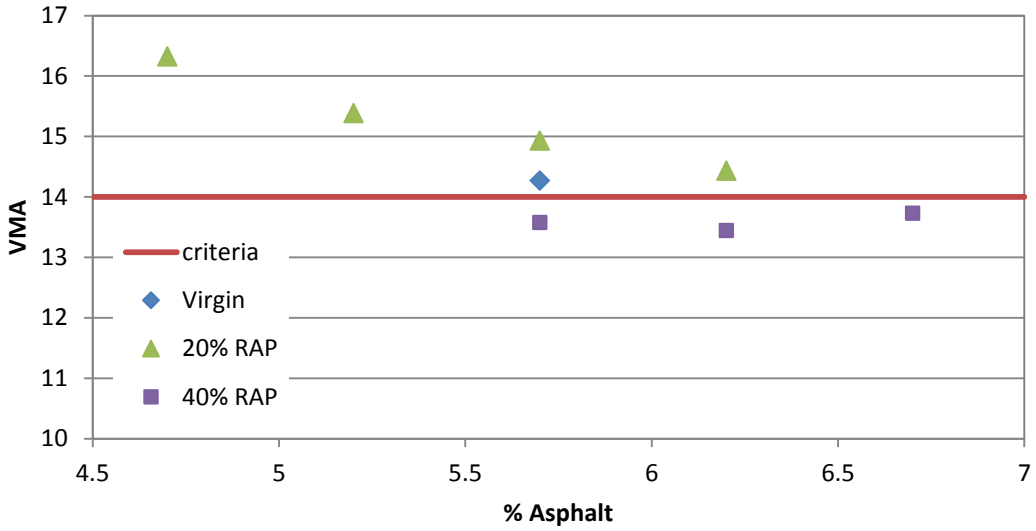

Figure 3.3 VMA versus Asphalt Content for Mix Design Specimens

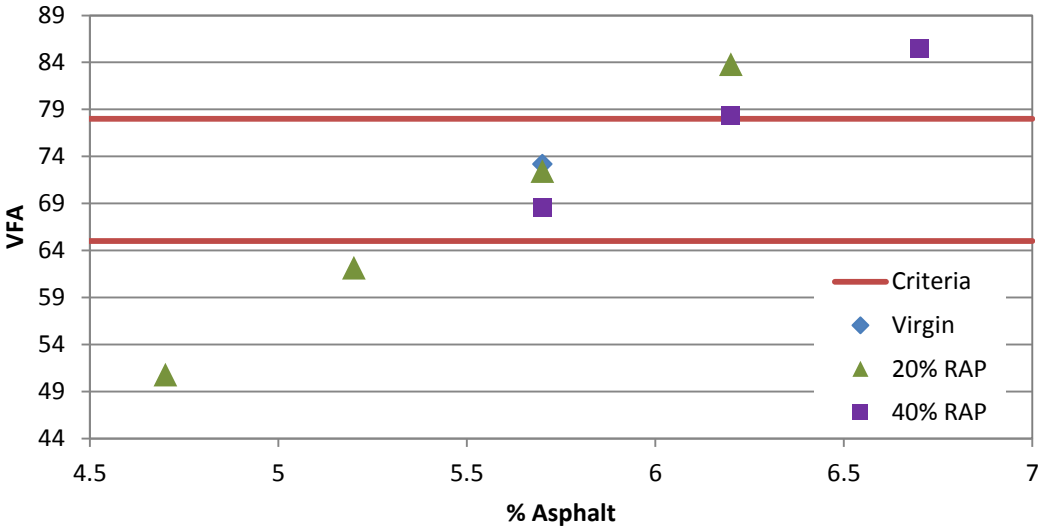

Figure 3.4 VFA versus Asphalt Content for Mix Design Specimens

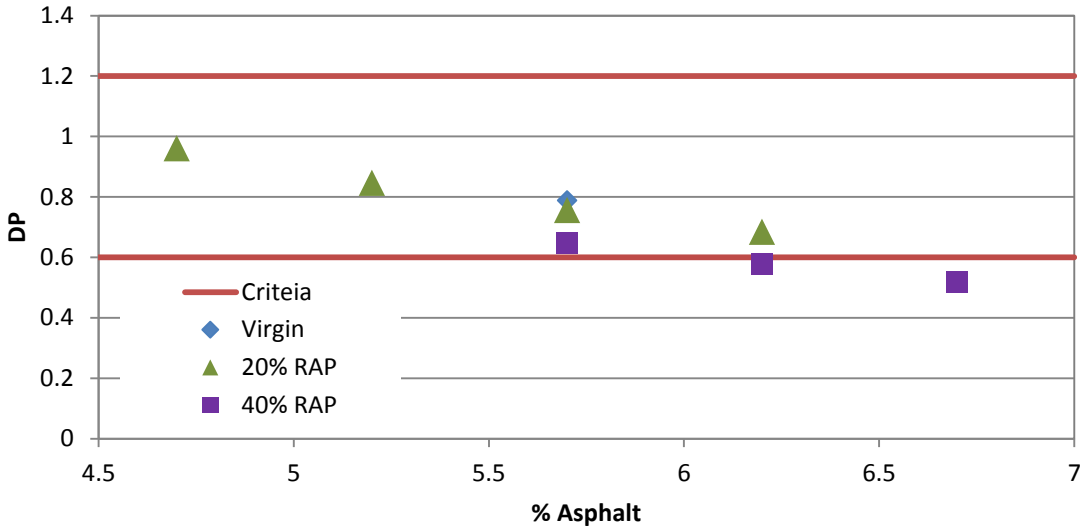

Figure 3.5 Dust Proportion versus Asphalt Content for Mix Design Specimens

CHAPTER 4 RESULTS

4.1 Binder Testing

The asphalt binder testing was conducted extracted and recovered asphalt binder from laboratory produced test specimens.

4.1.1 *PG Grading*

The asphalt binders were performance graded (PG) in accordance with AASHTO M320, *Standard Specification for Performance-Graded Asphalt Binder*. A master table with all of the PG information is shown as Table 4.1. As one would expect for the identical mixture condition (i.e. – binder grade and asphalt content), as the RAP content increases, both the high and low temperature PG grades increase. Figure 4.1 through Figure 4.3 show the high, intermediate and low temperature PG grades, respectively, determined from the extracted and recovered asphalt binders. The higher asphalt contents result in lower intermediate and high temperature grades and warmer low temperature grades, indicating that there is an effect of the amount of virgin asphalt on the recovered values, but it is not consistent with the high vs low temperatures.

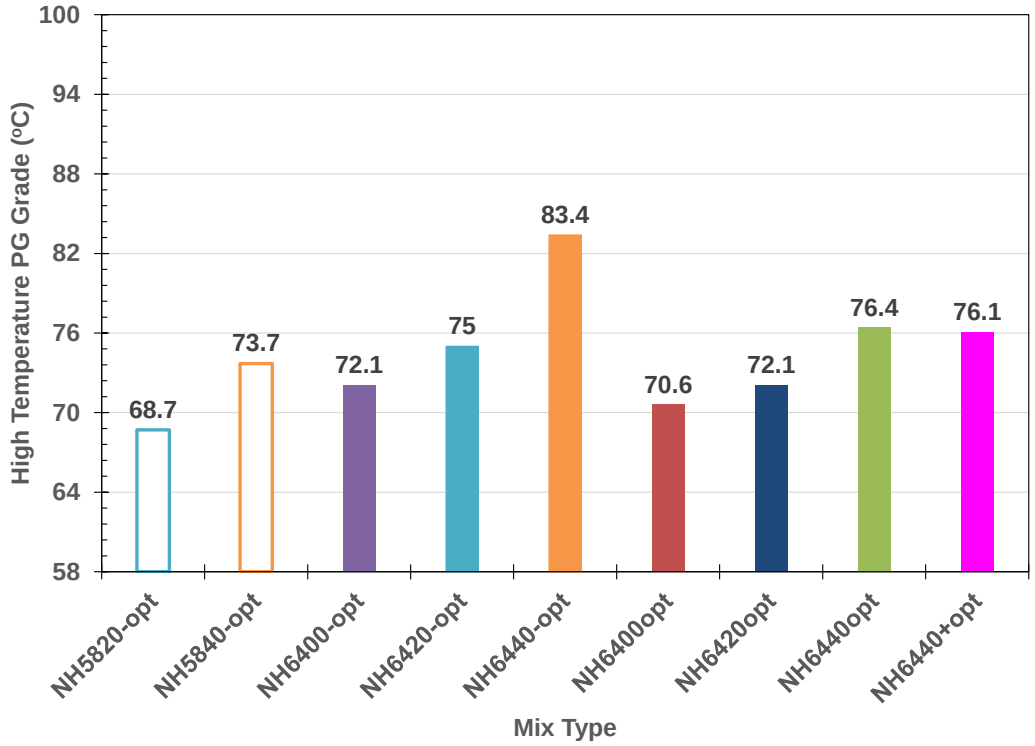

Figure 4.1 High Temperature PG Grades

Table 4.1 Summary of Asphalt Binder Performance Grading

Base Binder Grade	Sample Name	AC% Condition	RAP Content (%)	Performance Grade (PG) - AASHTO M320					
				High Temp (^{o}C)	Intermediate Temp (^{o}C)	Low Temperature			Final PG Grade
						AASHTO R29 (m-slope)	AASHTO R29 (Stiffness, S)	AASHTO R49 (C.C.)	
PG58-28	NH5820-opt	-Opt	20%	68.7	19.3	-26.9	-29.1	-27.1	64-22
	NH5840-opt		40%	73.7	22.3	-24.2	-28	-25	70-22
PG64-28	NH6400-opt	-Opt	0%	72.1	18.9	-30.2	-30.4	-27.9	70-28
	NH6420-opt		20%	75	20.1	-27.8	-29.3	-27	70-22
	NH6440-opt		40%	83.4	25.2	-19.9	-27	-23	82-16
	NH6400opt	Opt	0%	70.6	18.3	-28.8	-29.5	-27.8	70-28
	NH6420opt		20%	72.1	19.5	-26.5	-29.4	-26.6	70-22
	NH6440opt		40%	76.4	22.3	-16.3	-20.1	-24.5	76-16
	NH6440+opt	+Opt	40%	76.1	21.7	-16.1	-19.3	-24.1	76-16

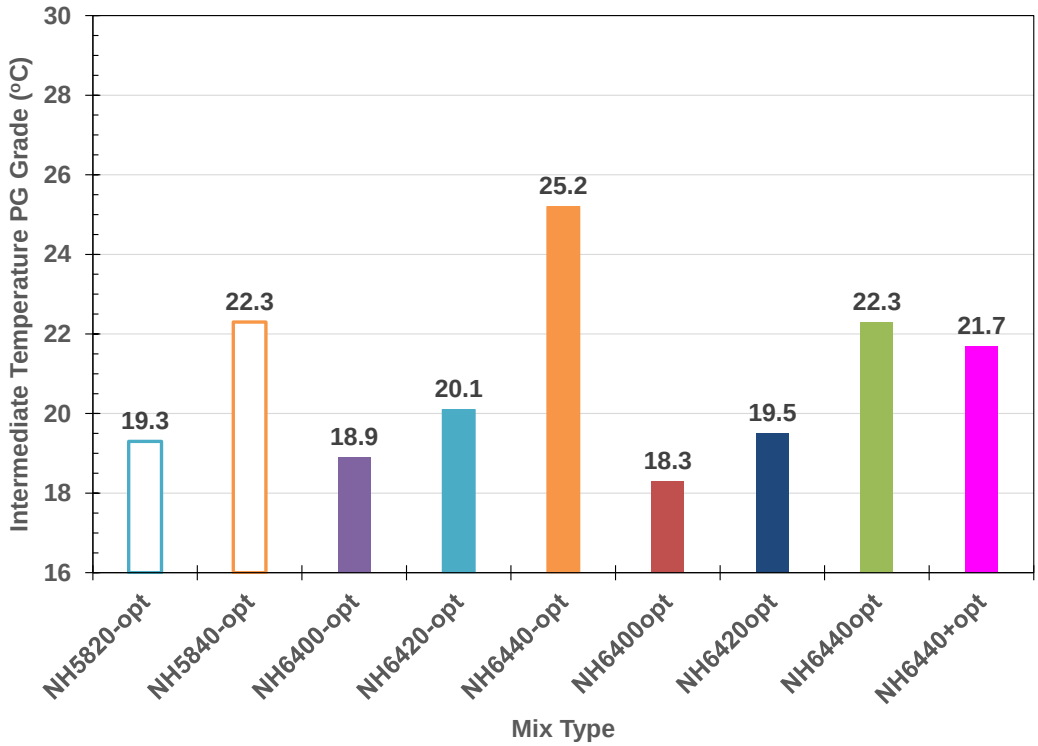

Figure 4.2 Intermediate Temperature PG Grades

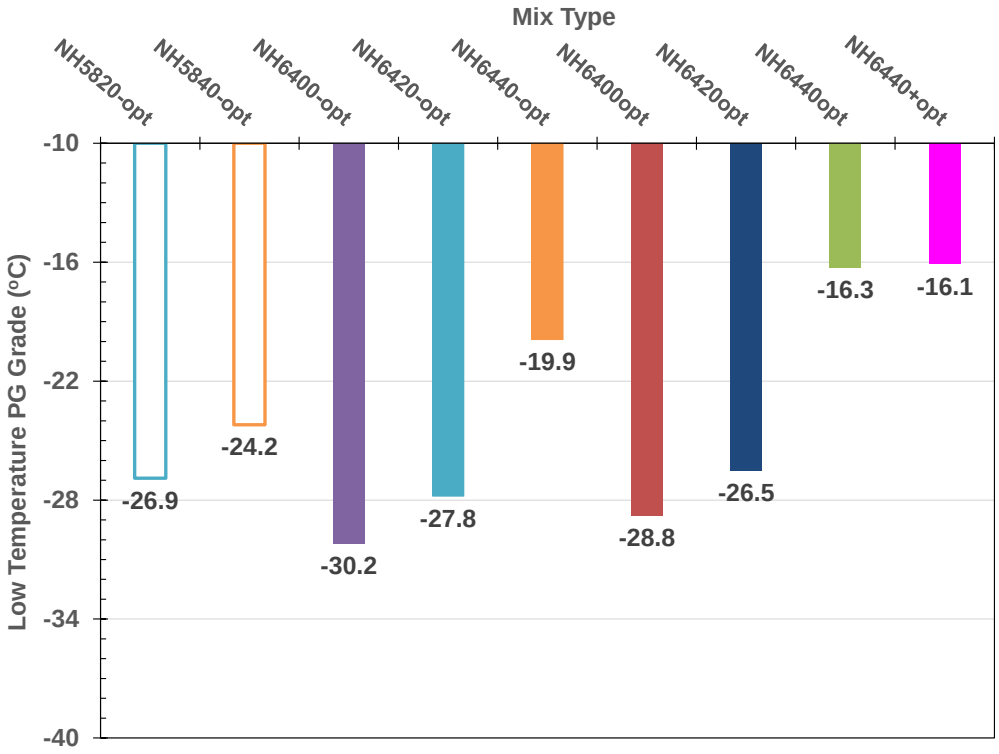

Figure 4.3 Low Temperature PG Grades

4.1.2 *Critical Cracking Temperature*

The low temperature critical cracking temperature was determined using the TSAR™ developed by Abatech Consulting Engineers and conforming to AASHTO R49, *Determination of Low-Temperature Performance Grade (PG) of Asphalt Binders.* The low temperature critical cracking temperature determined using AASHTO R49 and the low temperature binder grade, as determined using AASHTO R29, were plotted against one another and shown in Figure 4.4. A moderate correlation exists between the AASHTO M320 low temperature determination and the AASHTO R49 low temperature determination. Overall, Figure 4.4 indicates the m-value from AASHTO M320 correlated slightly better than the Stiffness (S).

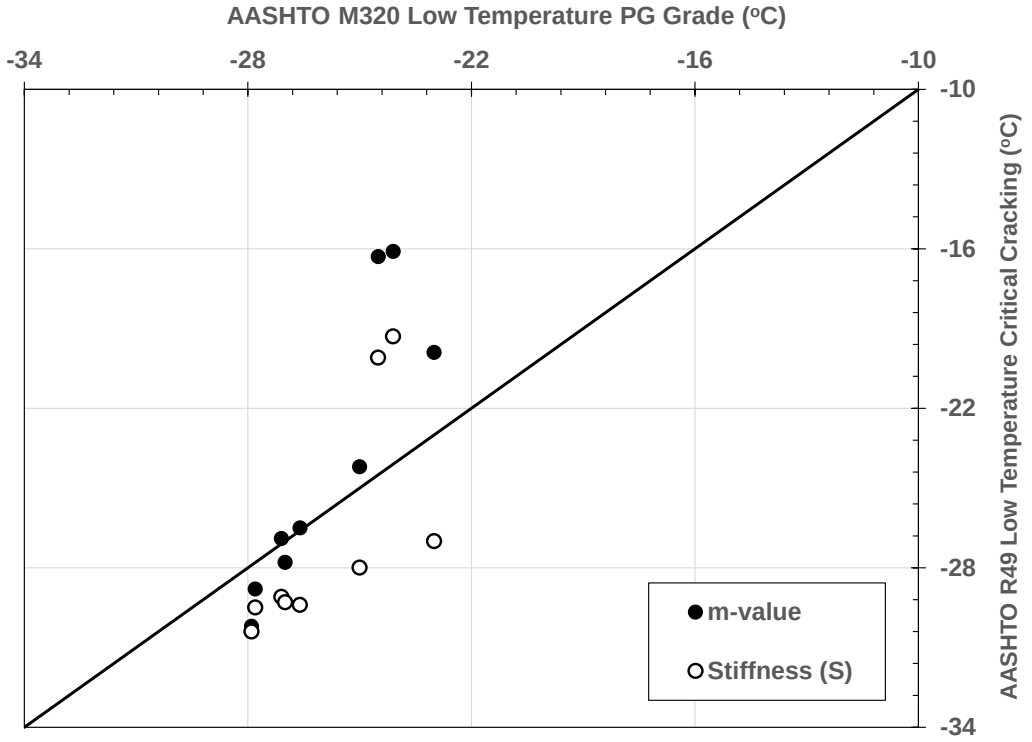

Figure 4.4 Low Temperature PG Grade Comparison – AASHTO R29 vs AASHTO R49

The analysis methodology described in AASHTO R49 allows for the determination of the low temperature critical cracking temperature at a multitude of cooling rate and starting temperature combinations, as long as there is enough test data to allow for the BBR thermal stress curve and DTT fracture stress curves to intersect. Results of the parametric low temperature critical cracking analysis is shown in Table 4.2 through Table 4.9. As the data in the tables suggests, the Cooling Rate is the more significant factor with respect to low temperature critical cracking temperatures. An increase (warmer) of a full low temperature PG grade results when changing from a 1°C/hr to 10°C/hr cooling rate. In fact, based on the parametric work, it was determined that the low temperature critical cracking temperature will get approximately 0.6°C warmer for every 1°C/hr increase in cooling rate.

Table 4.2 Cooling Rate vs Starting Temperature – NH5820-opt

NH5820-opt				
TCMODEL Critical Cracking Temperature (°C)				
Starting Temperature of cooling	Cooling Rate C/hr 1	Cooling Rate C/hr 2	Cooling Rate C/hr 5.6	Cooling Rate C/hr 10
10C	-27.1	-25.6	-23.4	-22.1
5C	-27.1	-25.7	-23.4	-22.1
0C	-27.1	-25.7	-23.4	-22.2
-5C	-27.2	-25.8	-23.6	-22.3

Table 4.3 Cooling Rate vs Starting Temperature – NH5840-opt

NH5840-opt				
TCMODEL Critical Cracking Temperature (°C)				
Starting Temperature of cooling	Cooling Rate C/hr 1	Cooling Rate C/hr 2	Cooling Rate C/hr 5.6	Cooling Rate C/hr 10
10C	-25.0	-23.3	-20.7	-19.2
5C	-25.0	-23.3	-20.7	-19.3
0C	-25.0	-23.4	-20.9	-19.5
-5C	-25.1	-23.5	-21.1	-19.8

Table 4.4 Cooling Rate vs Starting Temperature – NH6400-opt

NH6400-opt				
TCMODEL Critical Cracking Temperature (°C)				
Starting Temperature of cooling	Cooling Rate C/hr 1	Cooling Rate C/hr 2	Cooling Rate C/hr 5.6	Cooling Rate C/hr 10
10C	-27.8	-26.3	-23.9	-22.5
5C	-27.8	-26.3	-23.9	-22.5
0C	-27.9	-26.3	-23.9	-22.6
-5C	-27.9	-26.4	-24.0	-22.7

Table 4.5 Cooling Rate vs Starting Temperature – NH6400opt

NH6400opt				
TCMODEL Critical Cracking Temperature (°C)				
Starting Temperature of cooling	Cooling Rate C/hr 1	Cooling Rate C/hr 2	Cooling Rate C/hr 5.6	Cooling Rate C/hr 10
10C	-27.7	-26.2	-23.7	-22.3
5C	-27.7	-26.2	-23.8	-22.4
0C	-27.8	-26.2	-23.8	-22.4
-5C	-27.8	-26.3	-23.9	-22.6

Table 4.6 Cooling Rate vs Starting Temperature – NH6420-opt

NH6420-opt				
TCMODEL Critical Cracking Temperature (°C)				
Starting Temperature of cooling	Cooling Rate C/hr 1	Cooling Rate C/hr 2	Cooling Rate C/hr 5.6	Cooling Rate C/hr 10
10C	-26.9	-25.4	-23.1	-21.8
5C	-26.9	-25.4	-23.2	-21.9
0C	-27.0	-25.5	-23.2	-22.0
-5C	-27.0	-25.6	-23.4	-22.2

Table 4.7 Cooling Rate vs Starting Temperature – NH6420opt

NH6420opt				
TCMODEL Critical Cracking Temperature (°C)				
Starting Temperature of cooling	Cooling Rate C/hr 1	Cooling Rate C/hr 2	Cooling Rate C/hr 5.6	Cooling Rate C/hr 10
10C	-26.5	-25.0	-22.7	-21.3
5C	-26.5	-25.1	-22.7	-21.4
0C	-26.6	-25.1	-22.8	-21.5
-5C	-26.7	-25.3	-23.0	-21.8

Table 4.8 Cooling Rate vs Starting Temperature – NH6440-opt

NH6440-opt				
TCMODEL Critical Cracking Temperature (°C)				
Starting Temperature of cooling	Cooling Rate C/hr 1	Cooling Rate C/hr 2	Cooling Rate C/hr 5.6	Cooling Rate C/hr 10
10C	-22.8	-21.2	-18.8	-17.4
5C	-22.9	-21.3	-19.0	-17.6
0C	-23.0	-21.5	-19.2	-17.9
-5C	-23.3	-21.9	-19.7	-18.5

Table 4.9 Cooling Rate vs Starting Temperature – NH6440opt

NH6440opt				
TCMODEL Critical Cracking Temperature (°C)				
Starting Temperature of cooling	Cooling Rate C/hr 1	Cooling Rate C/hr 2	Cooling Rate C/hr 5.6	Cooling Rate C/hr 10
10C	-24.3	-21.8	-19.4	-18.1
5C	-24.4	-21.9	-19.5	-18.2
0C	-24.5	-22.0	-19.7	-18.3
-5C	-24.7	-22.3	-20.0	-18.7

4.1.3 *Rheological Analysis of Extracted Asphalt Binders*

4.1.3.1 G* Mastercurves

The impact of RAP content on the complex modulus master curves is shown in Figure 4.5 through Figure 4.7. The stiffness of the extracted and recovered binders increases with higher RAP contents. The increases are similar for both virgin binder grades and at optimum and optimum -0.5% asphalt contents. Figure 4.8 shows an increase in stiffness with a stiffer virgin binder grade for both RAP mixtures. Extracted binders from mixtures with lower asphalt content are stiffer than those at optimum asphalt content for virgin, 20%, and 40% mixtures shown in Figure 4.9 through Figure 4.11, respectively. However, the higher asphalt content did not impact the stiffness for the 40% RAP mixture in Figure 4.11.

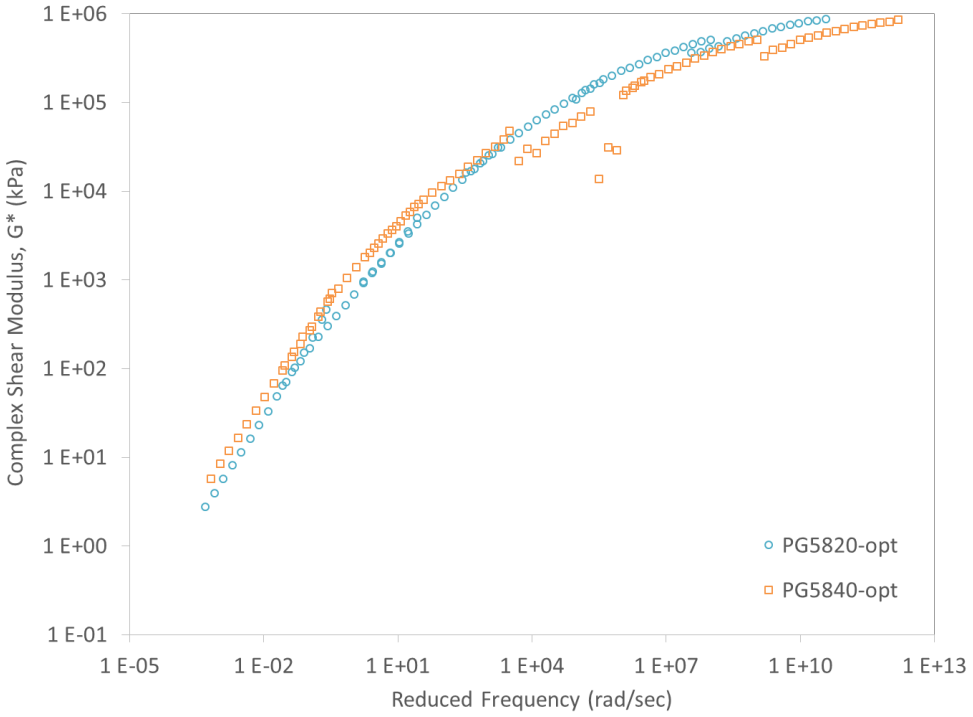

Figure 4.5 Complex Shear Modulus Mastercurves for Mixtures with PG 58-28 and Optimum-0.5% AC with Varying RAP Content

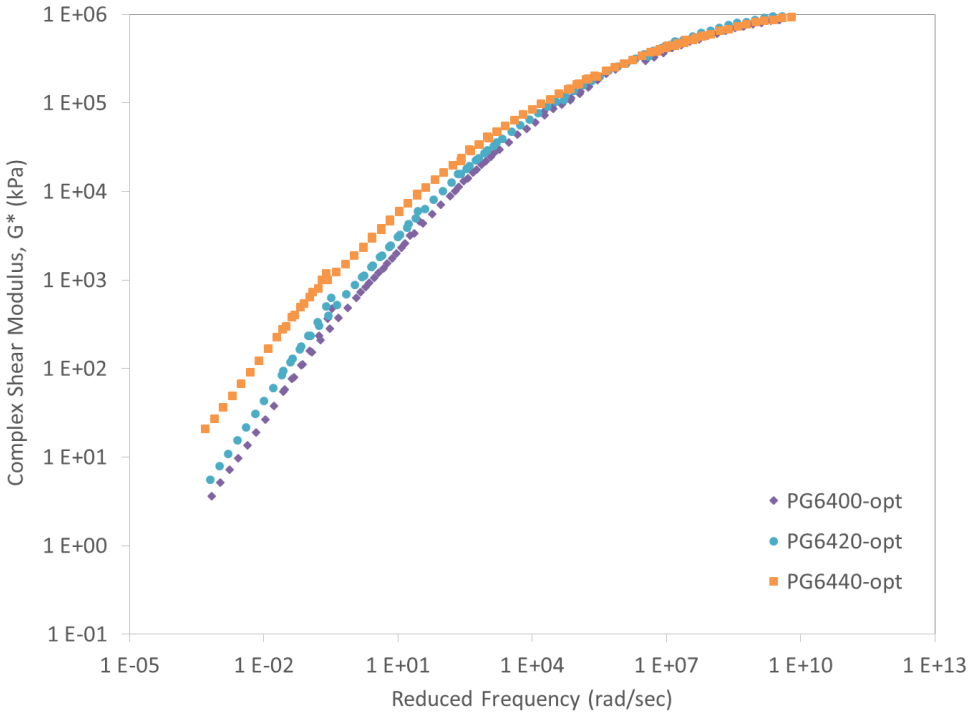

Figure 4.6 Complex Shear Modulus Mastercurves for Mixtures with PG 64-28 and Optimum-0.5% AC with Varying RAP Content

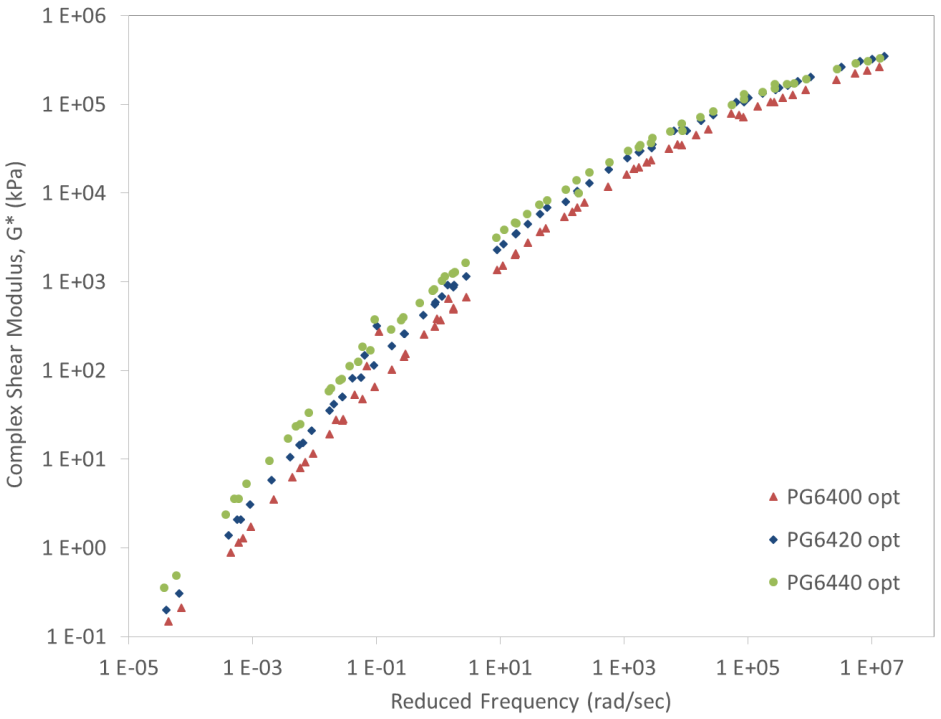

Figure 4.7 Complex Shear Modulus Mastercurves for Mixtures with PG 64-28 and Optimum AC with Varying RAP Content

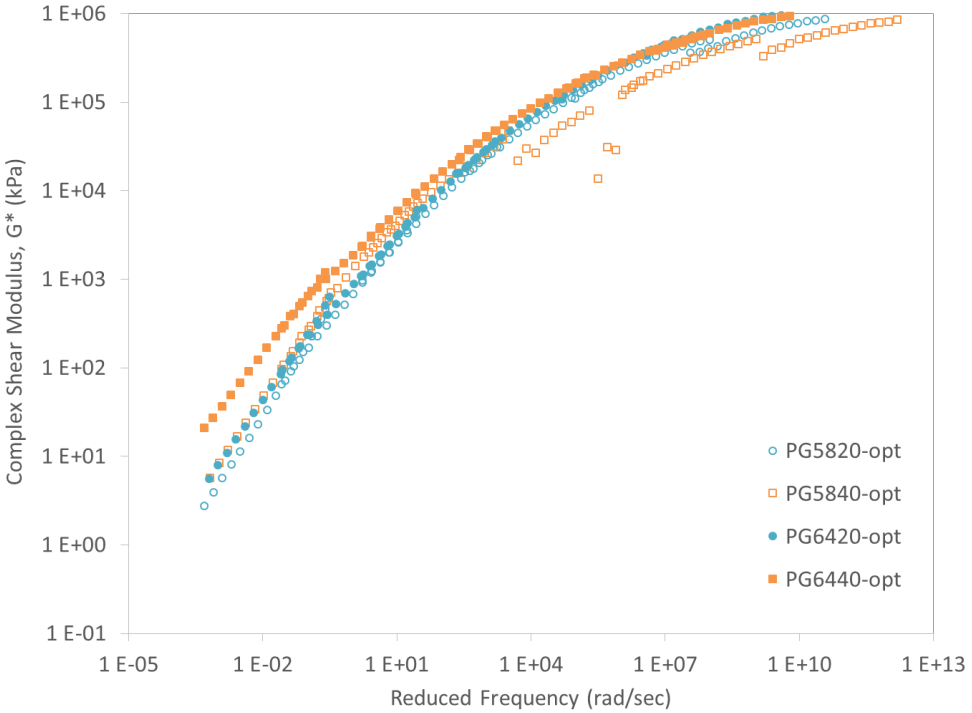

Figure 4.8 Complex Shear Modulus Mastercurves Showing Impact of Binder Grade for Mixtures Optimum -0.5% AC with Varying RAP Content

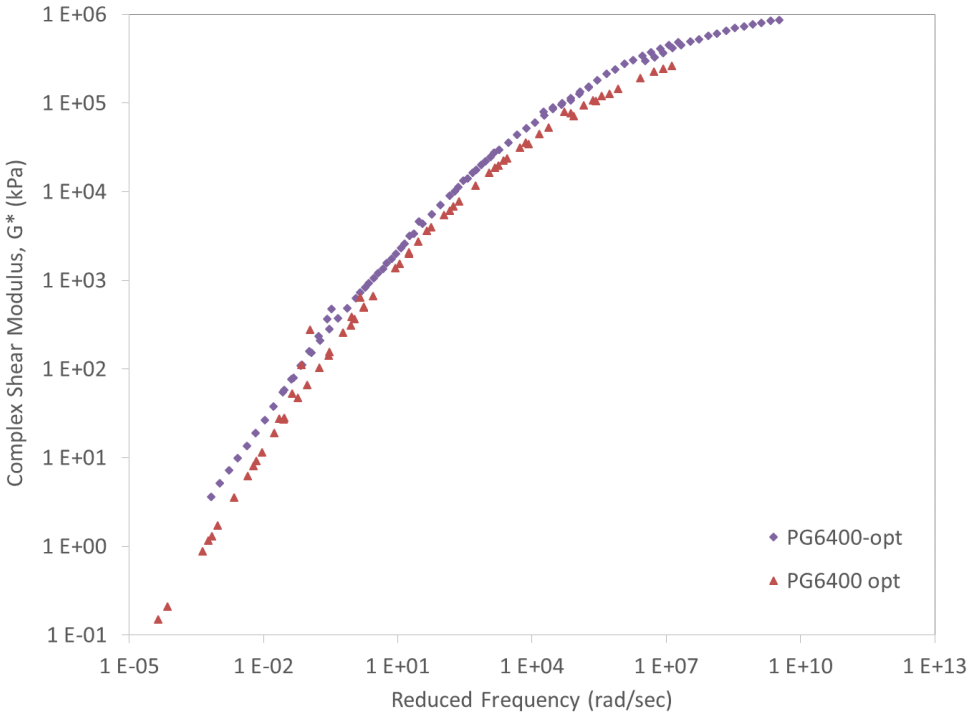

Figure 4.9 Complex Shear Modulus Mastercurves for PG 64-28 Virgin Mixture with Varying Asphalt Content

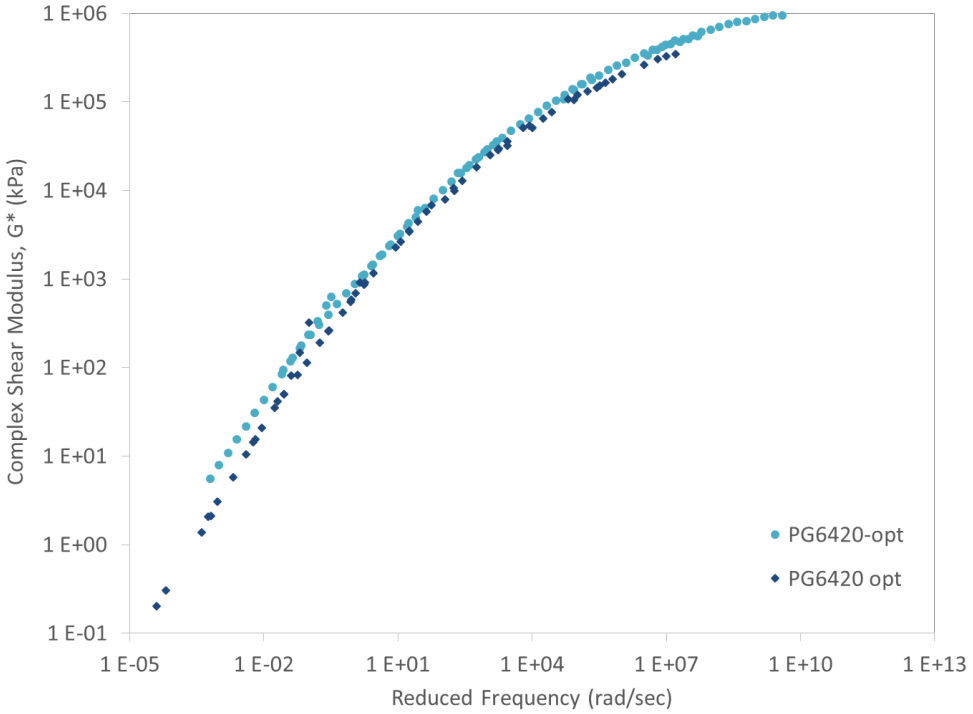

Figure 4.10 Complex Shear Modulus Mastercurves for PG 64-28 20% RAP Mixture with Varying Asphalt Content

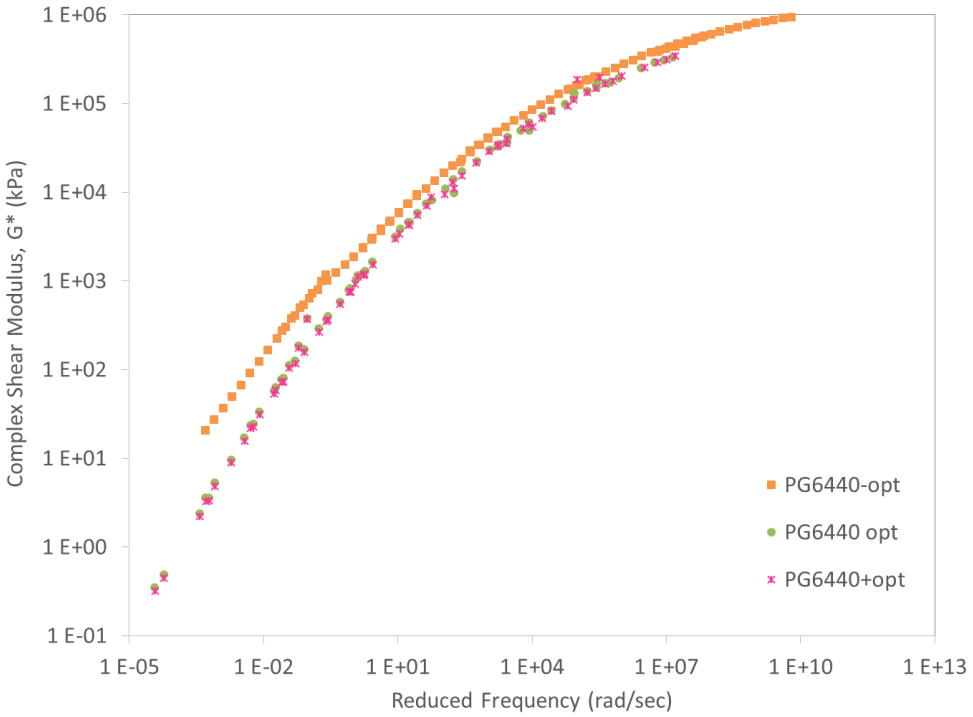

Figure 4.11 Complex Shear Modulus Mastercurves for PG 64-28 40% RAP Mixture with Varying Asphalt Content

4.1.3.2 Black Space Curves

Black Space curves of the extracted and recovered binders showing the impact of RAP content (Figure 4.12 through Figure 4.14), virgin asphalt binder grade (Figure 4.15) and asphalt content (Figure 4.16 through Figure 4.18) are shown below. In general, there are not any significant differences between the different binders, with the exception of the material from the PG 64-28 mixture with 40% RAP and low asphalt content that had lower phase angles than other materials.

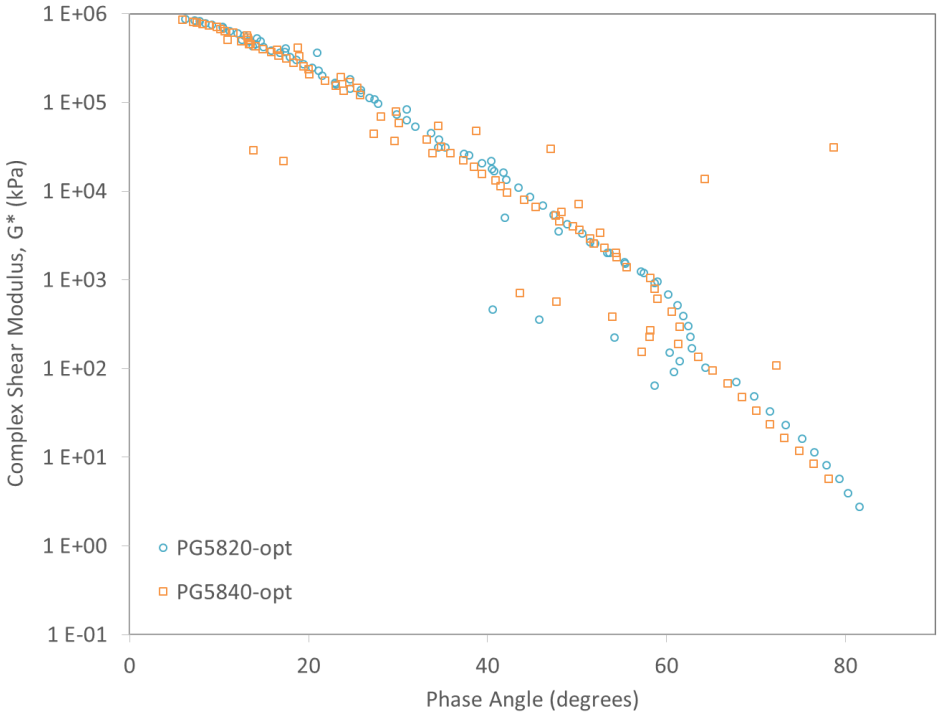

Figure 4.12 Black Space Curves for Mixtures with PG 58-28 and Optimum-0.5% AC with Varying RAP Content

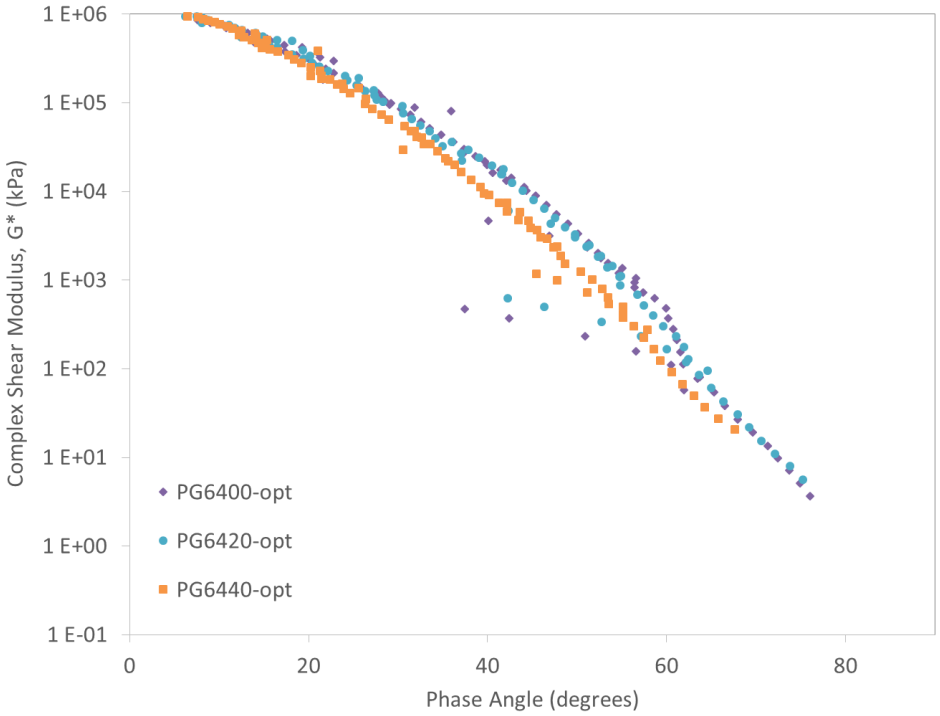

Figure 4.13 Black Space Curves for Mixtures with PG 64-28 and Optimum-0.5% AC with Varying RAP Content

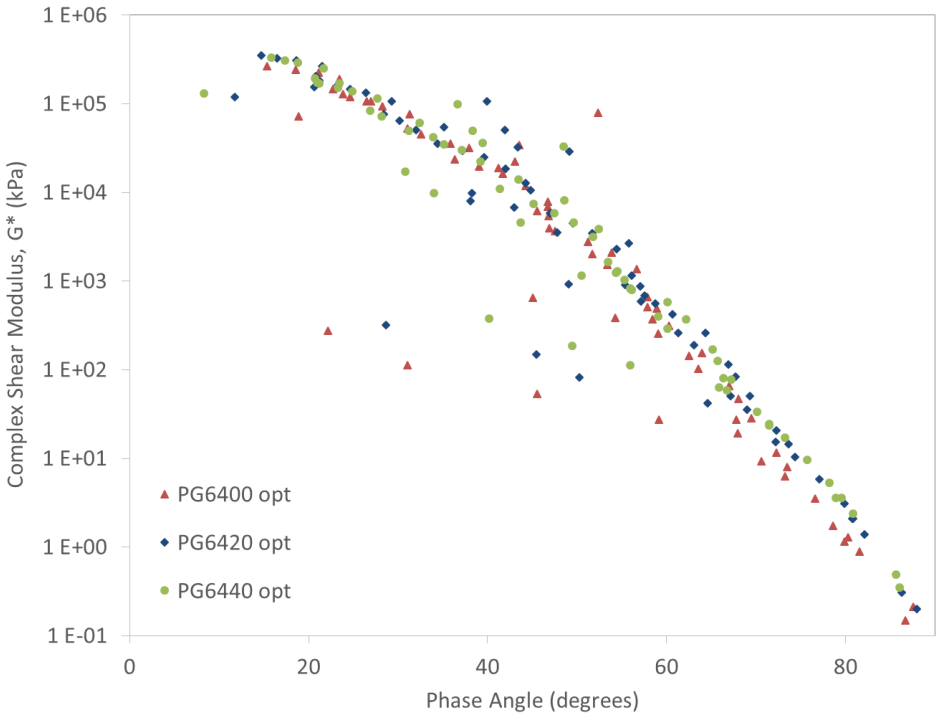

Figure 4.14 Black Space Curves for Mixtures with PG 64-28 and Optimum AC with Varying RAP Content

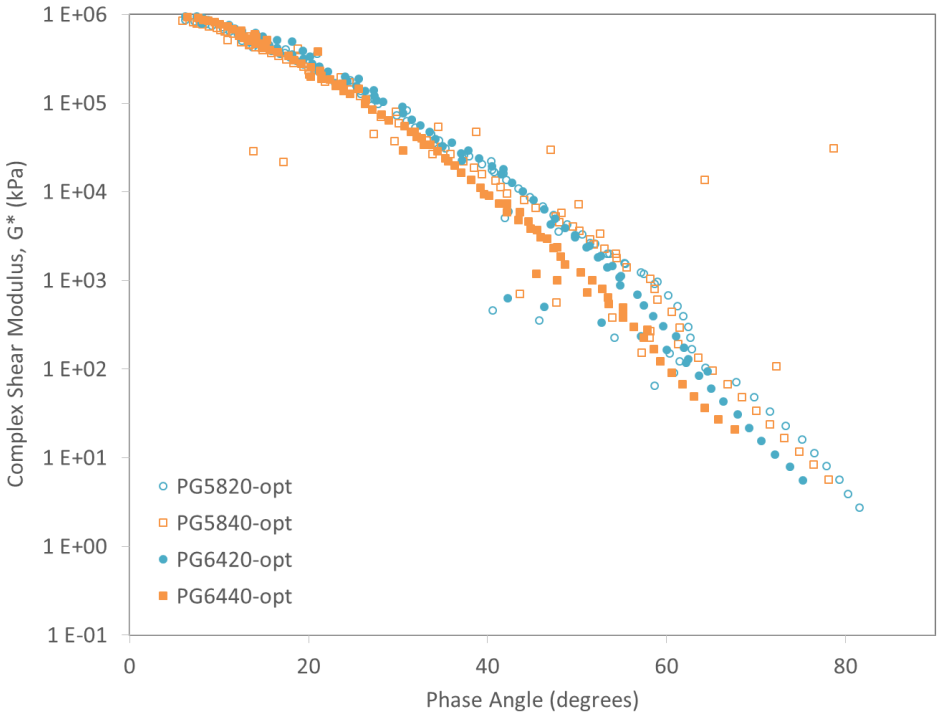

Figure 4.15 Black Space Curves Showing Impact of Binder Grade for Mixtures Optimum -0.5% AC with Varying RAP Content

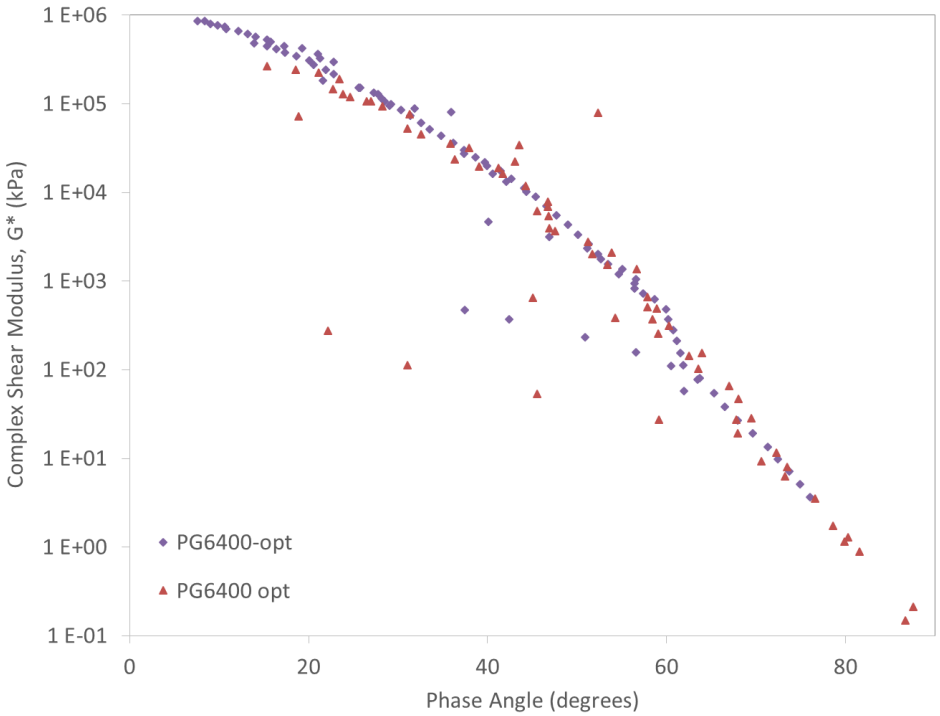

Figure 4.16 Black Space Curves for PG 64-28 Virgin RAP Mixture with Varying Asphalt Content

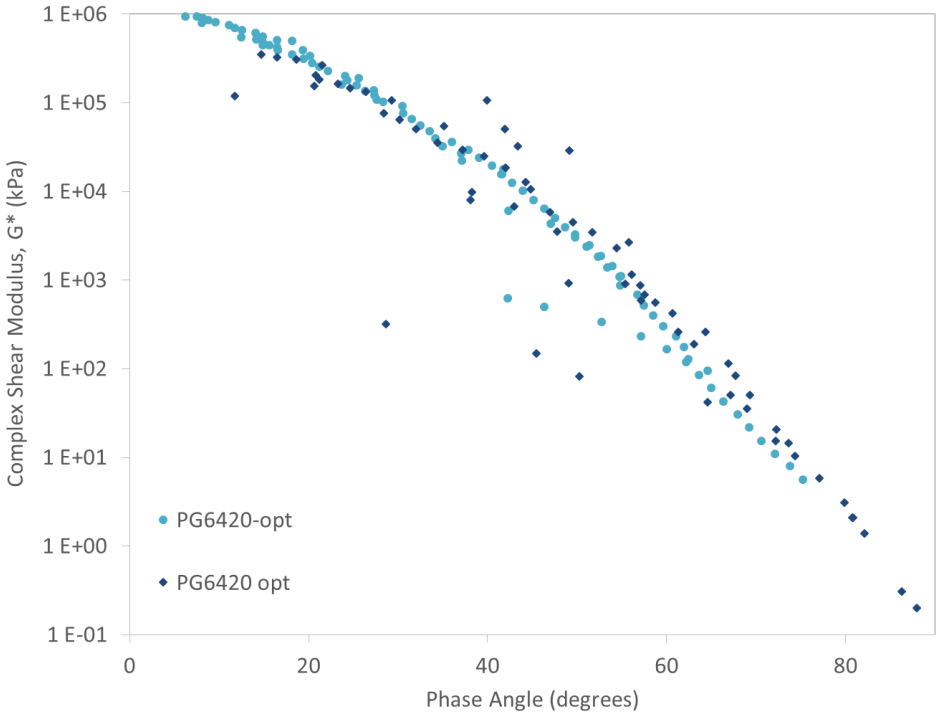

Figure 4.17 Black Space Curves for PG 64-28 20% RAP Mixture with Varying Asphalt Content

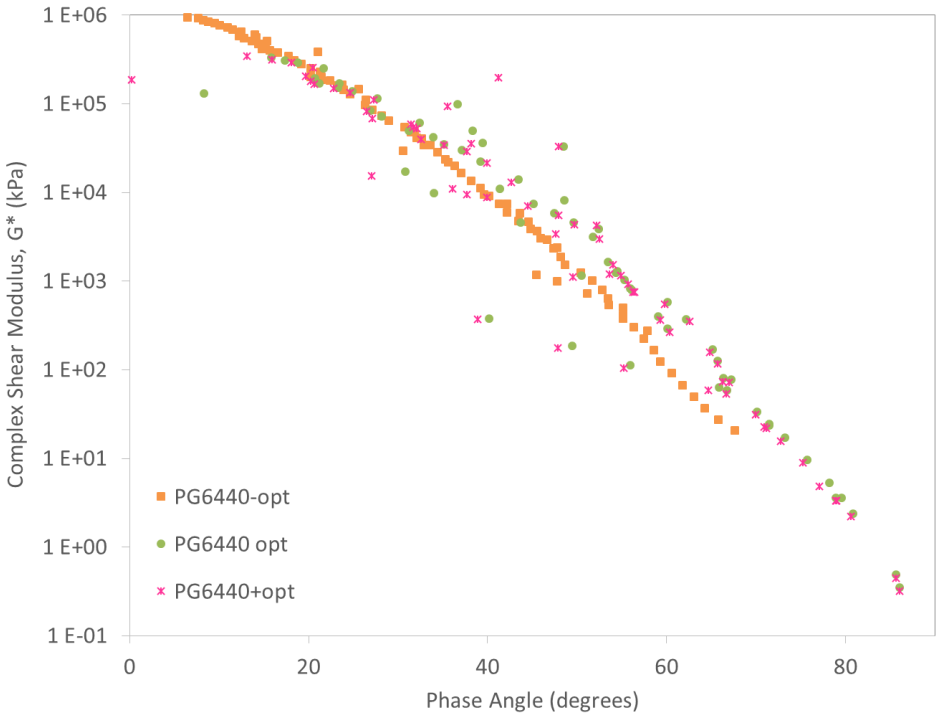

Figure 4.18 Black Space Curves for PG 64-28 40% RAP Mixture with Varying Asphalt Content

4.1.3.3 Glover-Rowe Parameter

Figure 4.19 and Figure 4.20 show the PG 58-28 and PG 64-28 asphalt binders, respectively, plotted in Black Space using the methodology proposed by Rowe (2011). As both figures indicate, as the RAP content increases and asphalt content decreases, the extracted/recovered asphalt binders move towards, and sometimes past, the recommended cracking thresholds.

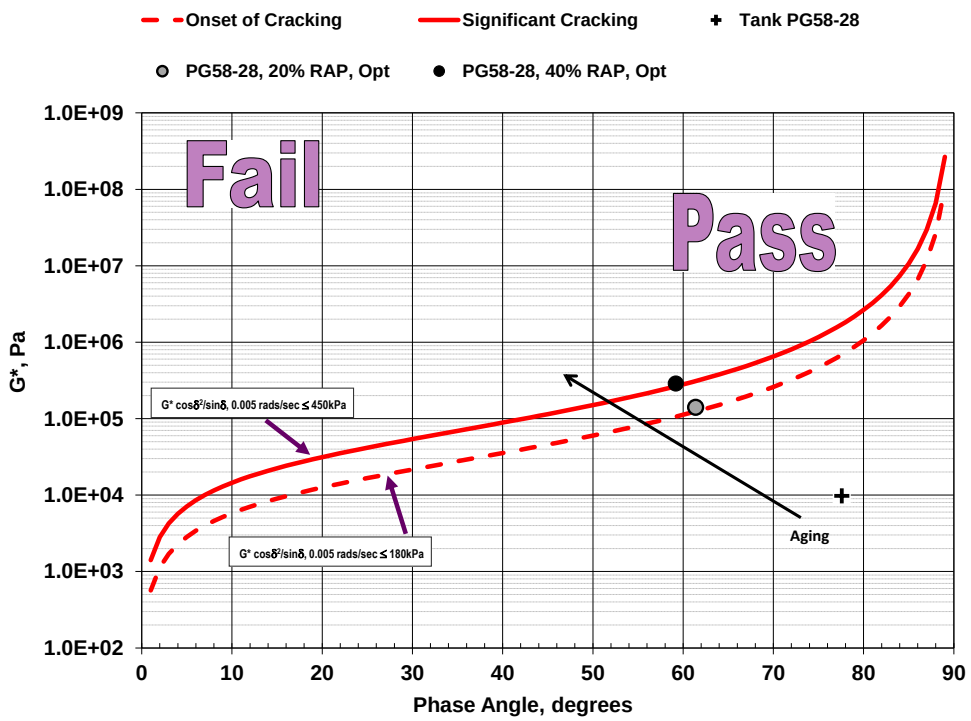

Figure 4.19 PG58-28 Asphalt Binders Plotted in Black Space

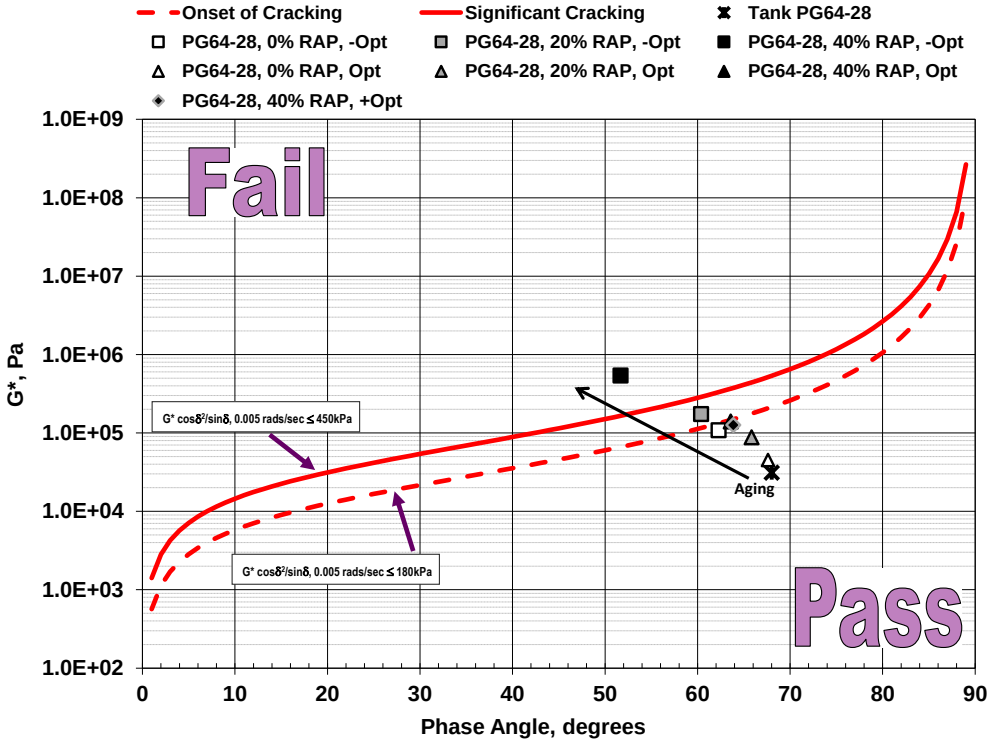

Figure 4.20 PG64-28 Asphalt Mixtures Plotted in Black Space

The Glover-Rowe parameter, calculated using equation 2-1, is shown independently in Figure 4.21. The test results show that the recovered asphalt binder most susceptible to fatigue cracking is the NH6440-opt asphalt binder. Meanwhile, the recovered binder least likely to result in fatigue cracking is the NH6400opt.

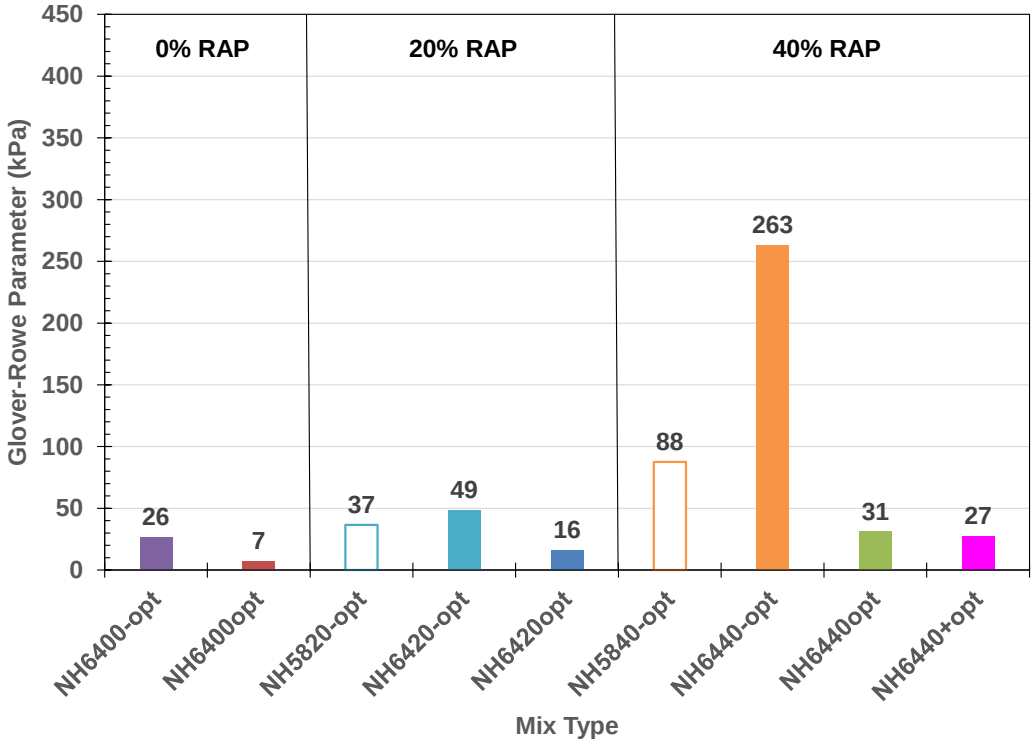

Figure 4.21 Calculated Glover-Rowe Parameter for Extracted/Recovered Asphalt Binders

The results from the Glover-Rowe parameter were compared with the fatigue cracking results from the Overlay Tester. The test results are shown in Figure 4.22. The results from the Glover-Rowe asphalt binder analysis compare well to the Overlay Tester mixture fatigue cracking test results.

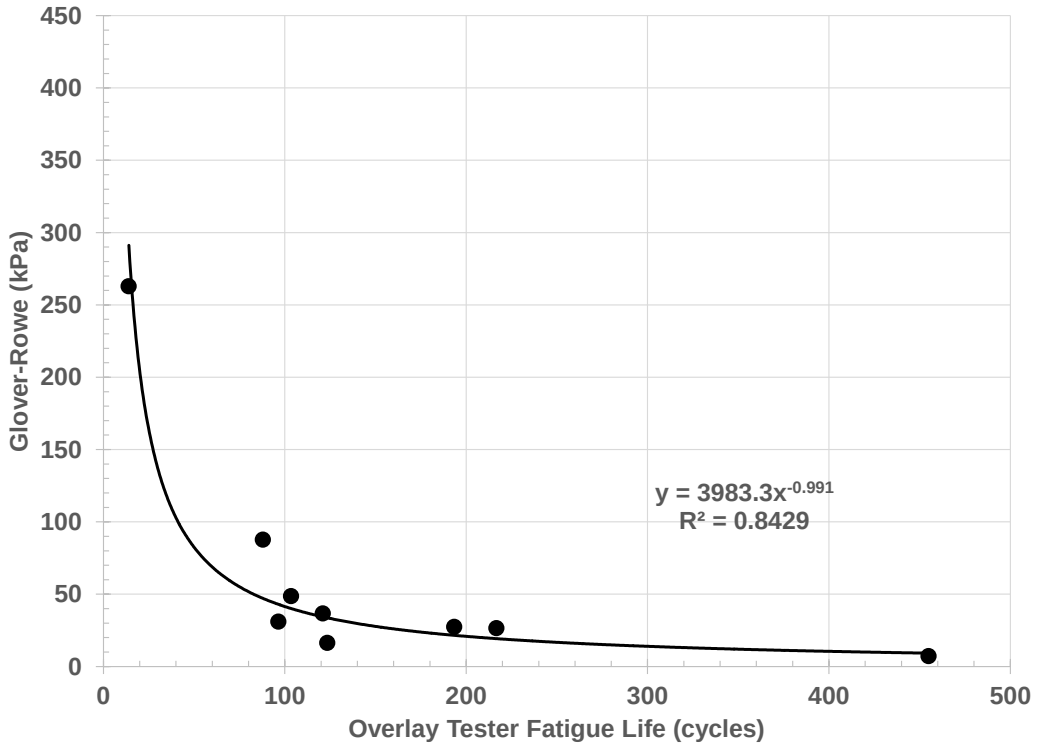

Figure 4.22 Comparison between Glover-Rowe Parameter (Recovered Binder) and Overlay Tester Fatigue Cracking (Asphalt Mixtures)

4.3.1.2 – Cross-over Frequency and R-Value

Figure 4.23 and Figure 4.24 show the extracted and recovered binders plotted in Cross-over Frequency – R-value Space. As the RAP content increases, the data shifts from the upper left quadrant of the space to the lower right quadrant of the space. This indicates that the Cross-over Frequency – R-value Space is sensitive to the RAP content in the asphalt mixtures.

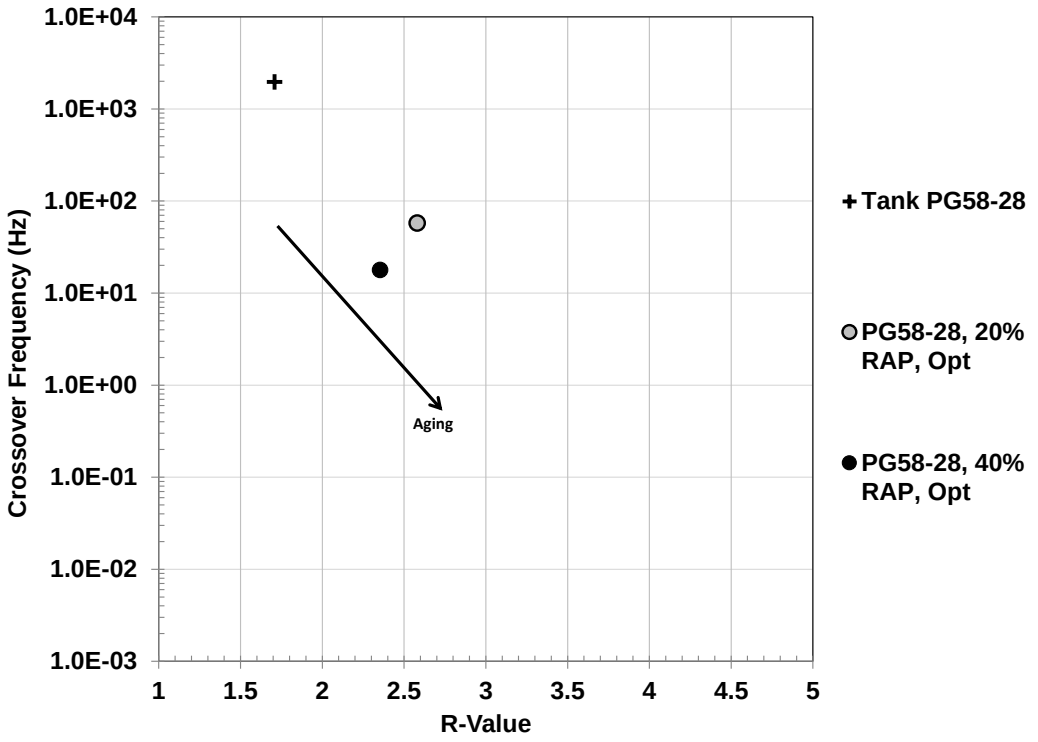

Figure 4.23 Cross-over Frequency – R-value Space for PG58-28 Asphalt Mixtures

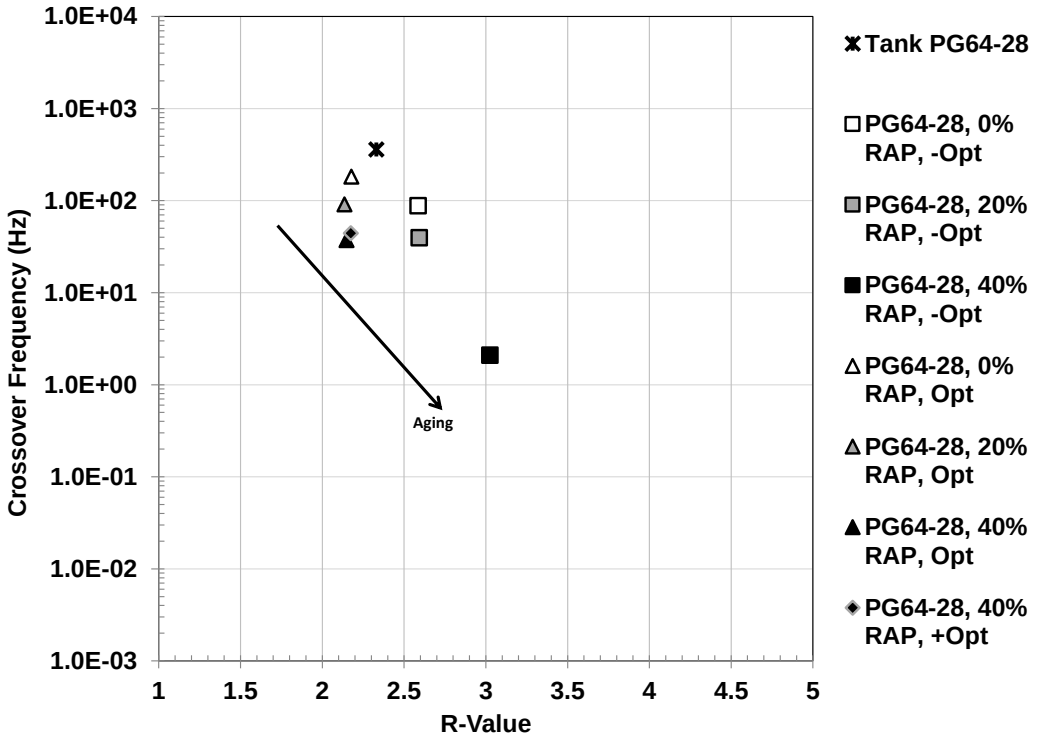

Figure 4.24 Cross-over Frequency – R-value Space for PG64-28 Asphalt Mixtures

Similar to the mixture comparisons with the Glover-Rowe Parameter, the measured Cross-over Frequency of the recovered asphalt binders were compared with the Overlay Tester fatigue cracking of the asphalt mixtures. Figure 4.25 shows that the Cross-over Frequency of the recovered asphalt binder compares well to the mixture fatigue cracking results from the Overlay Tester.

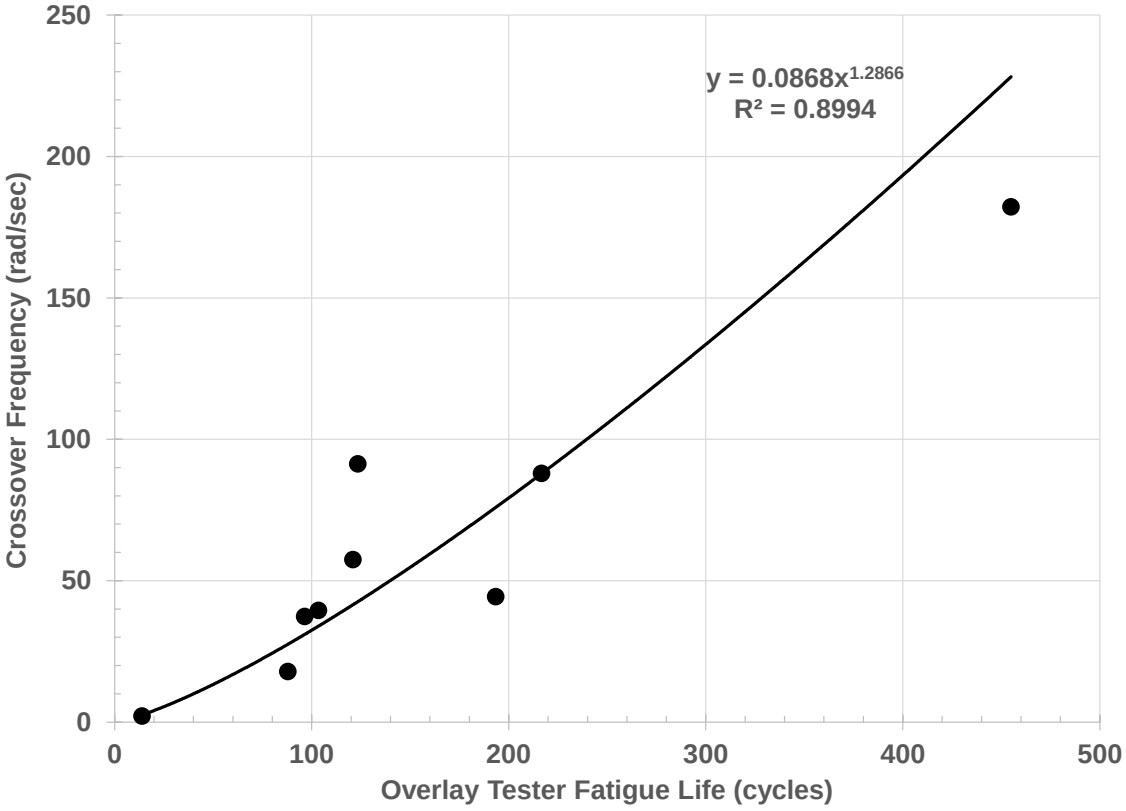

Figure 4.25 Cross-over Frequency (Asphalt Binder) Compared to Overlay Tester Fatigue Cracking (Asphalt Mixtures)

4.1.4 *Multiple Stress Creep Recovery*

The results from the MSCR testing are shown in Table 4.10. The J_{nr} values meet the criteria for either Heavy (J_{nr} < 2.0 1/kPa) or Very Heavy (J_{nr} < 1.0 1/kPa) traffic at the virgin performance grade temperature. This indicates that they should all perform satisfactorily under expected traffic.

Table 4.10 MSCR Test Results

Sample Name	AC% Condition	RAP Content (%)	Multiple Stress Creep Recovery					
			58C		64C		70C	
			J_{nr} (1/kPa)	% Rec	J_{nr} (1/kPa)	% Rec	J_{nr} (1/kPa)	% Rec
NH5820-opt	-Opt	20%	0.81	6.3%	2.17	1.6%	5.29	0.2%
NH5840-opt		40%	0.34	15.4%	0.97	5.8%	2.56	1.4%
NH6400-opt	-Opt	0%	0.48	17.1%	1.33	6.4%	3.31	1.9%
NH6420-opt		20%	0.31	22.4%	0.85	10.2%	2.26	3.0%
NH6440-opt		40%	0.06	45.6%	0.19	31.2%	0.54	16.1%
NH6400opt	Opt	0%	0.61	15.2%	1.56	5.9%	3.97	1.4%
NH6420opt		20%	0.46	14.2%	1.30	4.8%	3.35	1.4%
NH6440opt		40%	0.22	22.3%	0.65	10.5%	1.79	3.2%
NH6440+opt	+Opt	40%	0.23	22.5%	0.67	10.7%	1.82	3.4%

4.2 Mixture Testing

4.2.1 *Dynamic Modulus*

Figure 4.26 through Figure 4.28 show the dynamic modulus test results for the NH6400-opt, NH6420-opt, and NH6440-opt mixtures with 0%, 20%, 40% RAP, respectively. All the mixtures contain 0.5% below the optimum binder content and have the base binder of PG 64-28. As these graphs show, the replicate results collapse well with each other in all cases. Figure 4.29 shows the effect of RAP content on the stiffness of the mix at 0.5% below the optimum binder content. As this graph suggests, incorporating RAP in the mixture increased the stiffness of the mixture and, as the RAP percentage increased, the stiffness increased, too. This increase is more pronounced when the RAP percentage increased from 20 to 40 percent.

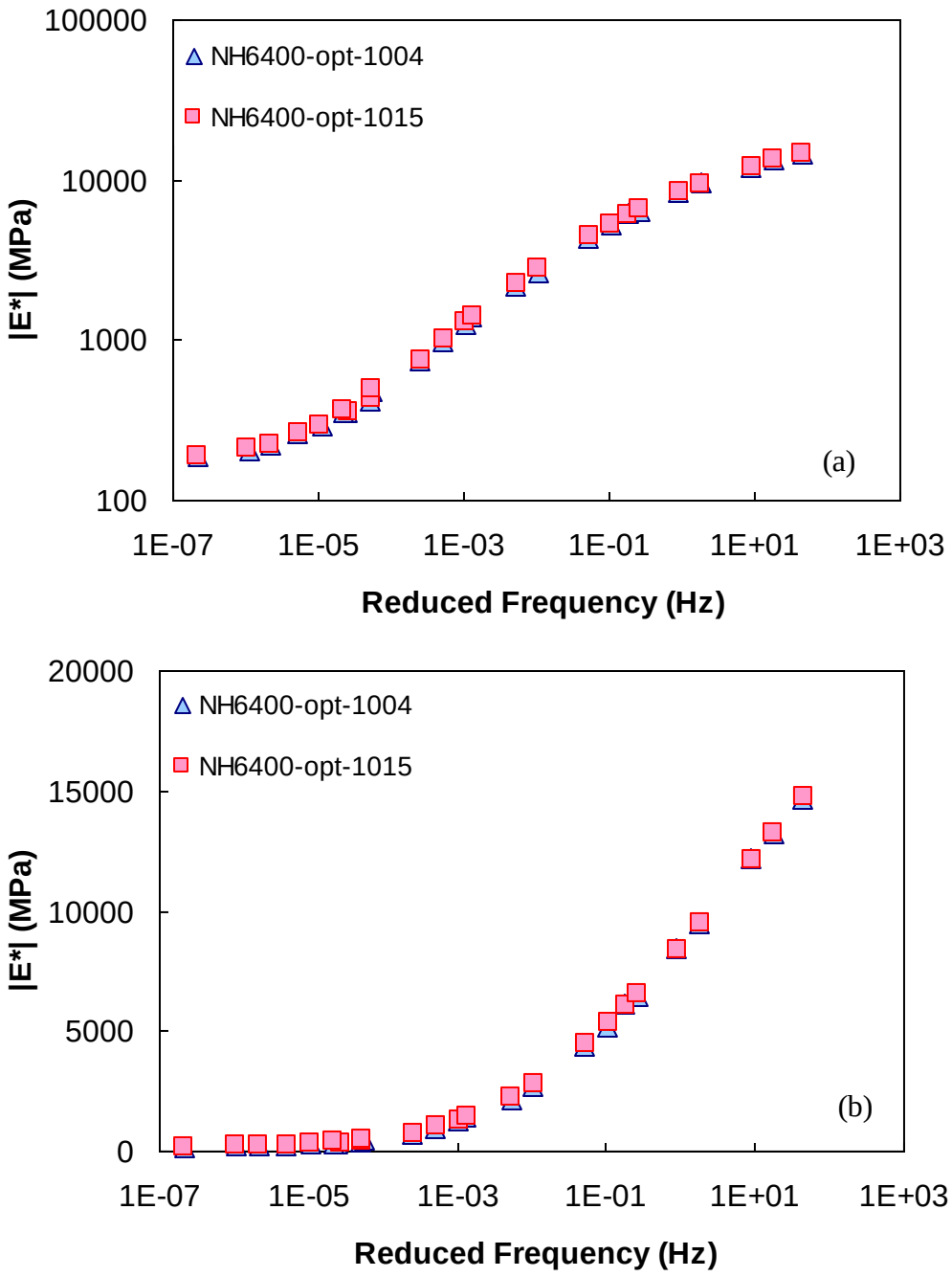

Figure 4.26 Dynamic modulus test results for NH6400-opt mixture in (a) logarithmic scale and (b) semi-logarithmic scale

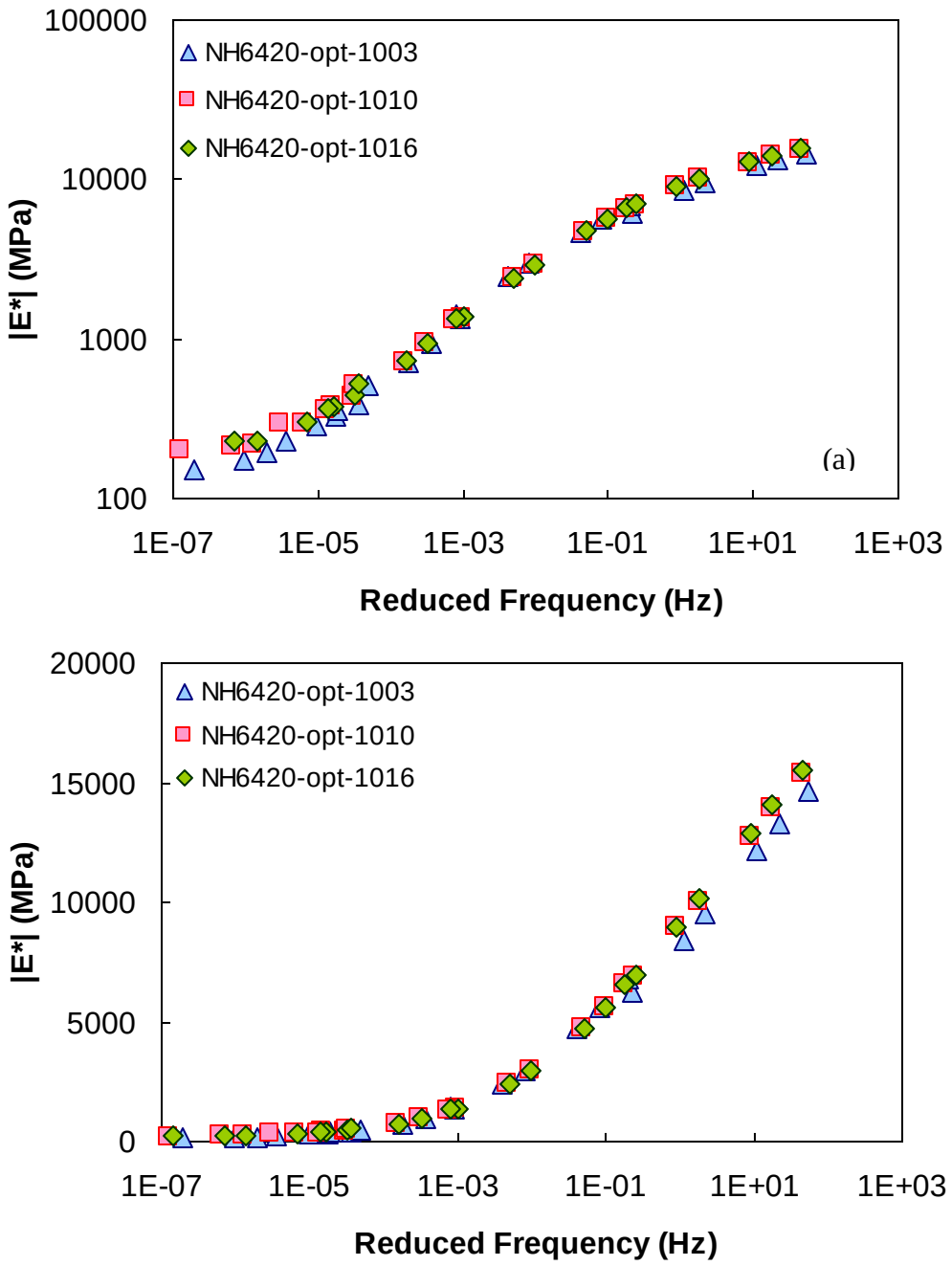

Figure 4.27 Dynamic modulus test results for NH6420-opt mixture in (a) logarithmic scale and (b) semi-logarithmic scale

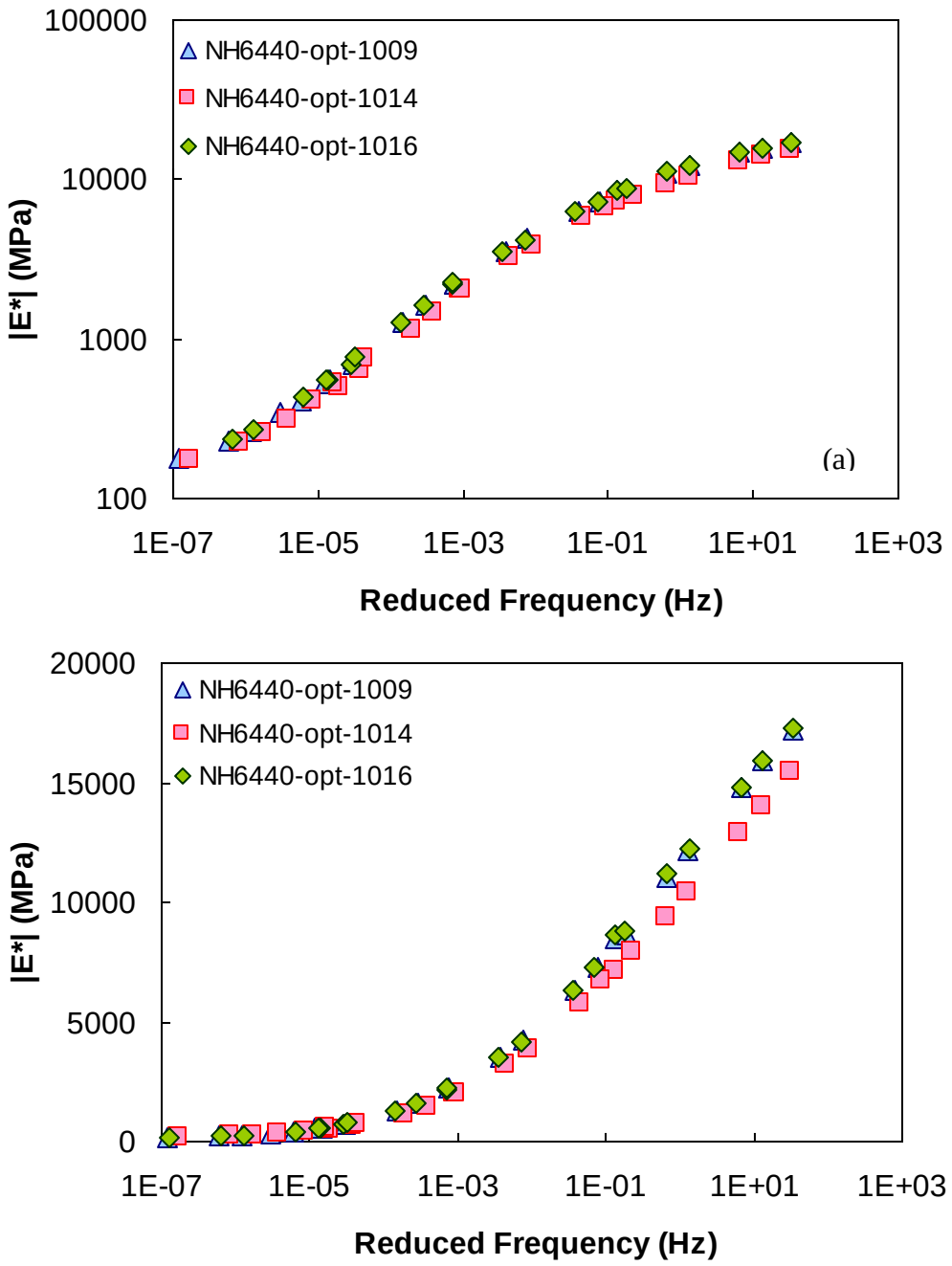

Figure 4.28 Dynamic modulus test results for NH6440-opt mixture in (a) logarithmic scale and (b) semi-logarithmic scale

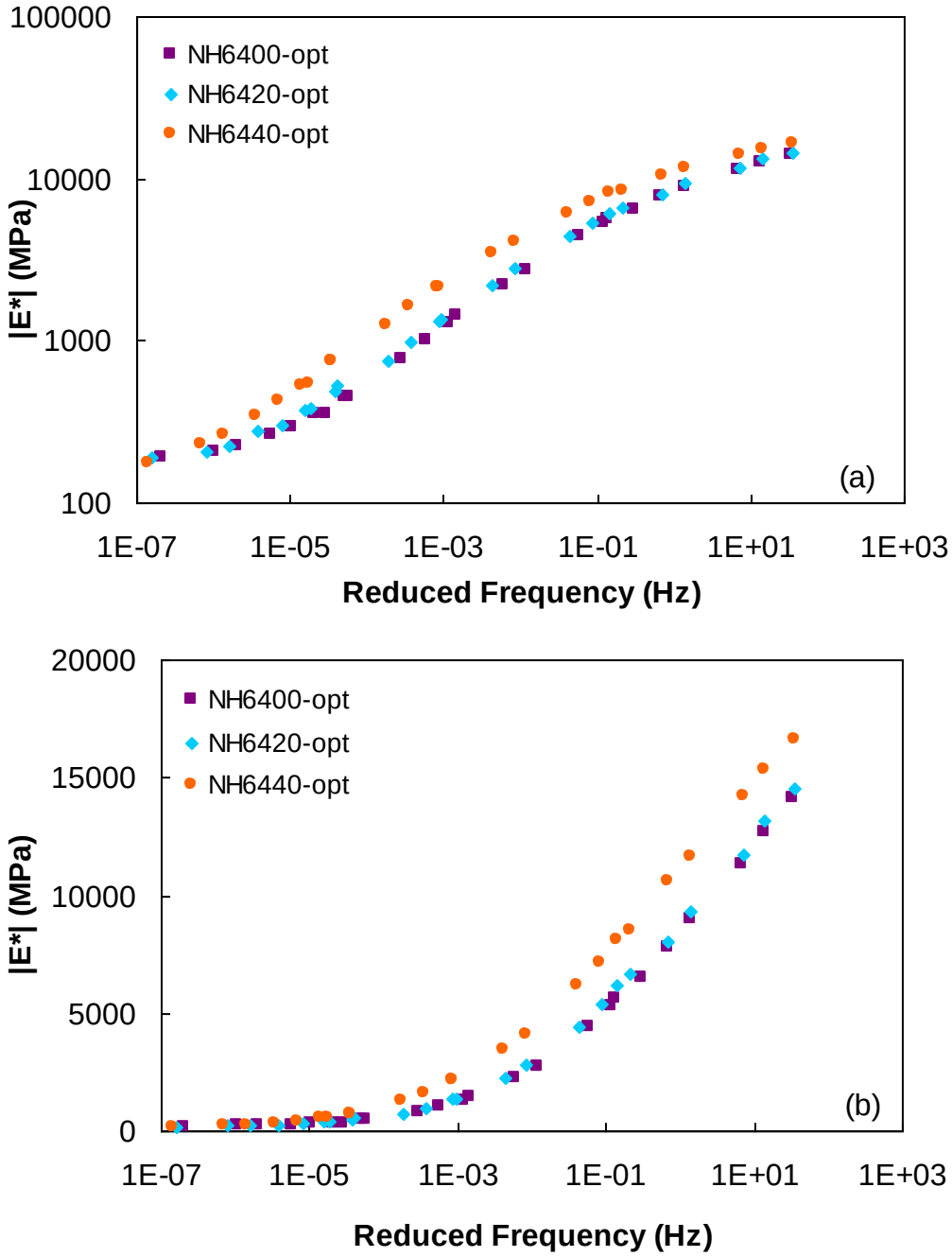

Figure 4.29 Effect of RAP% on dynamic modulus test results for PG 64-28 mixture with AC of 0.5% below the optimum in (a) logarithmic scale and (b) semi-logarithmic scale

Figure 4.30 through Figure 4.32 show the dynamic modulus test results for the NH6400opt, NH6420opt, and NH6440opt mixtures with 0%, 20%, 40% RAP, respectively. All the mixtures contain the optimum binder content and have the base binder of PG 64-28. As these graphs show, the replicate results collapse well with each other in all cases. Figure 4.29 shows the effect of RAP content on the stiffness of the mix at the optimum asphalt content. As this graph suggests, incorporating RAP in the mixture increased the stiffness

of the mixture and, as the RAP percentage increased, the stiffness increased, too. This increase is more pronounced when the RAP percentage increased from 20% to 40 percent.

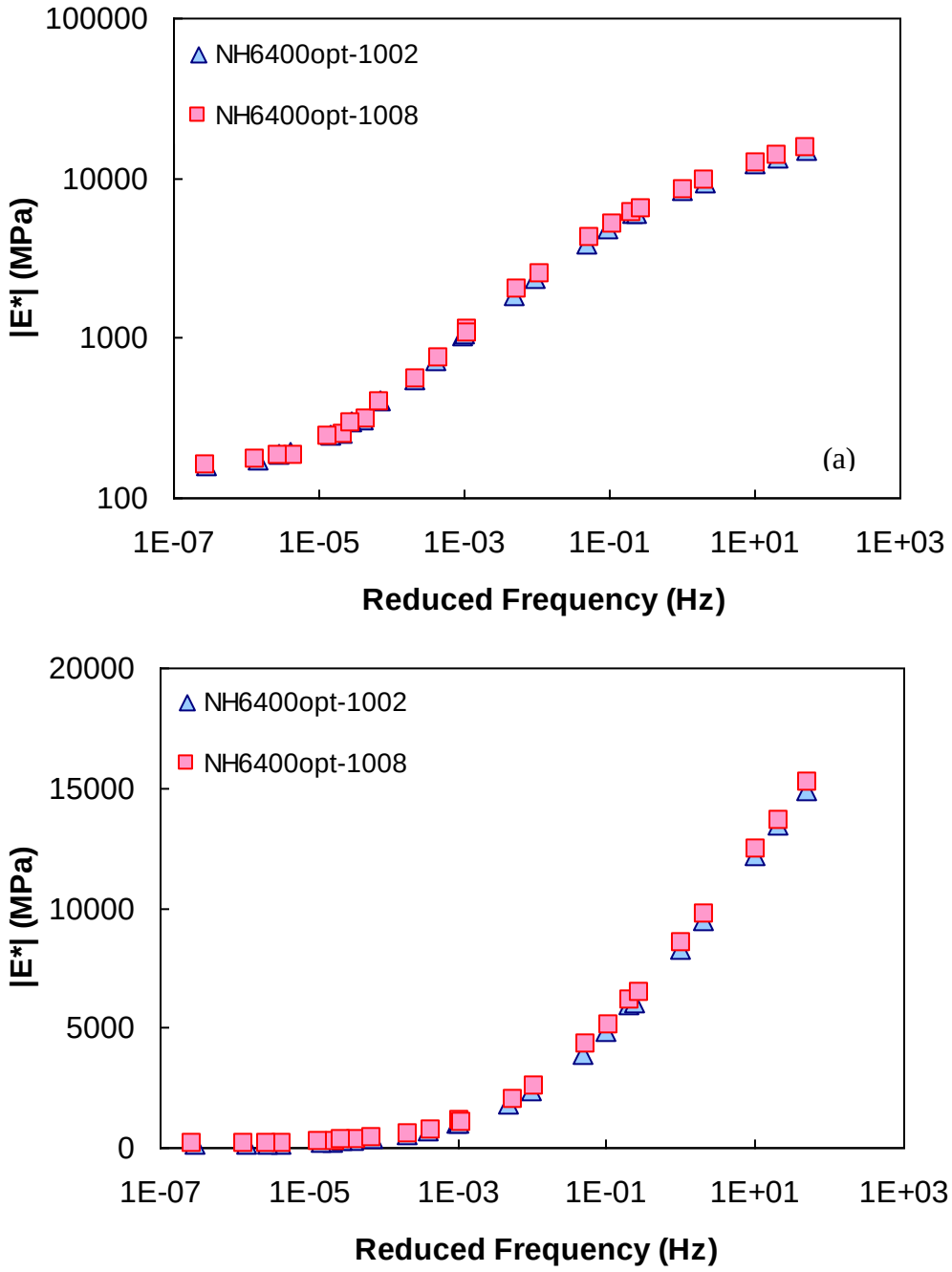

Figure 4.30 Dynamic modulus test results for NH6400opt mixture in (a) logarithmic scale and (b) semi-logarithmic scale

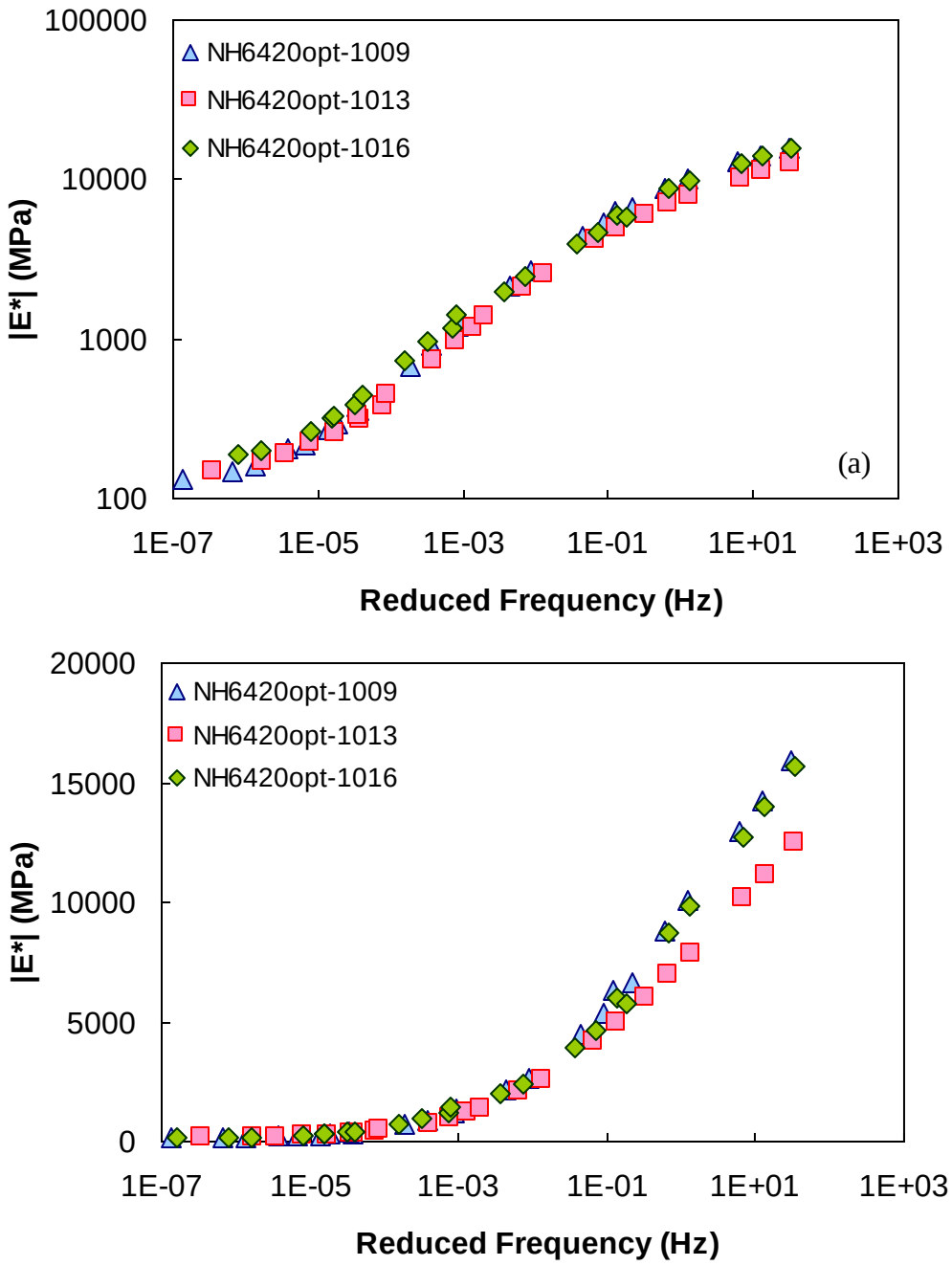

Figure 4.31 Dynamic modulus test results for NH6420opt mixture in (a) logarithmic scale and (b) semi-logarithmic scale

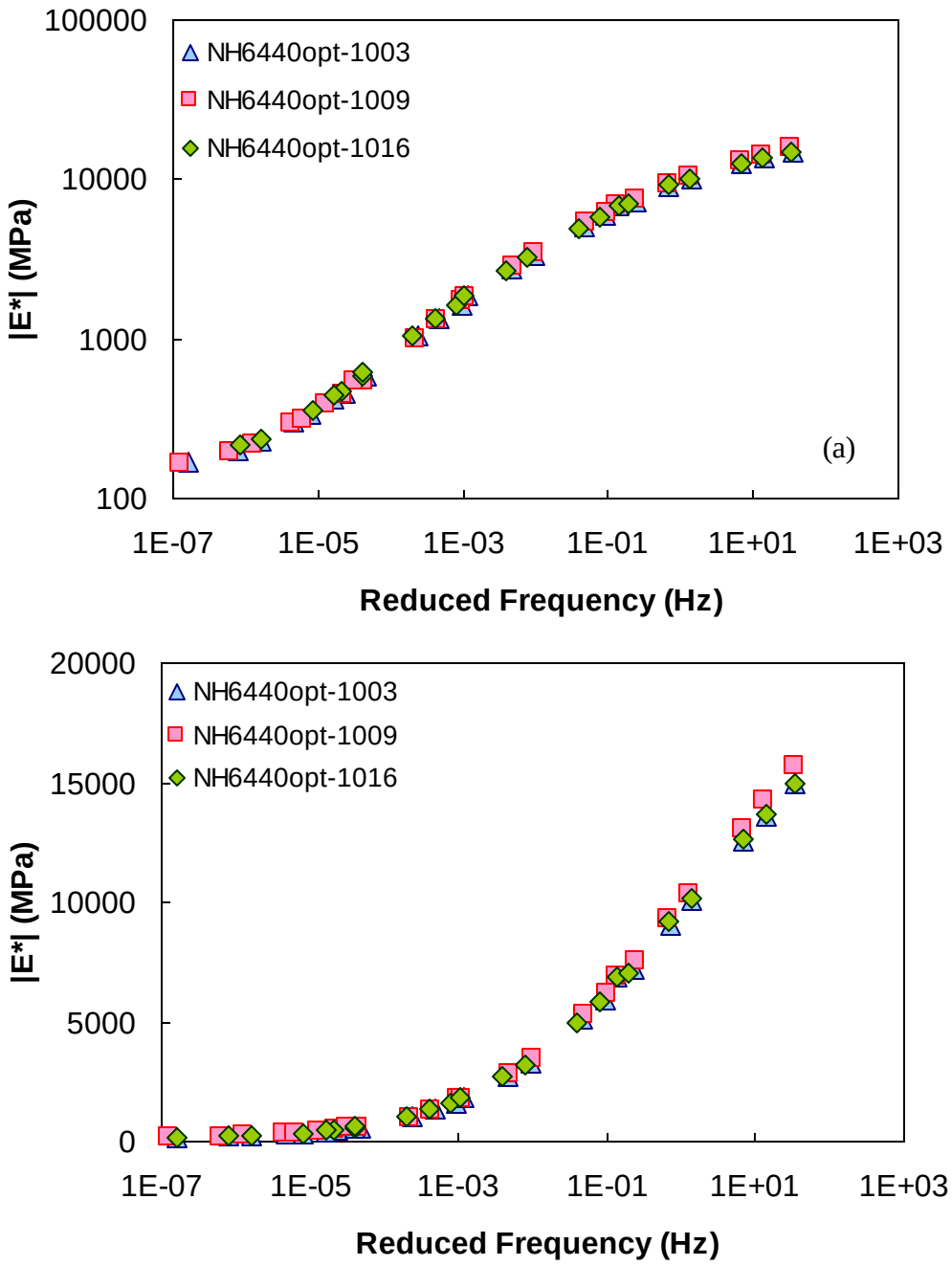

Figure 4.32 Dynamic modulus test results for NH6440opt mixture in (a) logarithmic scale and (b) semi-logarithmic scale

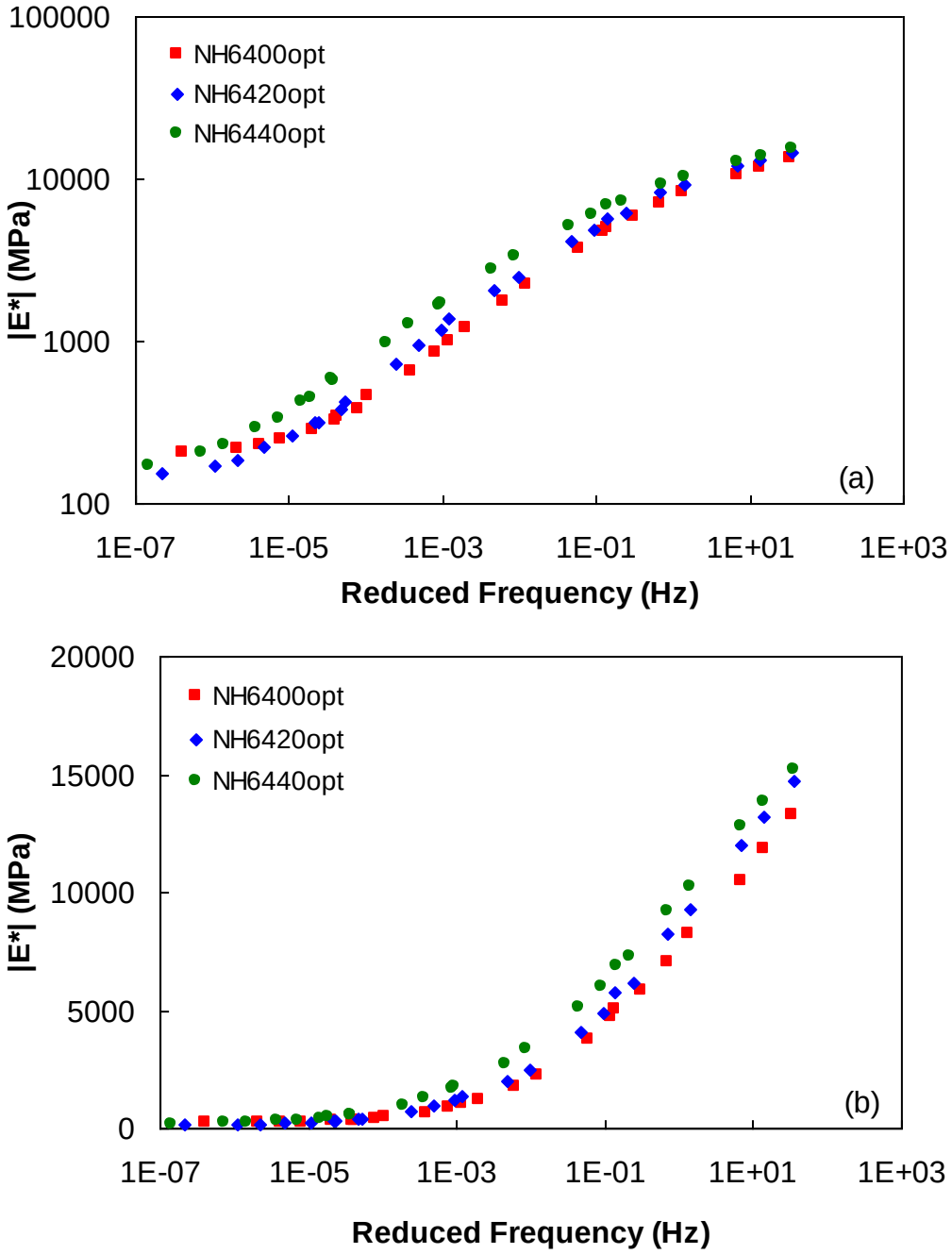

Figure 4.33 Effect of RAP% on dynamic modulus test results for PG 64-28 mixture with with optimum AC in (a) logarithmic scale and (b) semi-logarithmic scale

Figure 4.34 and Figure 4.35 show the dynamic modulus test results for the NH5820-opt and NH5840-opt mixtures with 20% and 40% RAP, respectively. Both mixtures contain 0.5% lower binder content than the optimum binder content and have a base binder of PG 58-28. As these graphs show, the replicate results collapse well with each other in all cases. Figure 4.36 shows the effect of RAP% on dynamic modulus test results for PG 58-28 mixture with AC of 0.5% below the optimum. As this graph shows, as the RAP percentage

increases from 20% in the NH5820-opt mixture to 40% in the NH5840-opt mixture, the stiffness increases too. In other words, it seems that incorporating RAP in the PG 58-28 mixtures affects the mixture properties in terms of dynamic modulus testing also.

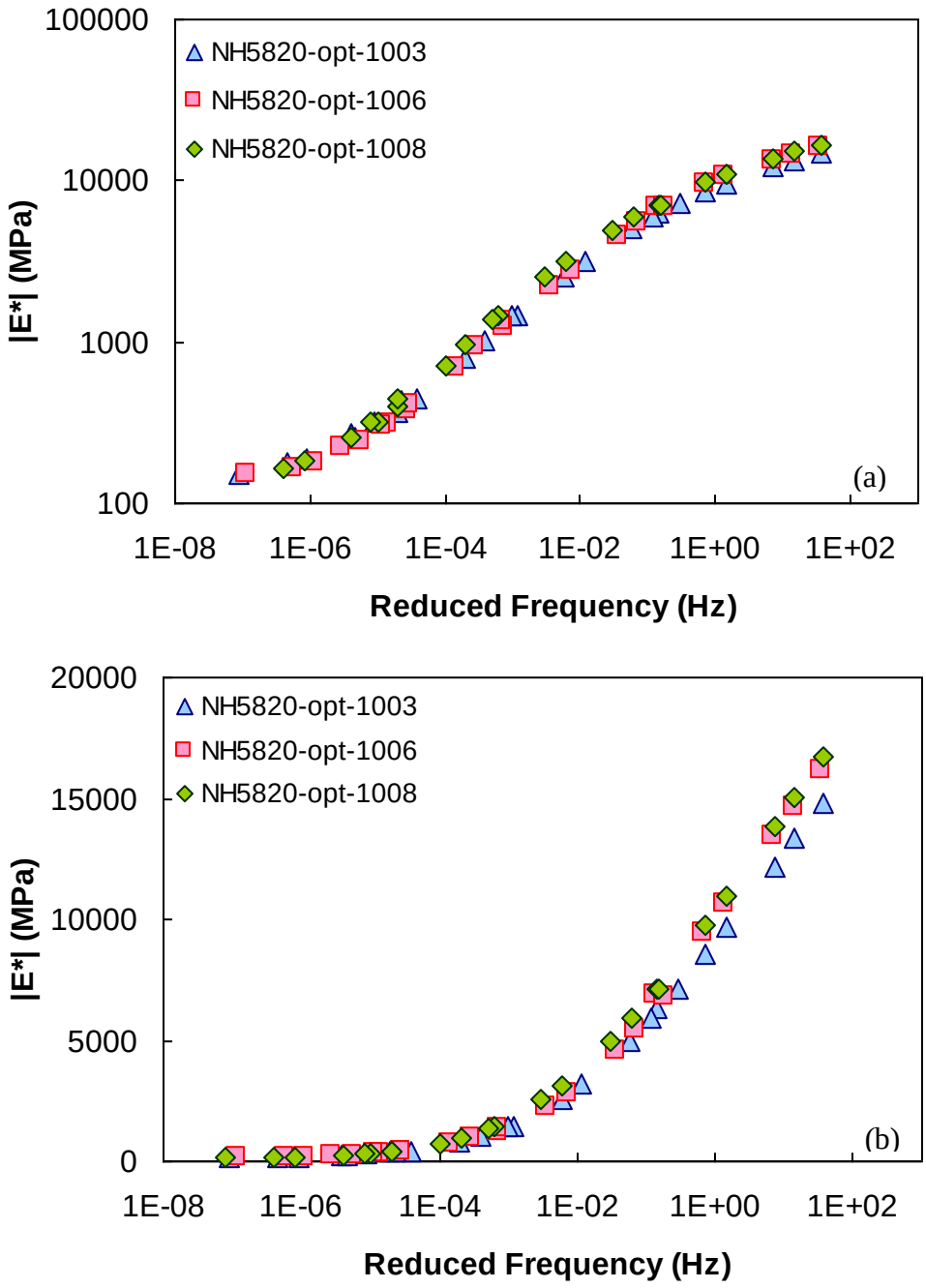

Figure 4.34 Dynamic modulus test results for NH5820-opt mixture in (a) logarithmic scale and (b) semi-logarithmic scale

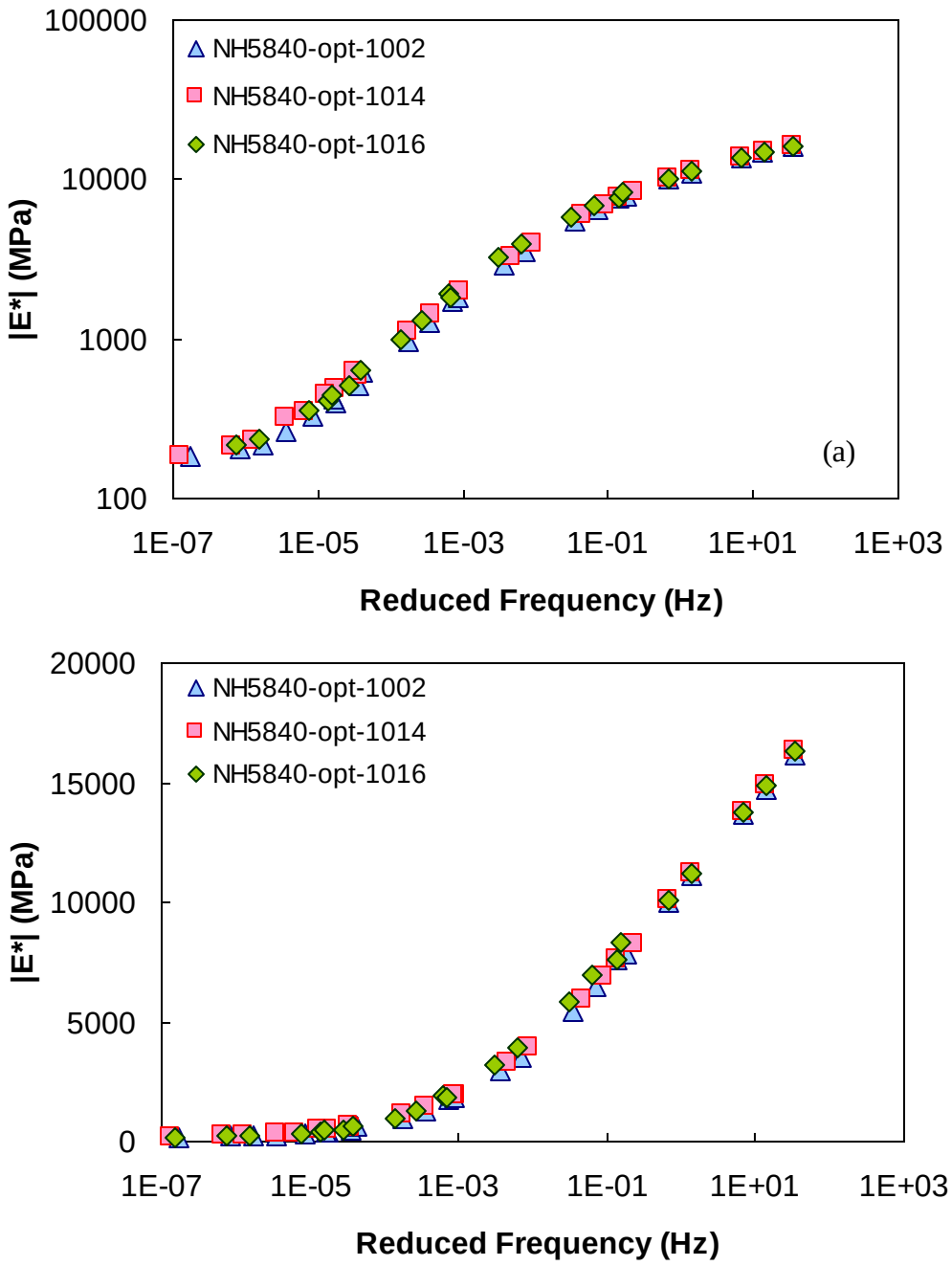

Figure 4.35 Dynamic modulus test results for NH5840-opt mixture in (a) logarithmic scale and (b) semi-logarithmic scale

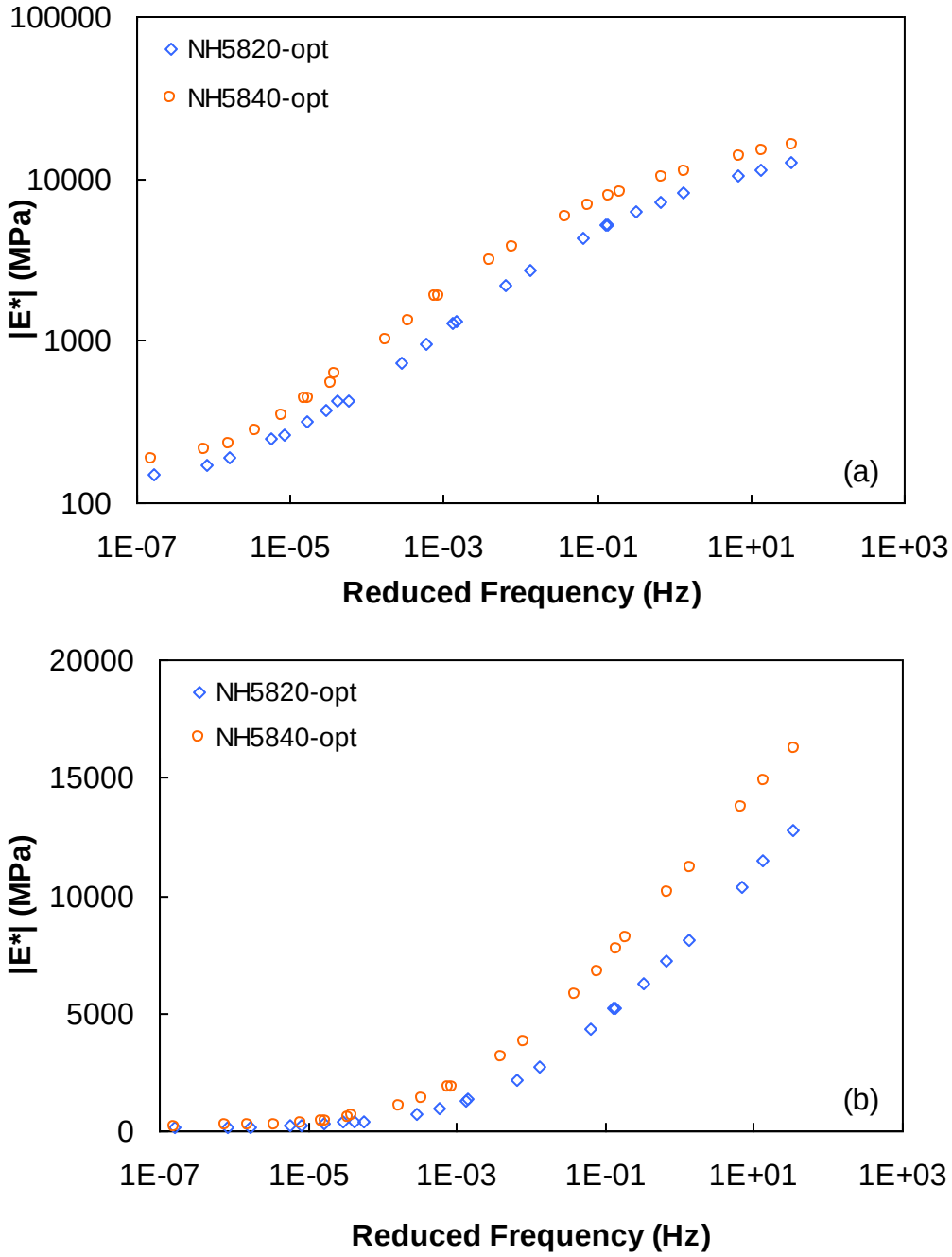

Figure 4.36 Effect of RAP% on dynamic modulus test results for PG 58-28 mixture with AC of 0.5% below the optimum in (a) logarithmic scale and (b) semi-logarithmic scale

Figure 4.37 and Figure 4.38 show the effect of binder content at 20% and 40% RAP, respectively. According to these figures, increasing the binder content decreased the stiffness of the mixture. The effect of the softer binder on the stiffness value is compared in Figure 4.39 and Figure 4.40 for 20% and 40% RAP mixtures, respectively. As these graphs suggest, using softer binder reduced the stiffness of the mixtures to some extent.

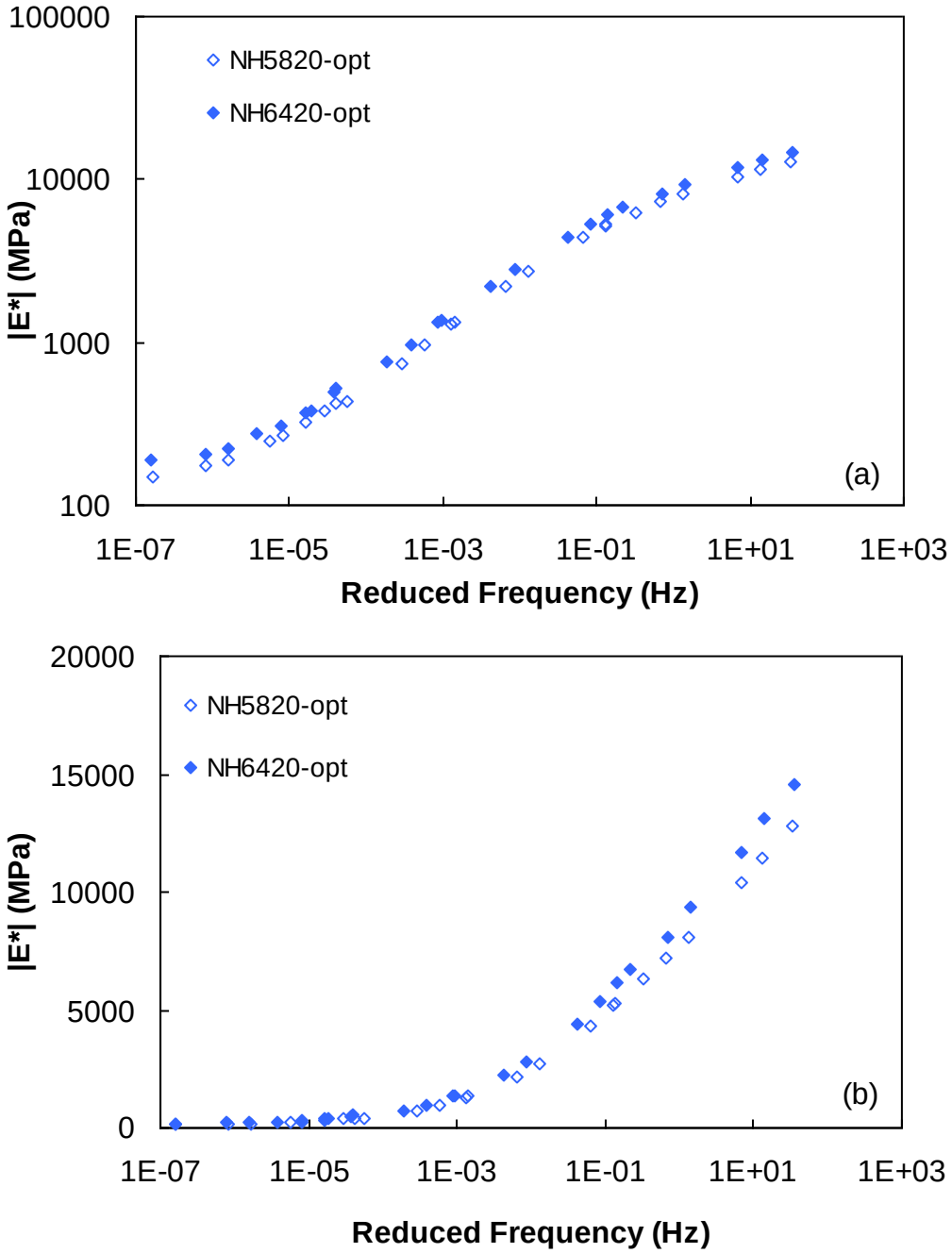

Figure 4.37 Effect of binder grade on the dynamic modulus of 20% RAP mixtures in (a) logarithmic scale and (b) semi-logarithmic scale

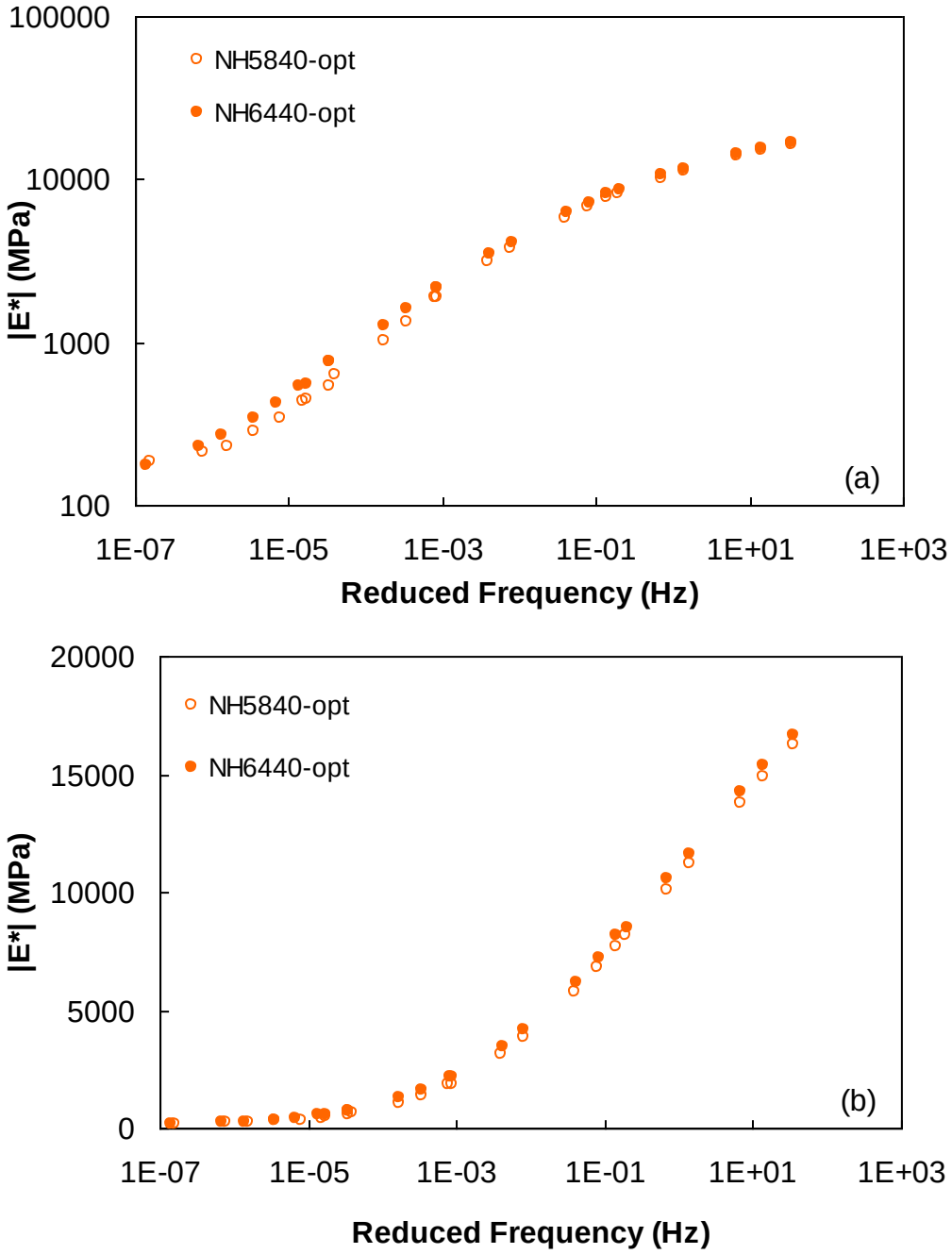

Figure 4.38 Effect of binder grade on the dynamic modulus of 40% RAP mixtures in (a) logarithmic scale and (b) semi-logarithmic scale

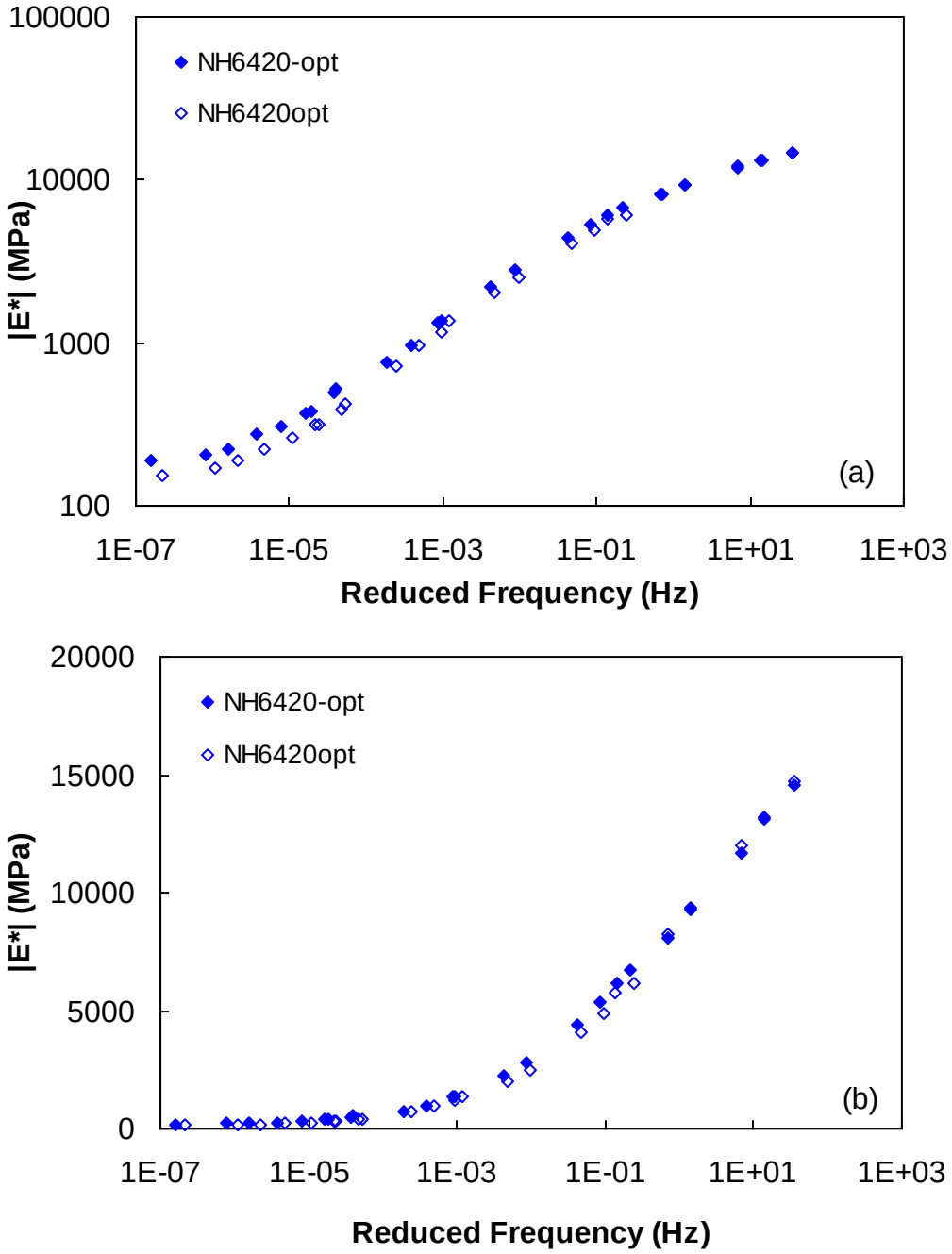

Figure 4.39 Effect of binder content on the dynamic modulus of 20% RAP mixtures in (a) logarithmic scale and (b) semi-logarithmic scale

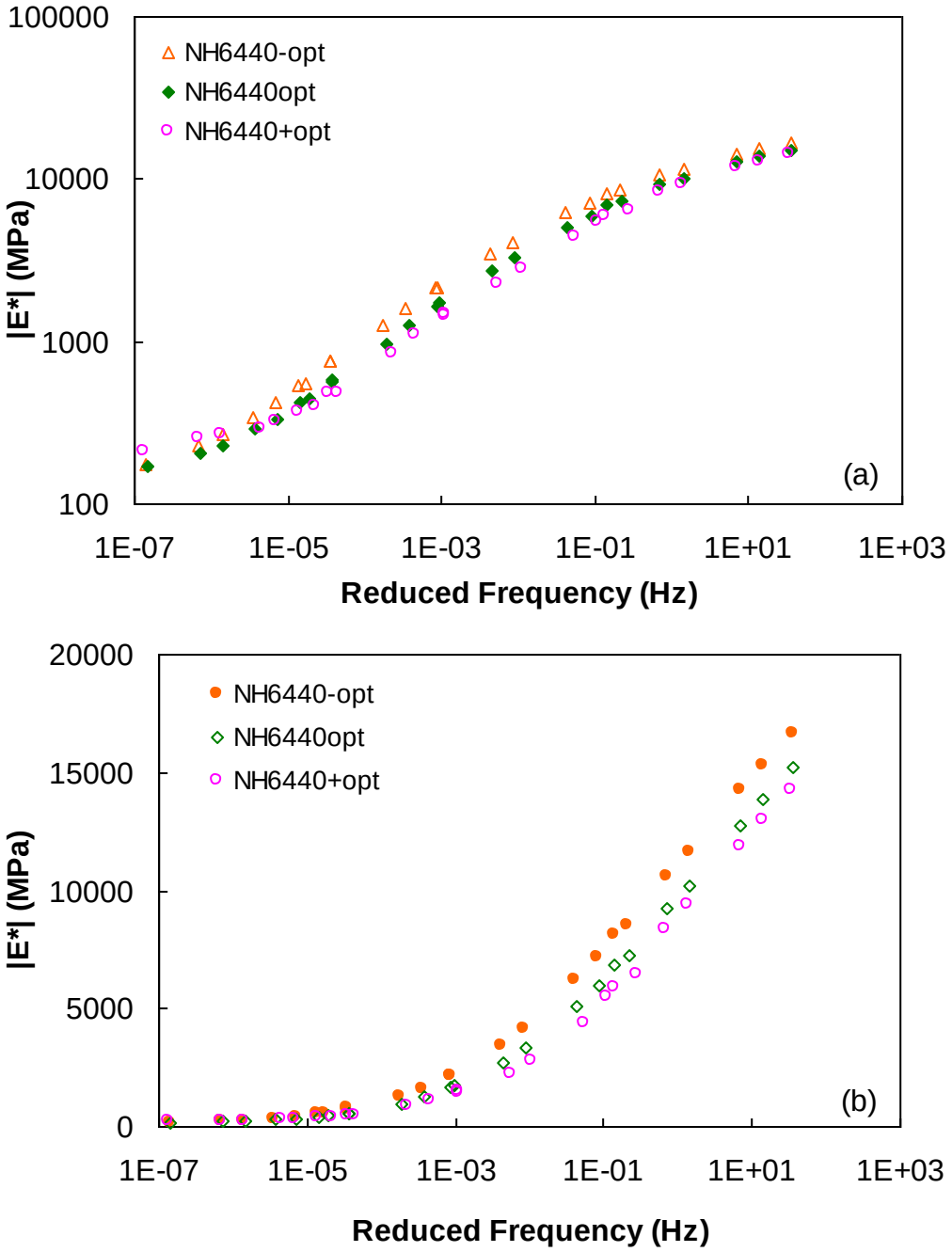

Figure 4.40 Effect of binder content on the dynamic modulus of 40% RAP mixtures in (a) logarithmic scale and (b) semi-logarithmic scale

4.2.2 *Fatigue*

The fatigue behavior of the mixtures was evaluated using S-VECD testing conducted in crosshead mode of loading at 13°C and 10 Hz for the PG 64-28 mixtures and at 12°C and 10 Hz for the PG 58-28 mixtures. Figure 4.41 through Figure 4.49 show the individual results for fatigue testing of all the study mixtures.

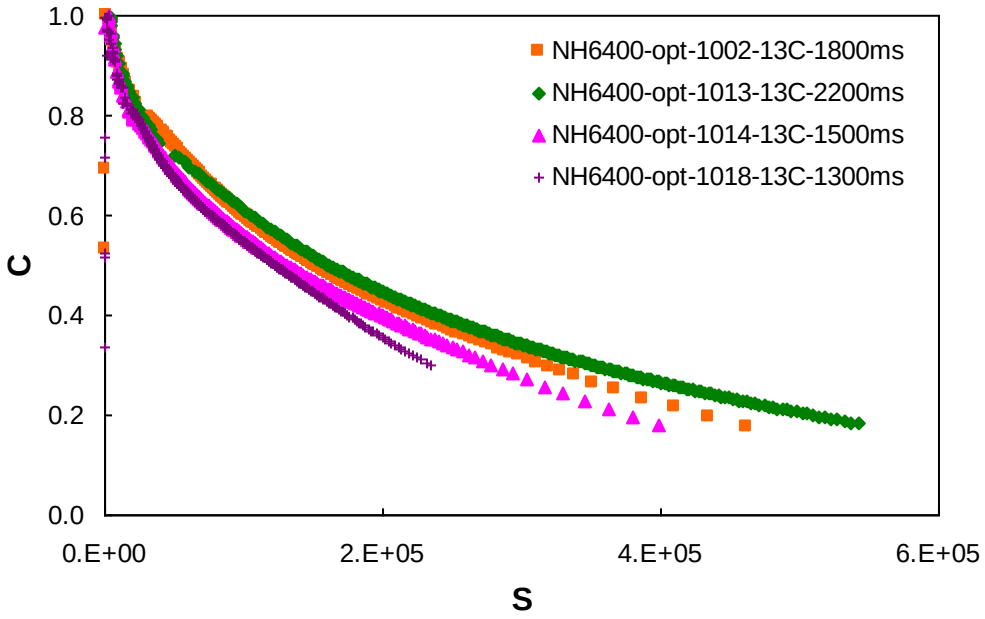

Figure 4.41 Individual results for NH6400-opt mixture at 13°C

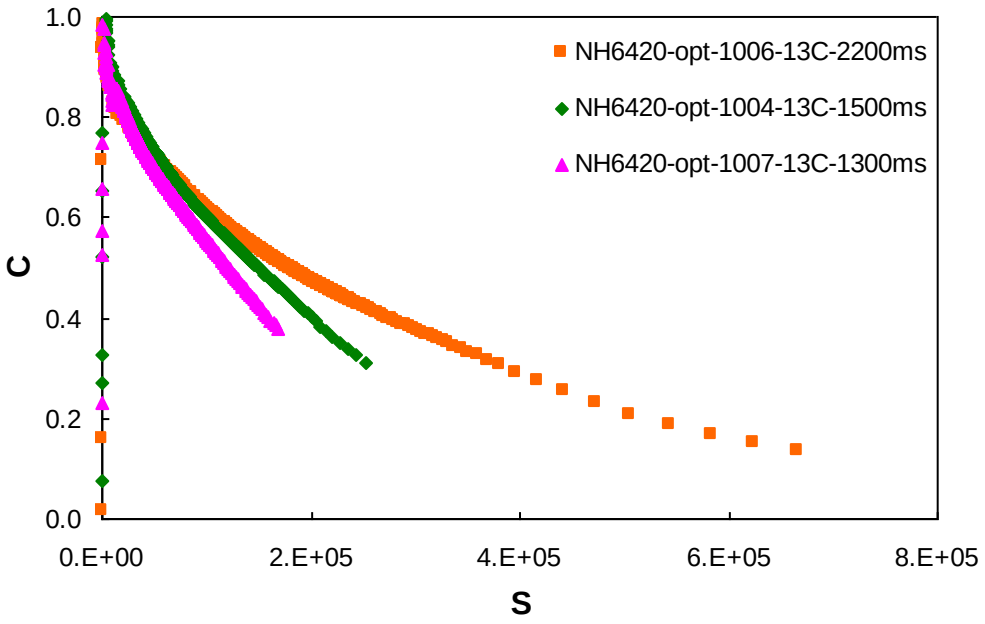

Figure 4.42 Individual results for NH6420-opt mixture at 13°C

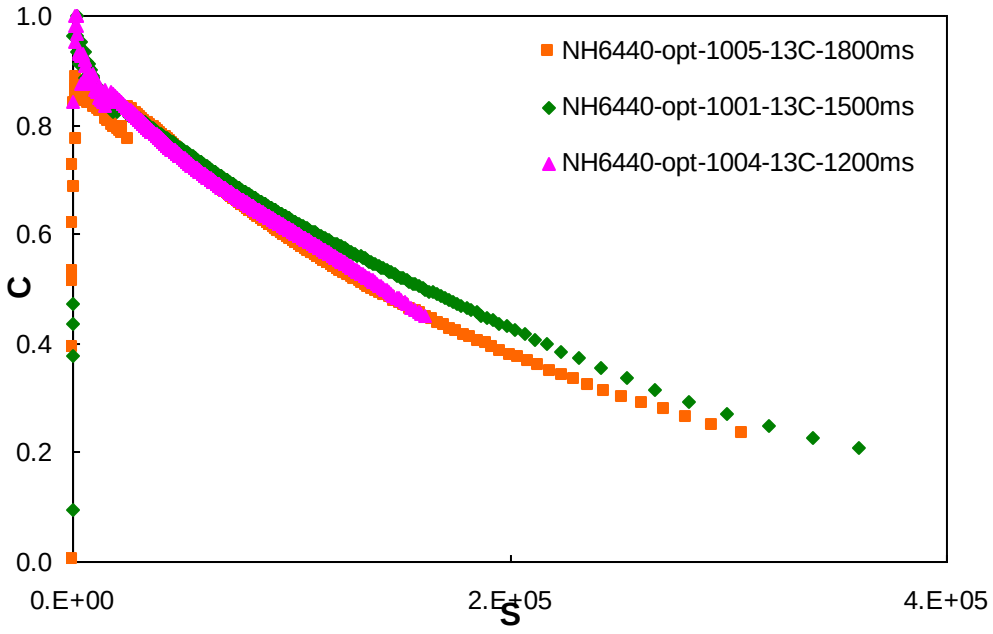

Figure 4.43 Individual results for NH6440-opt mixture at 13°C

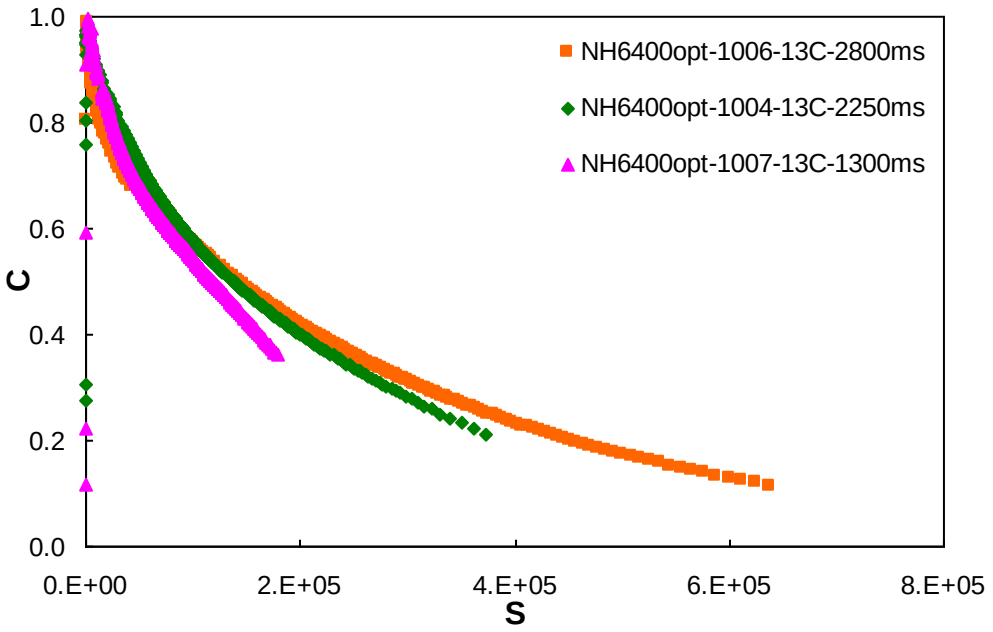

Figure 4.44 Individual results for NH6400opt mixture at 13°C

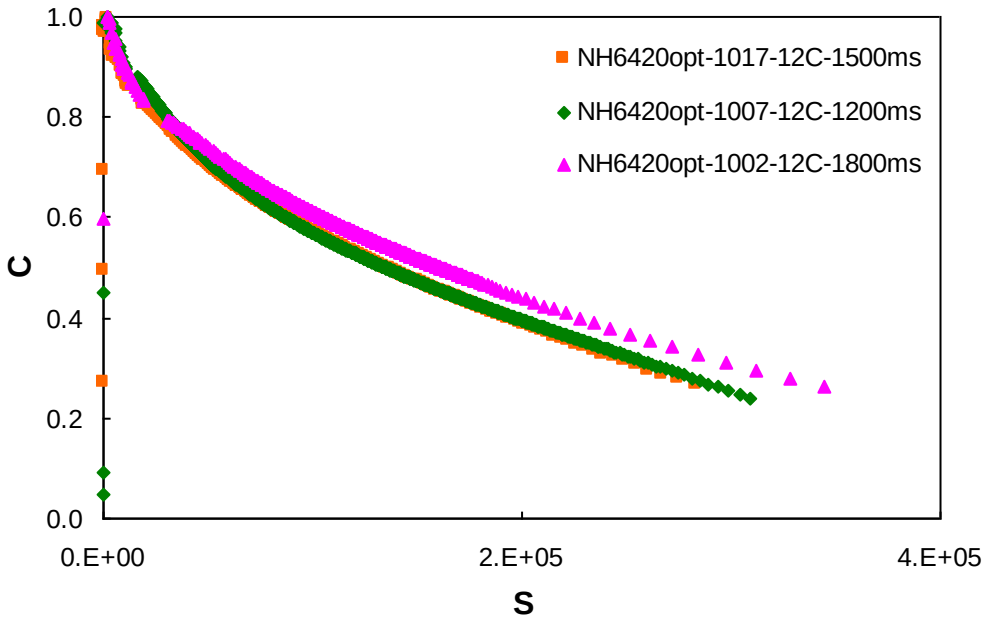

Figure 4.45 Individual results for NH6420opt mixture at 13°C

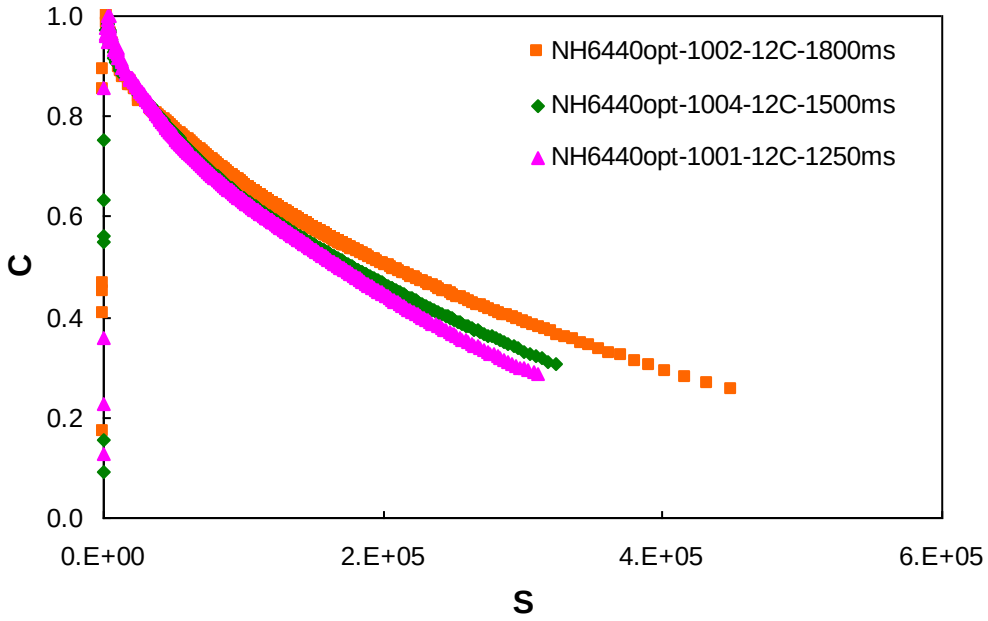

Figure 4.46 Individual results for NH6440opt mixture at 13°C

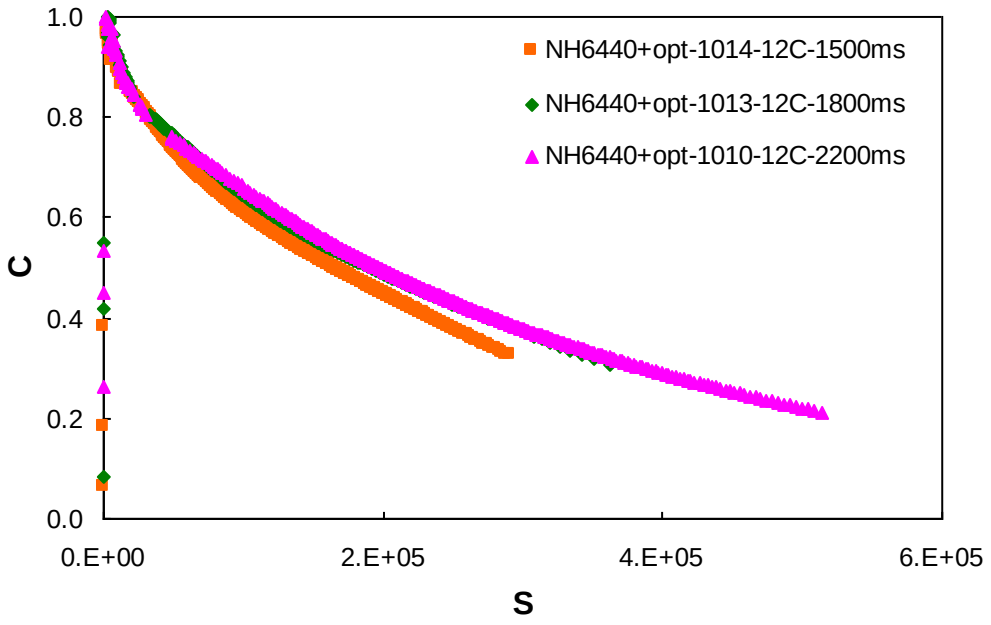

Figure 4.47 Individual results for NH6440+opt mixture at 13°C

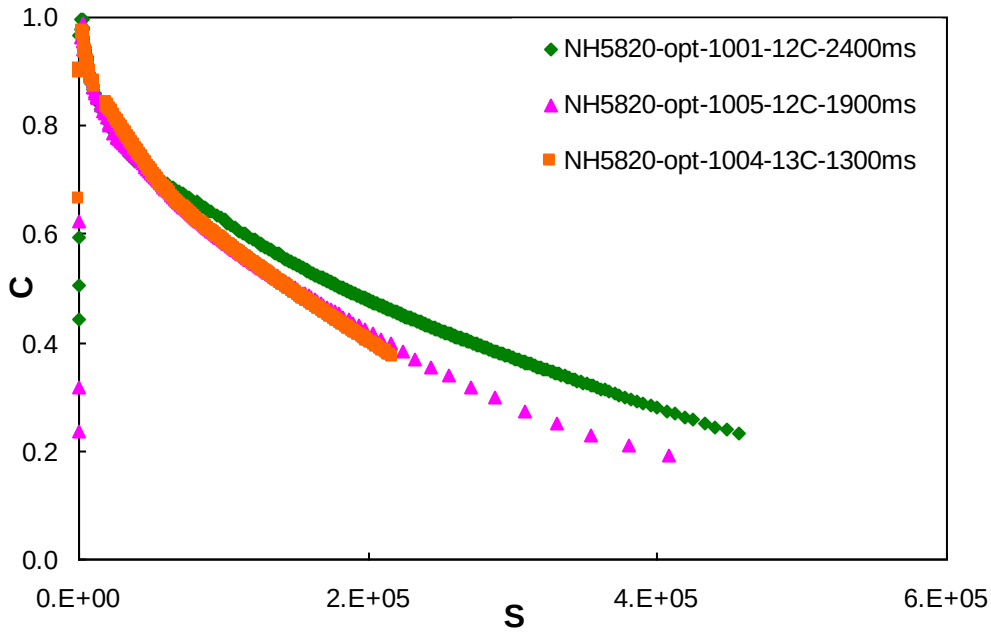

Figure 4.48 Individual results for NH5820-opt mixture at 12°C

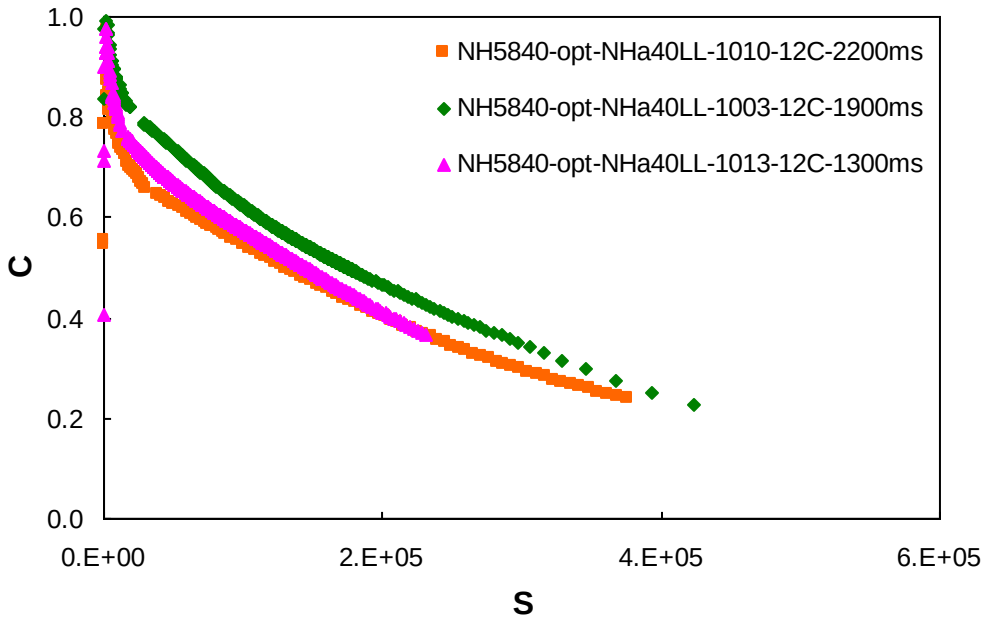

Figure 4.49 Individual results for NH5840-opt mixture at 12°C

Figure 4.50 through Figure 4.55 compares the fitted C vs. S curves for all the study mixtures from different aspects. Figure 4.50 and Figure 4.51 show the effects of RAP content. In general, high RAP mixtures show higher curves than the others. The mixtures with the same virgin binder grade are clustered together with similar damage characteristic curves. The curves for the PG 58-28 mixtures are above those for the PG 64-28 mixtures. Figure 4.52 and Figure 4.53 show the effect of binder content at each RAP level. Here, as the binder content increases, the curve moves up. This trend is more pronounced for 40% RAP mixtures (Figure 4.53). The effect of softer binder is shown in Figure 4.54 and Figure 4.55. The performance of the 20% RAP mixtures is similar, whereas for the 40% RAP mixtures, the PG 58-28 mixture shows a slightly higher curve.

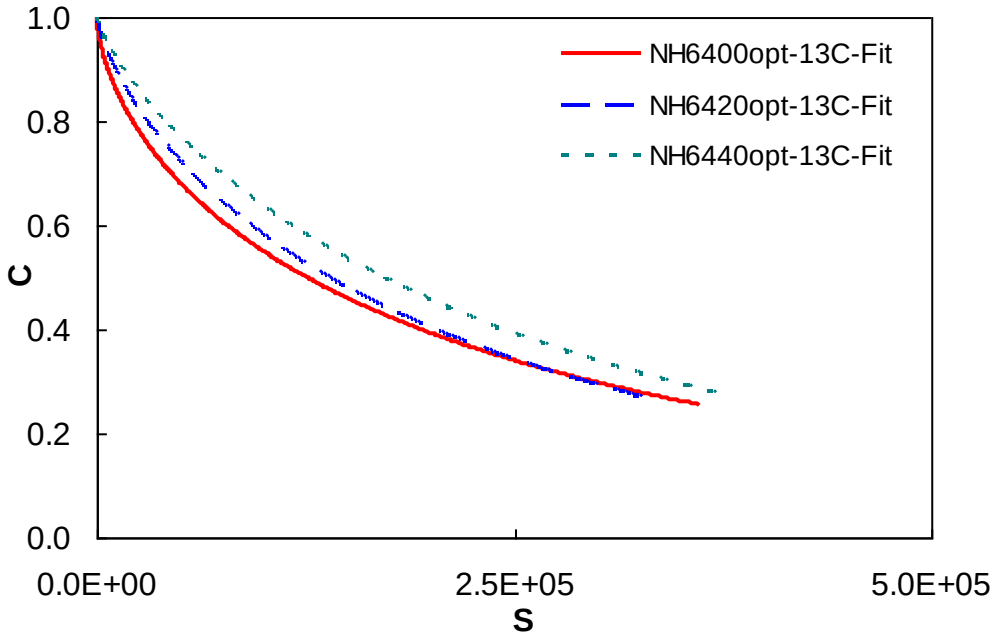

Figure 4.50 Evaluation of the effect of RAP content at the optimum AC on the mixture characteristic curve

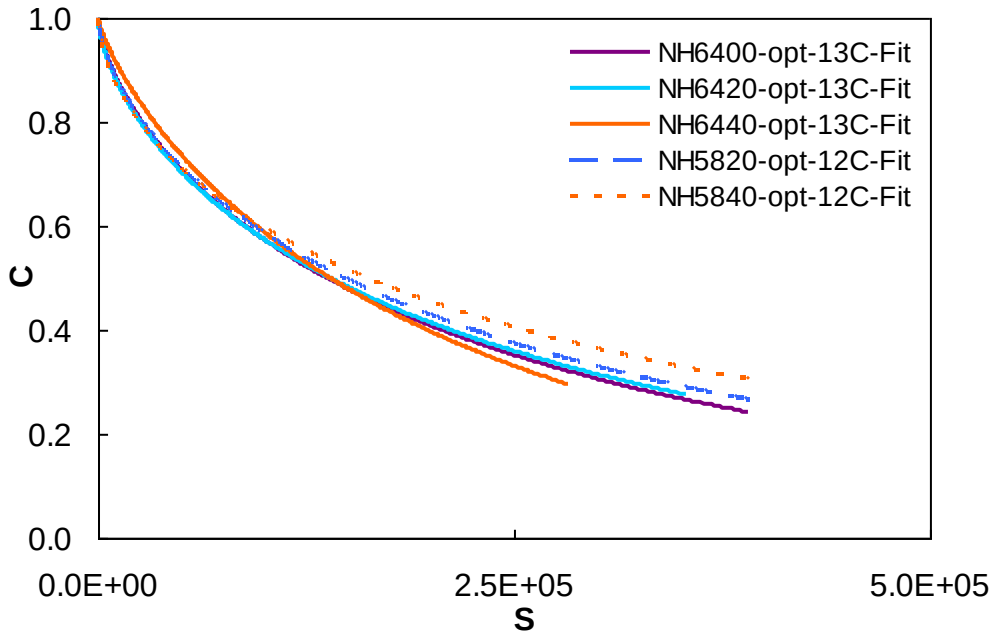

Figure 4.51 Evaluation of the effect of RAP content at 0.5 percent below the optimum AC on the mixture characteristic curve

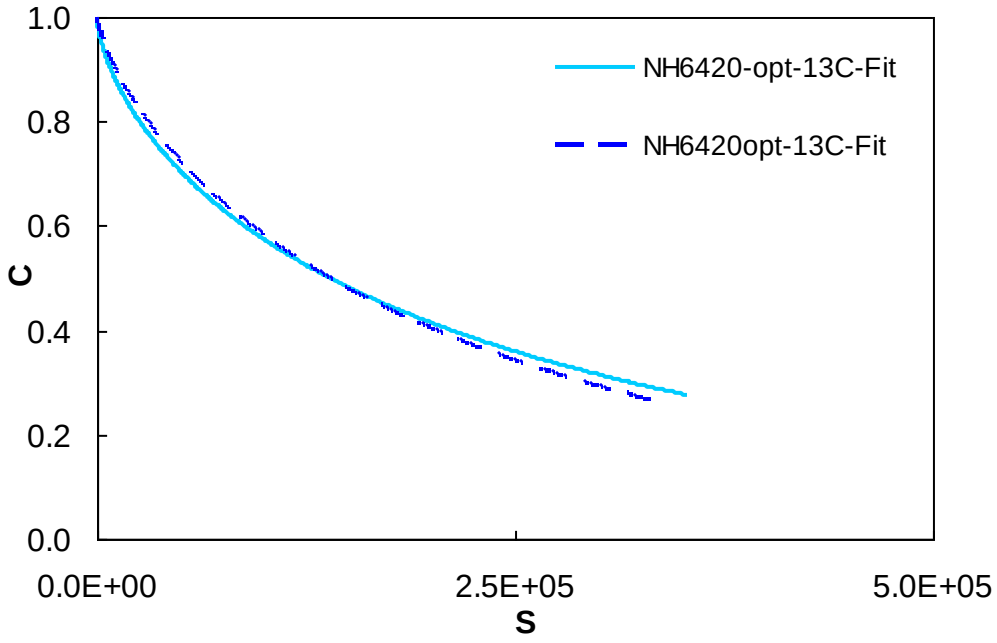

Figure 4.52 Evaluation of the effect of binder content at 20% RAP on the mixture characteristic curve

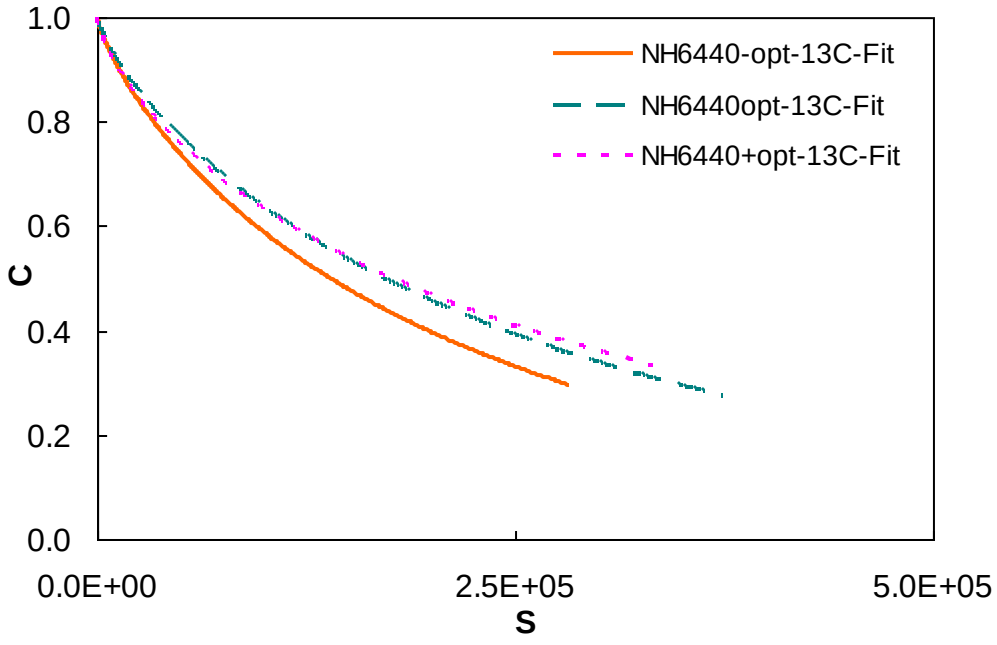

Figure 4.53 Evaluation of the effect of binder content at 40% RAP on the mixture characteristic curve

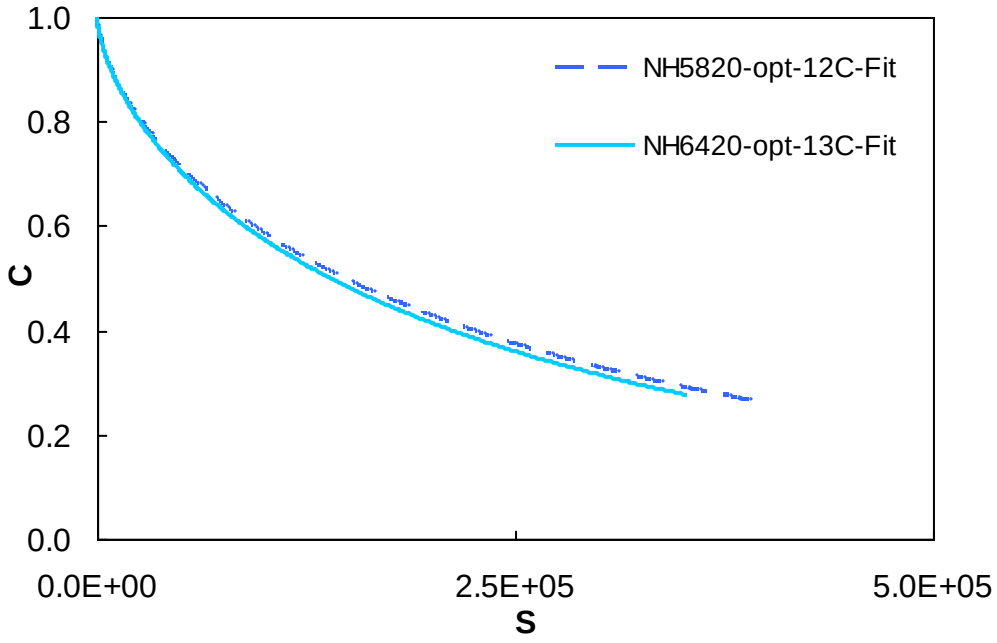

Figure 4.54 Evaluation of the effect of binder base PG grade at 20% RAP on the mixture characteristic curve

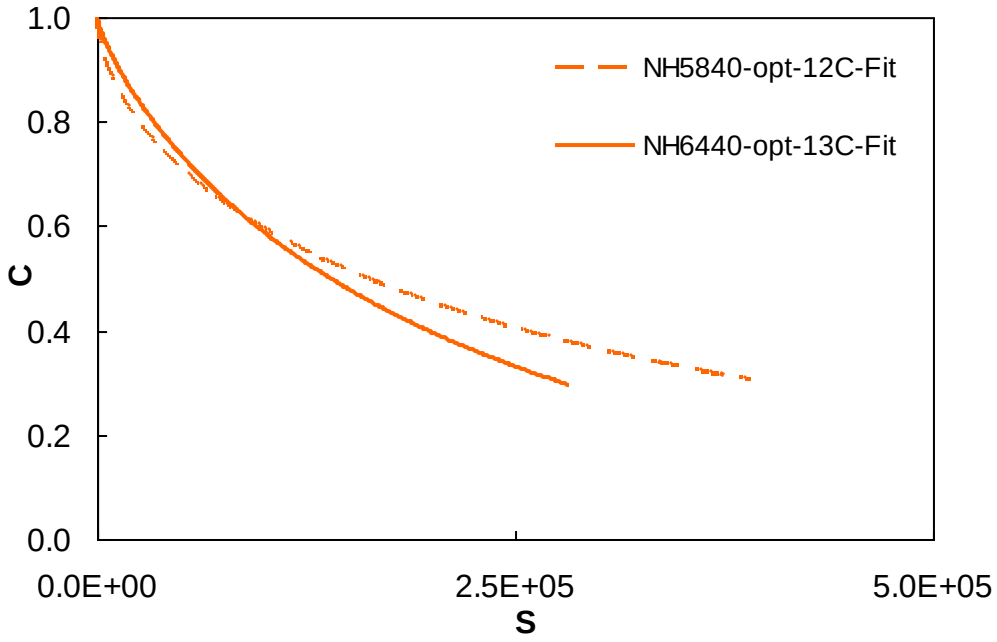

Figure 4.55 Evaluation of the effect of binder base PG grade at 40% RAP on the mixture characteristic curve

The S-VECD failure criterion was applied to all the study mixtures and the results are shown in Figure 4.56 through Figure 4.61. The positions of the failure criterion lines can be used as a relative comparison of the expected fatigue resistance of the mixtures. Mixtures with better fatigue resistance have failure criterion lines that are located towards the upper right corner with shallower slopes, meaning that at the same level, the G^R will correspond to a higher N_f value (i.e., better performance). However, in order to compare the fatigue resistance of the different mixtures, they must be considered within a specific pavement structure. This pavement evaluation was conducted in this project using the LVECD software and the results are presented in a subsequent section.

Figure 4.56 through Figure 4.57 compare the fatigue failure criterion for all the study mixtures from different aspects. Figure 4.56 and Figure 4.57 show the effects of incorporating RAP into the mixture. The failure criterion lines move down with increases in RAP content, suggesting a decrease in fatigue resistance. This change is more pronounced for mixtures with the binder content that is lower than the optimum binder content (Figure 4.57). Figure 4.58 and Figure 4.59 show the effects of binder content at 20% and 40% RAP, respectively. Lowering the binder content in both cases decreased the fatigue resistance. This reduction is more pronounced when the binder content dropped below the optimum binder content in both cases. The effects of using the softer binder is shown in Figure 4.60 and Figure 4.61 for 20% and 40% RAP, respectively. In both cases the softer binder indicates better fatigue resistance. Also, it is observed that as the RAP content increases, the impact of the binder PG decreases, and the performance of the mixtures with the different binders becomes increasingly similar, which is likely due to the increased amount of recycled material. Also, it is interesting to note that, in general, adding RAP seems to shift only the failure criterion lines, whereas the binder content and binder grade appear to change the slopes as well.

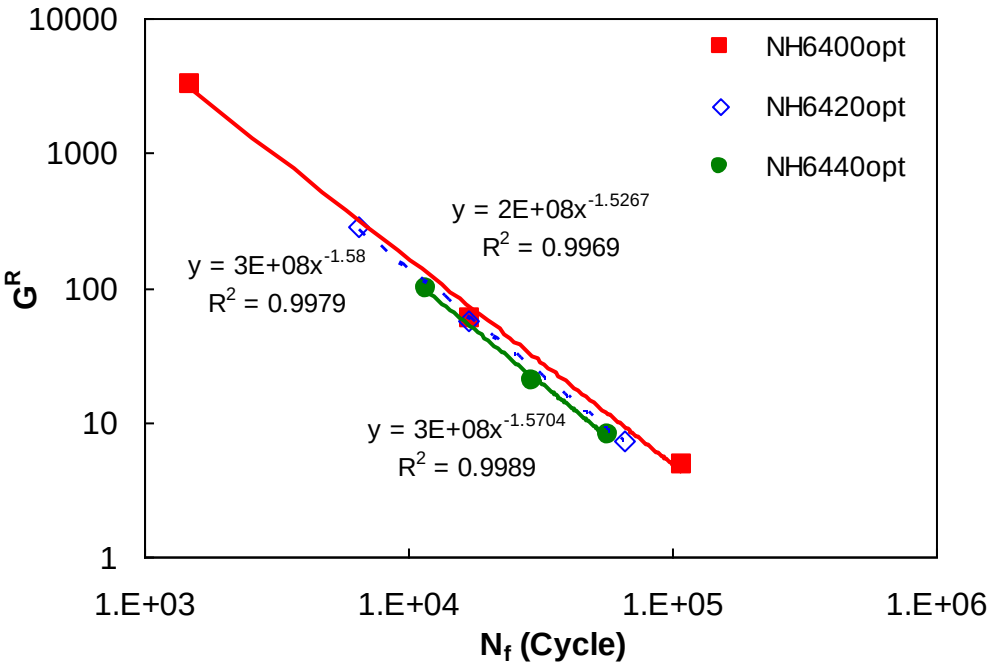

Figure 4.56 Evaluation of the effect of RAP content at the optimum AC on the mixture characteristic curve

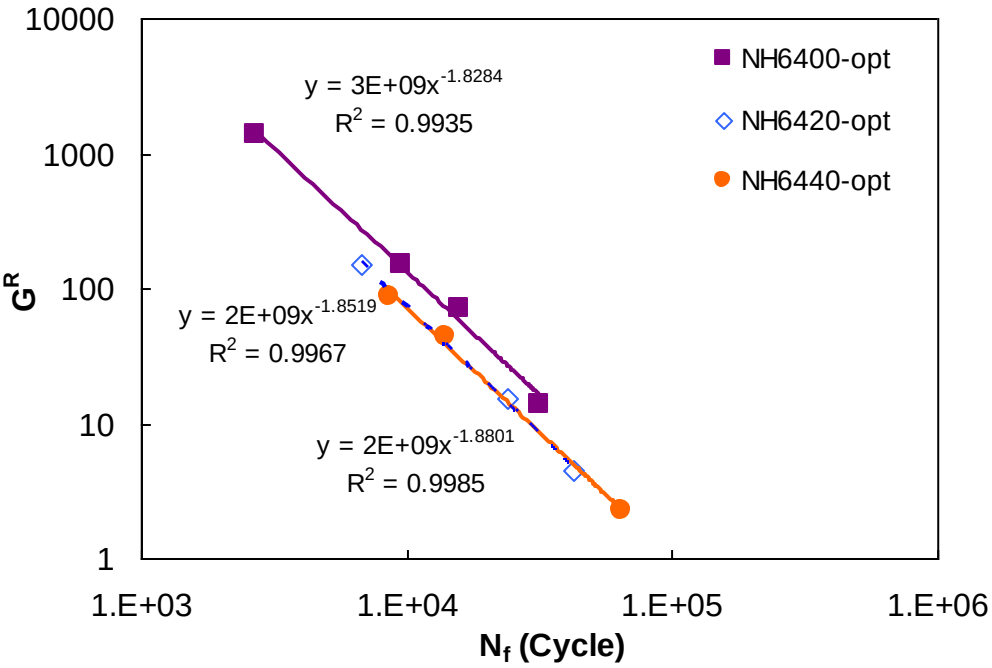

Figure 4.57 Evaluation of the effect of RAP content at 0.5 percent below the optimum AC on the mixture characteristic curve

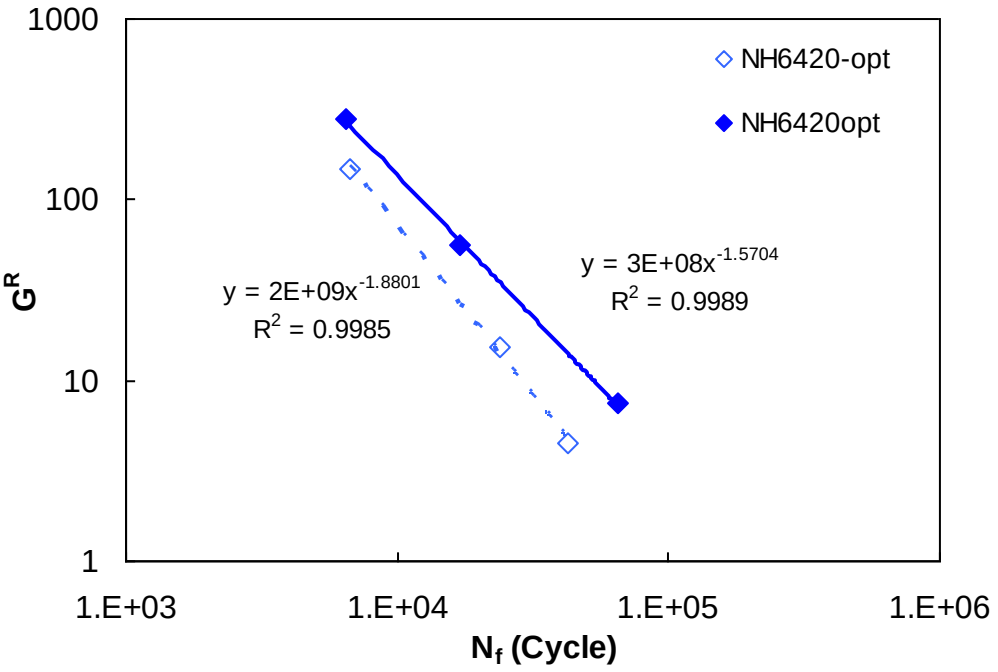

Figure 4.58 Evaluation of the effect of binder content at 20% RAP on the mixture characteristic curve

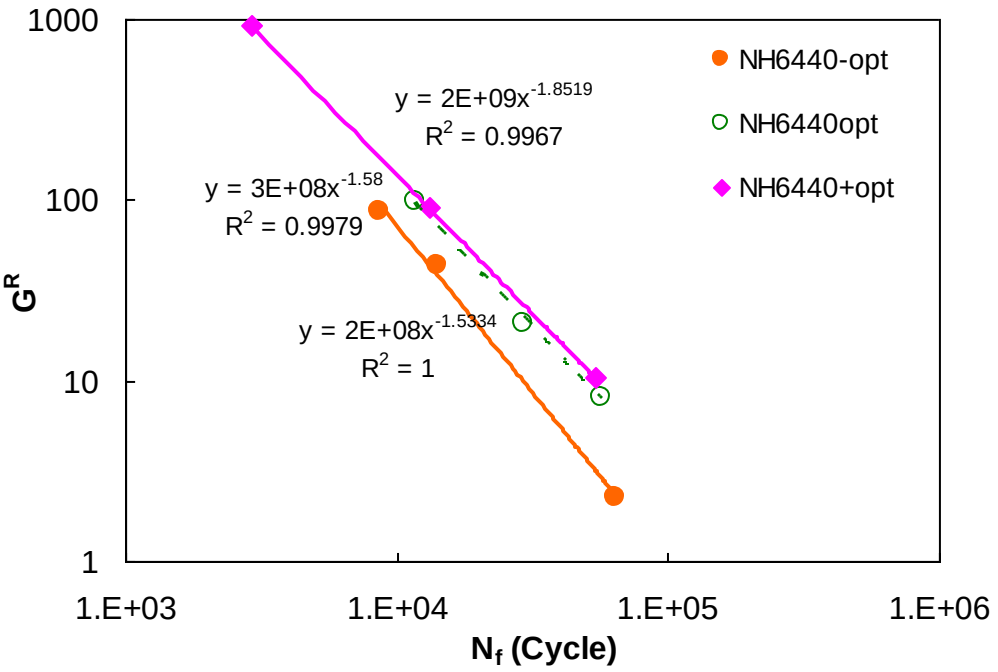

Figure 4.59 Evaluation of the effect of binder content at 40% RAP on the mixture characteristic curve

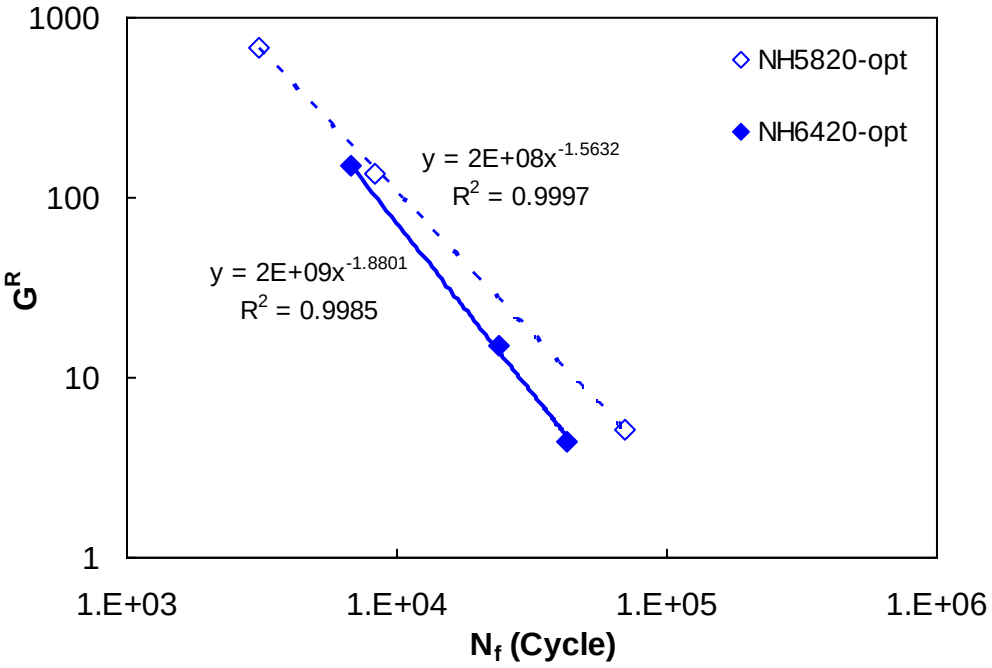

Figure 4.60 Evaluation of the effect of binder base PG grade at 20% RAP on the mixture characteristic curve

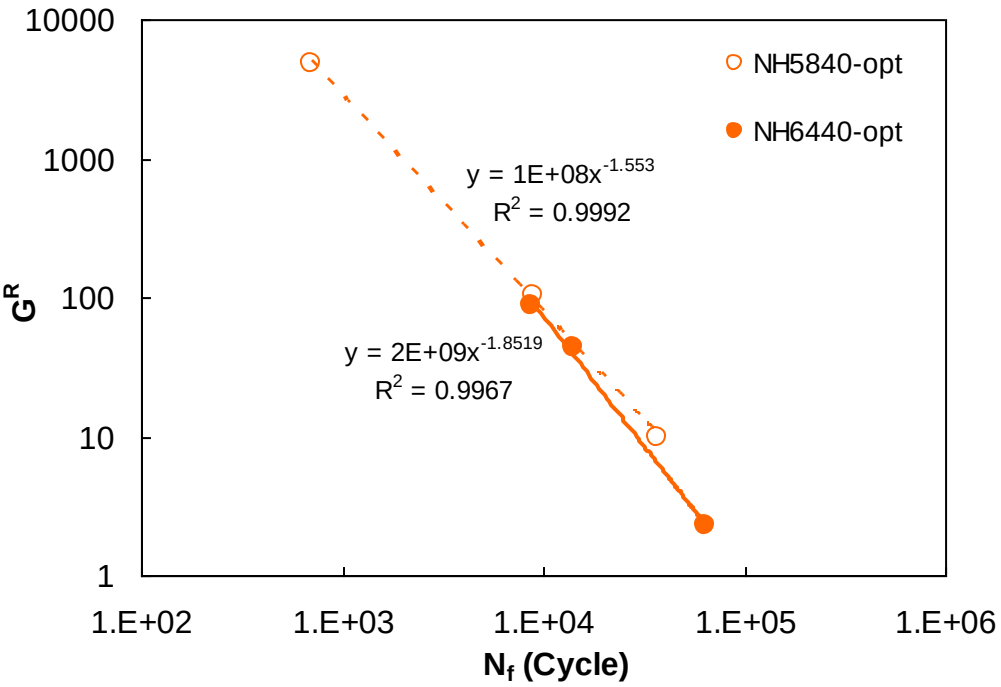

Figure 4.61 Evaluation of the effect of binder base PG grade at 40% RAP on the mixture characteristic curve

4.2.3 *Permanent Deformation*

The rutting characterization tests, i.e., the TSS tests, were performed using all the mixtures. As previously indicated, the TSS tests are composed of a reference test and three MSS tests. Figure 4.62 through Figure 4.70 show TSS test results for all the study mixtures.

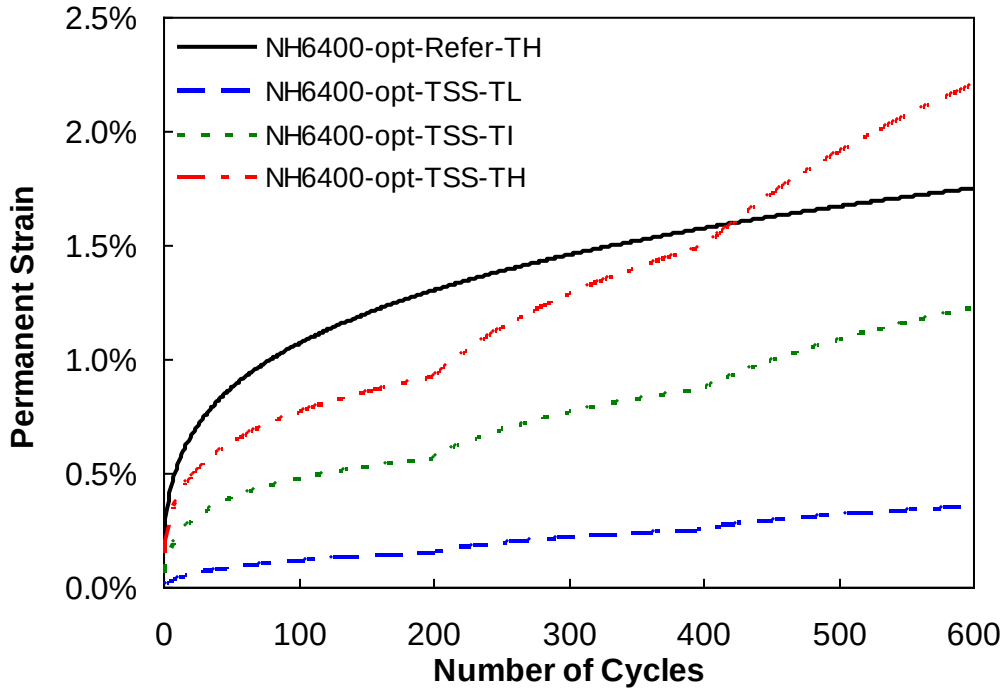

Figure 4.62 TSS test results for NH6400-opt mixture

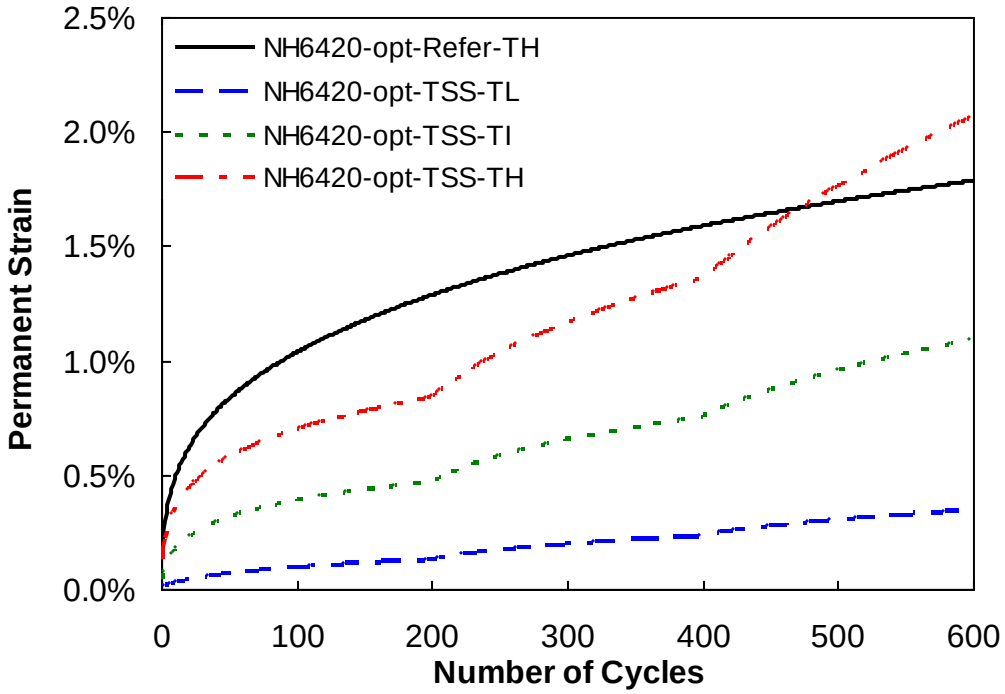

Figure 4.63 TSS test results for NH6420-opt mixture

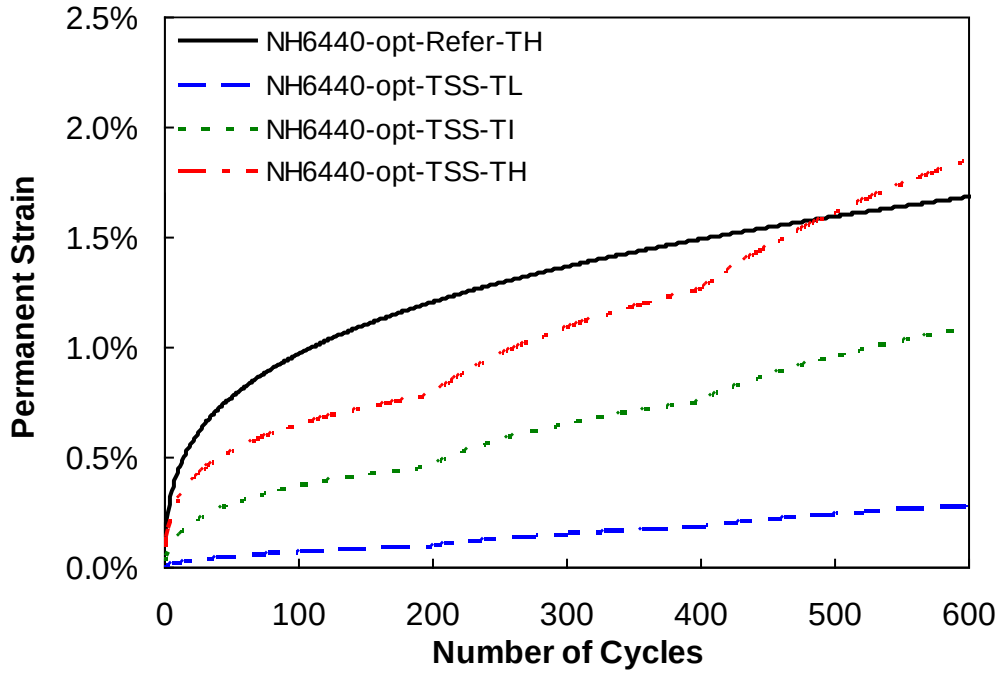

Figure 4.64 TSS test results for NH6440-opt mixture

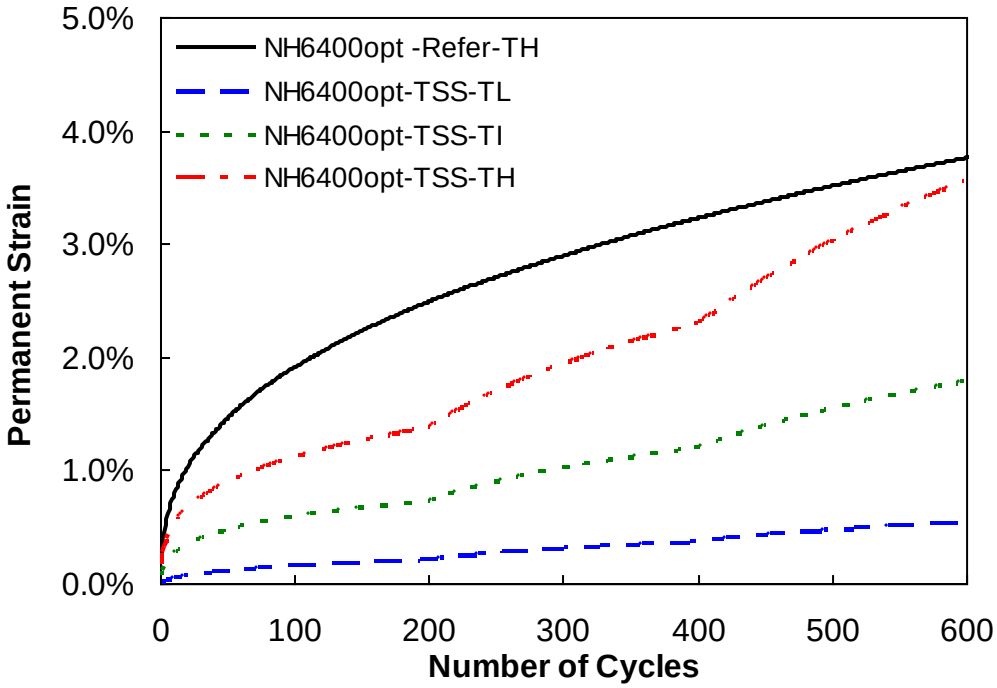

Figure 4.65 TSS test results for NH6400opt mixture

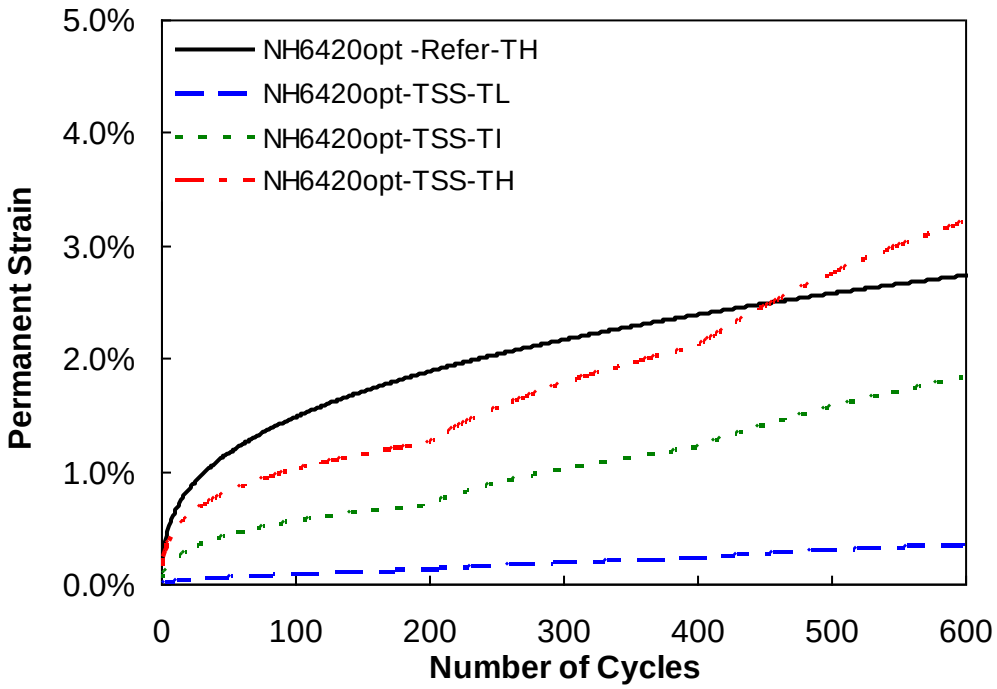

Figure 4.66 TSS test results for NH6420opt mixture

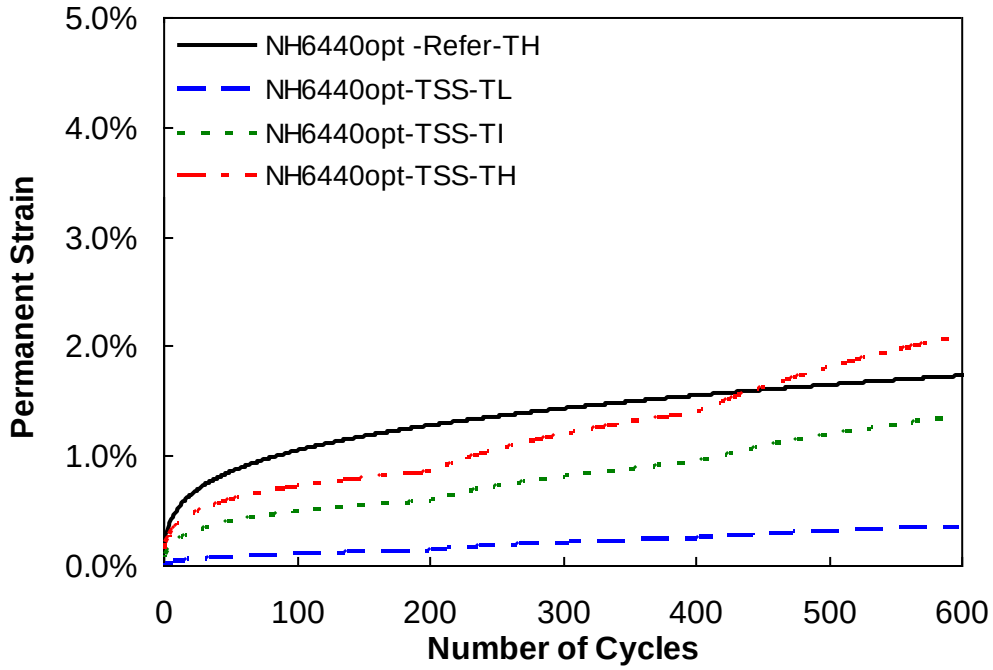

Figure 4.67 TSS test results for NH6440opt mixture

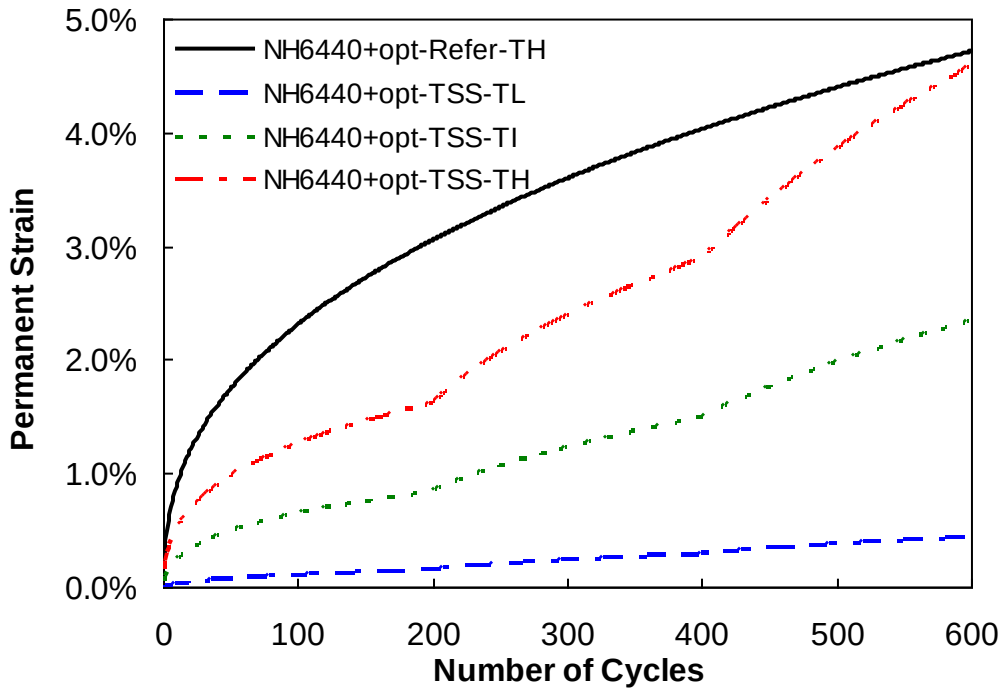

Figure 4.68 TSS test results for NH6440+opt mixture

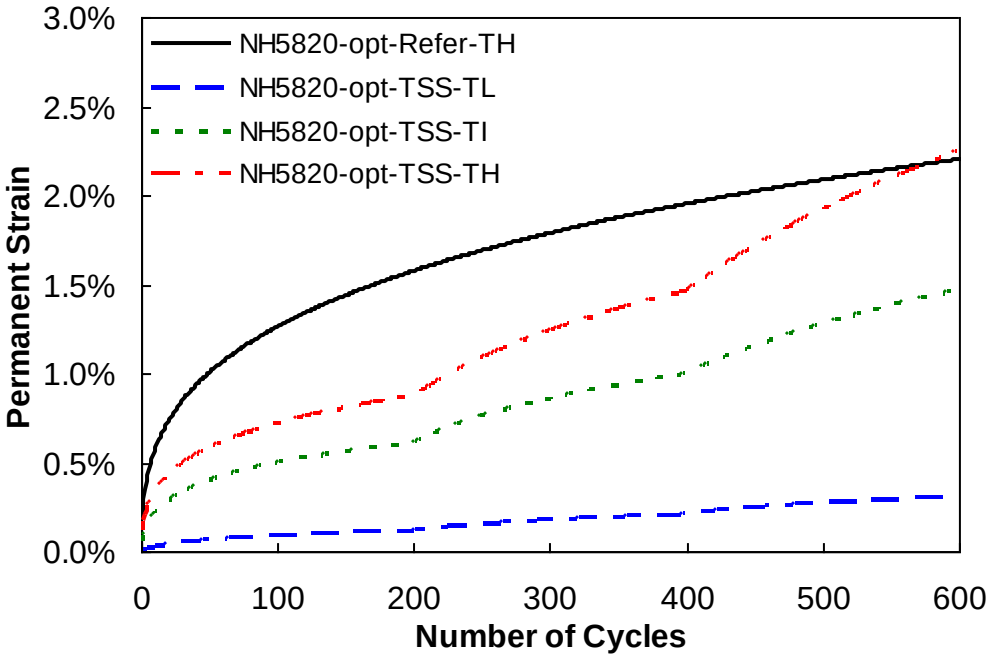

Figure 4.69 TSS test results for NH5820-opt mixture

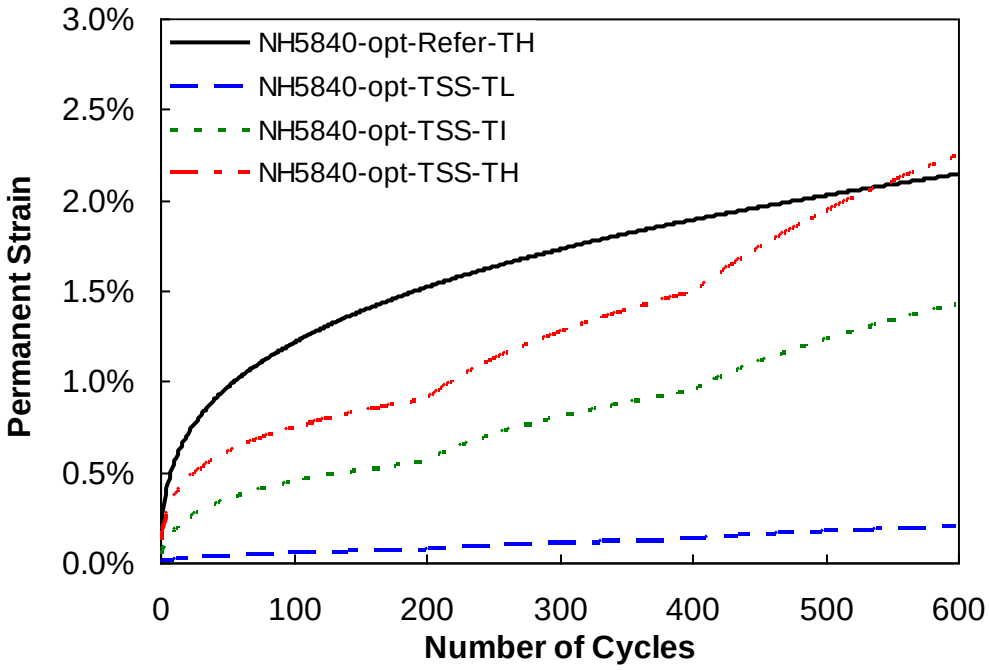

Figure 4.70 TSS test results for NH5840-opt mixture

Figure 4.71 and Figure 4.72 show the effects of incorporating RAP into the mixture at different asphalt binder content levels. As expected, by incorporating more RAP into the mixture, the rutting resistance increased. Figure 4.73 and Figure 4.74 show the effects of

binder content at 20% and 40% RAP, respectively. Generally, as the binder content increased, the rutting resistance decreased. This decrease seems to be much more pronounced when the asphalt content exceeds the optimum binder content, as the NH6440+opt mixture shows the poorest rutting resistance among all the study mixtures. The effect of using softer binder is shown in Figure 4.75 and Figure 4.76 for 20% and 40% RAP, respectively. In both cases, the stiffer binder shows better rutting resistance, which is due to the increase in the mixture's stiffness.

In general, as the mixture's stiffness increases, the rutting resistance improves. This finding suggests that the dynamic modulus data, which have been captured in the viscoelastic domain, could be related to the rutting resistance of the mixture to some extent. It is interesting to note also that these results agree well with the binder rutting data (MSCR test results). The binder data show improvement in rutting resistance as the RAP percentage increased or the binder content decreased or when the stiffer base binder was used.

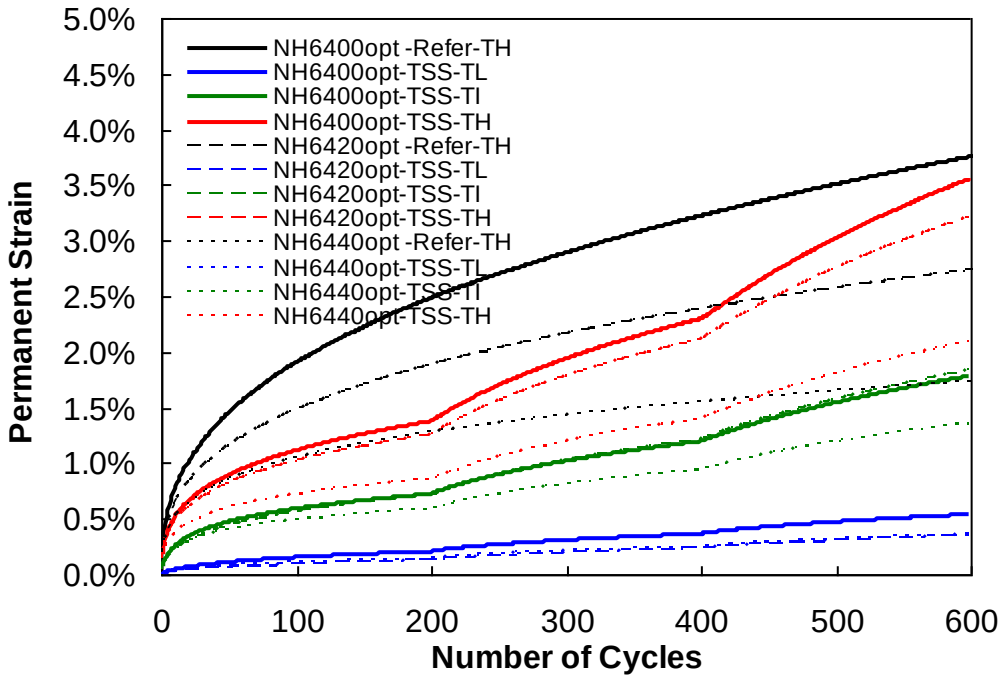

Figure 4.71 Evaluation of the effect of RAP content at the optimum AC on the mixture characteristic curve

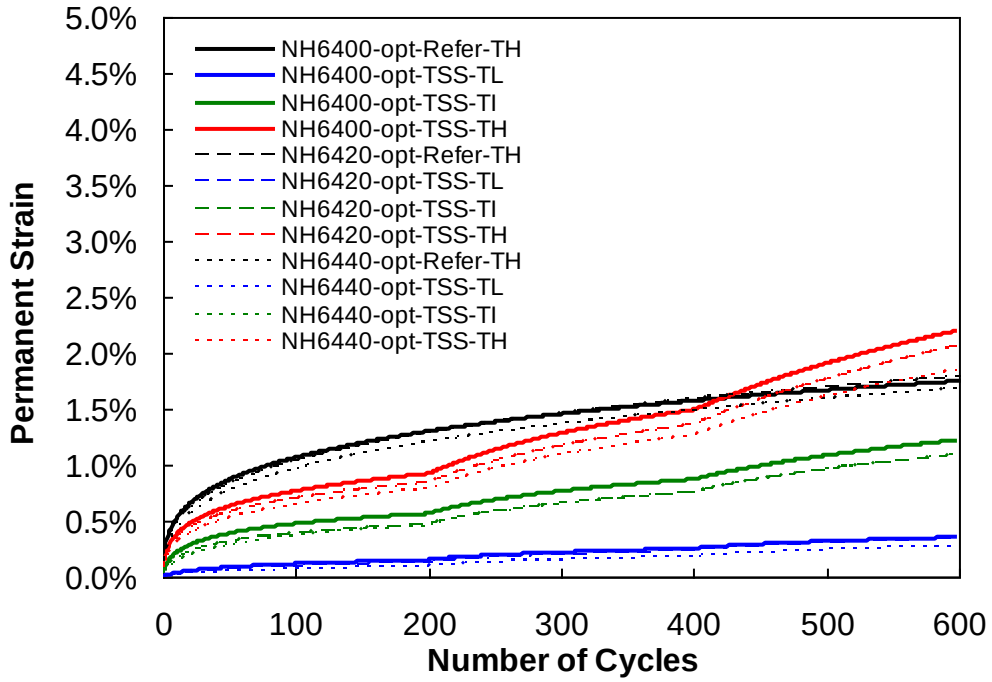

Figure 4.72 Evaluation of the effect of RAP content at 0.5 percent below the optimum AC on the mixture characteristic curve

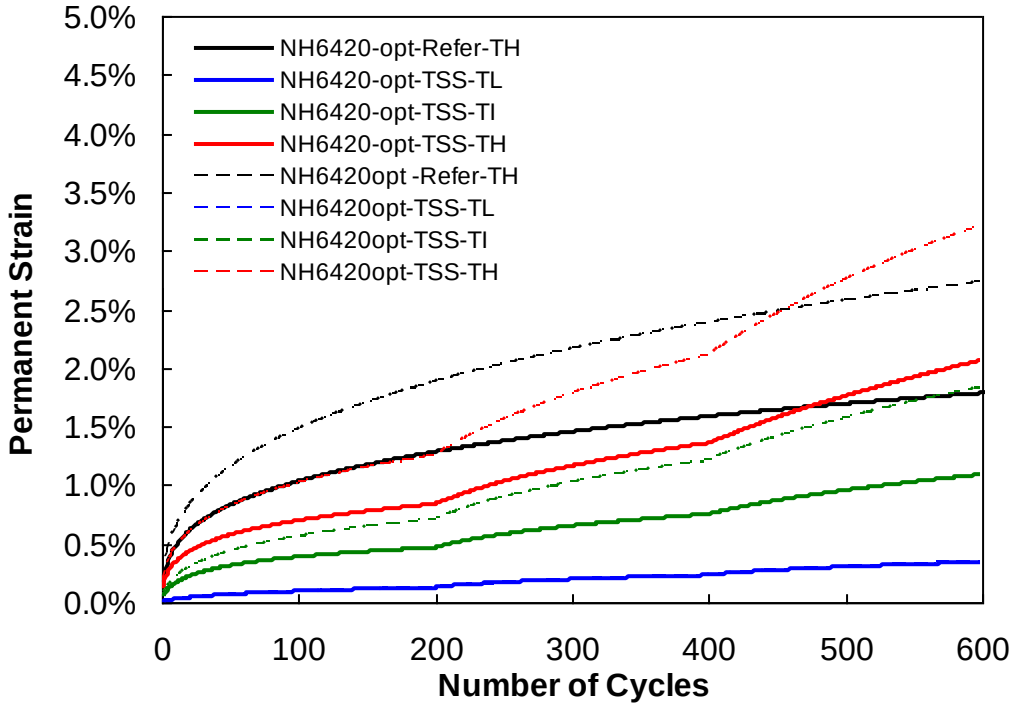

Figure 4.73 Evaluation of the effect of binder content at 20% RAP on the mixture characteristic curve

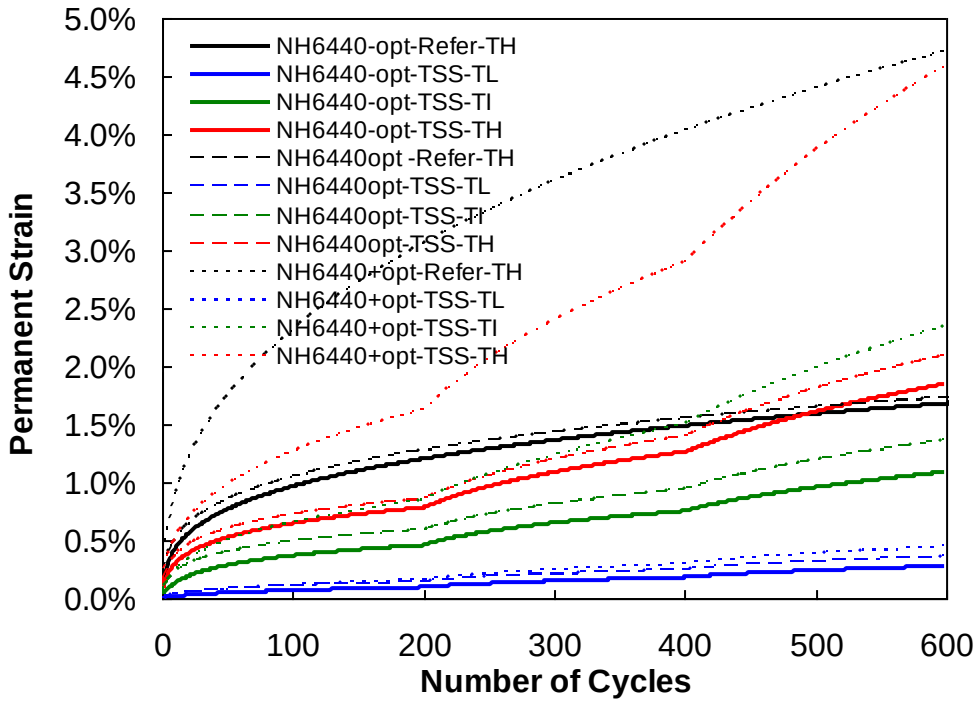

Figure 4.74 Evaluation of the effect of binder content at 40% RAP on the mixture characteristic curve

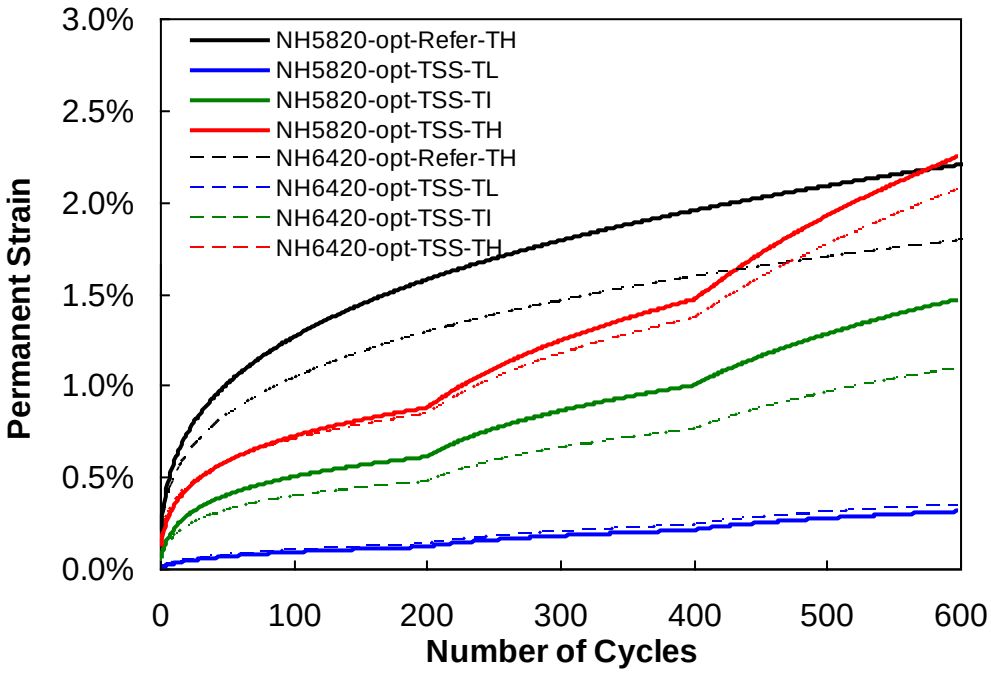

Figure 4.75 Evaluation of the effect of binder base PG grade at 20% RAP on the mixture characteristic curve

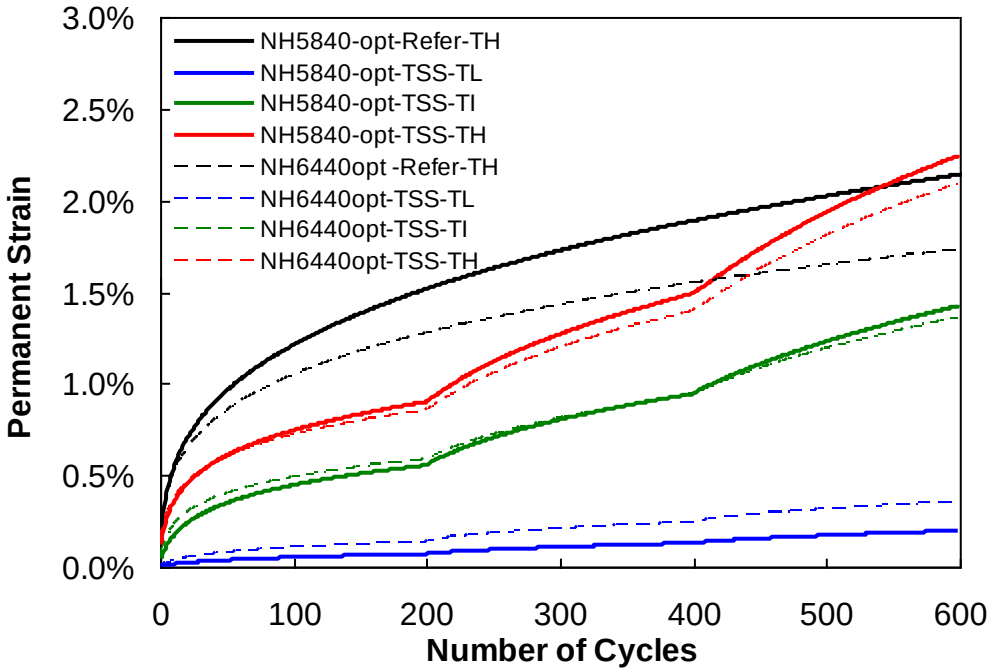

Figure 4.76 Evaluation of the effect of binder base PG grade at 40% RAP on the mixture characteristic curve

4.2.4 *Low Temperature*

The asphalt mixtures were evaluated for their respective mixture low temperature cracking in accordance with AASHTO TP10, Method for Thermal Stress Restrained Specimen Tensile Strength. The TSRST started at an initial temperature of 4°C and then cooled the specimens at a rate of 10°C/hr. The failure temperature and standard deviation are shown in Table 4.11. The results indicate that as RAP content increases for the respective asphalt binder grade, the cracking temperature becomes warmer. Also, the drop in the binder content from the optimum has a negative effect on the RAP mixtures. However, the impact is greater for the 40% RAP mixtures relative to the 20% RAP mixtures. Adding additional binder beyond the optimum binder content for the 40% RAP mixture did not show any improvement in the low temperature cracking.

Table 4.11 Low Temperature Cracking Results Using the TSRST

Base Binder Grade	Sample Name	AC% Condition	RAP Content (%)	Temperature Average	Temperature Standard Deviation
PG58-28	NH5820-opt	-Opt	20%	-22.60	0.94
	NH5840-opt		40%	-20.80	1.21
PG64-28	NH6400-opt	-Opt	0%	-23.30	0.58
	NH6420-opt		20%	-22.40	1.34
	NH6440-opt		40%	-19.30	1.42
	NH6400opt	Opt	0%	-23.50	0.96
	NH6420opt		20%	-23.00	2.18
	NH6440opt		40%	-21.30	1.57
	NH6440+opt	+Opt	40%	-21.10	1.75

4.2.5 *Overlay Tester*

The results of the overlay testing are shown in Figure 4.77; the virgin mixtures have the best performance overall. The resistance to crack propagation decreases with increasing RAP content and decreasing asphalt content, as would be expected. At the 20% RAP level, the change in asphalt content and use of a softer binder grade do not significantly affect the performance of the mixture whereas a significant impact is seen at the 40% RAP level.

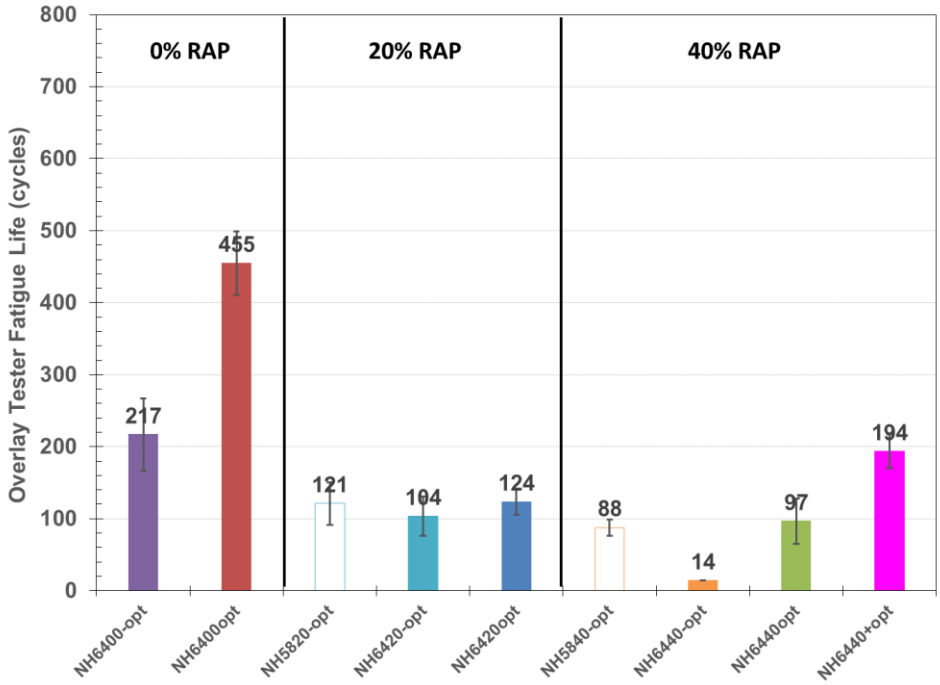

Figure 4.77 Overlay test results for Phase III Mixtures

4.3 Pavement Analysis

The inputs required for the LVECD simulations are the standard components needed for most pavement simulations: design time, structural layout, traffic, and climate. The typical design time for asphalt pavements is 20 years, so the simulations are run to 20 years at the same traffic rate to predict future performance.

Figure 4.78 presents the pavement structure that was used in the LVECD simulations. Simulation was done on thin (strain-controlled) and thick (stress-controlled) pavement structures. In the thin pavement case, the asphalt concrete layer is 100 mm (4 inches) thick with an aggregate base of 200 mm (8 inches), while for the thick pavement a full depth asphalt layer of 300 mm (12 inches) is used. The asphalt layer is described as viscoelastic with damage. Therefore, these layers need the Prony series representation of the dynamic modulus values, shift factors, and S-VECD model values. The aggregate base and subgrade were modeled using linear elastic properties. The layer properties used in the analysis are listed in Table 4.12.

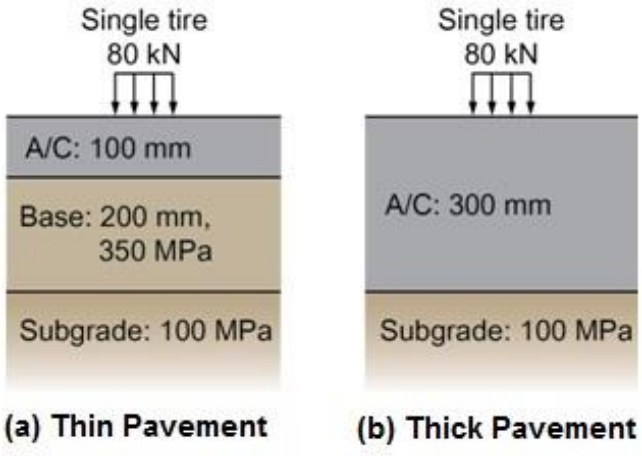

Figure 4.78 Pavement structure used in LVECD simulations for (a) thin pavement, and (b) thick pavement

Table 4.12 Design Structure

Layer	Modulus (MPa)	Poisson's Ratio	Material Type
AC	$\|E^*\|$	0.30	Viscoelastic with Damage
Aggregate Base	350	0.35	Linear Elastic
Subgrade	100	0.35	Linear Elastic

The traffic information used in this analysis is listed in Table 4.13. For convenience, a single tire with corresponding equivalent single-axle loads (ESALs) (the standard axle loading of 18 kips on one axle) is applied at the center of the pavement. The LVECD model simulates 20 years of asphalt concrete pavement performance using climate and traffic data. The average annual daily truck traffic (AADTT) count is 2000, so the total ESALs are 14.4 million for 20-year simulations.

Table 4.13 Traffic Inputs for LVECD

Vehicle	ESAL
Design Velocity (kph)	100
AADTT	2000
Pressure Distribution	Constant
Contact Area	Rectangular
Aspect Ratio (length/width)	11/7
Tire Pressure (MPa)	0.21
Growth Type	No Growth
Lane Distribution Factor	1

For the climate data, the pavement was assumed to be placed in Boston, Massachusetts. The LVECD program uses pavement temperatures obtained from the Enhanced Integrated Climatic Model (EICM). The EICM program provides hourly temperatures of asphalt pavements in terms of pavement depth.

Simulations were conducted using different measured properties from the SVECD testing for the asphalt layers while keeping all the other conditions constant. To evaluate fatigue, the LVECD program calculated the damage growth (i.e., reduction of the secant pseudo modulus) and the damage factor that is defined in Equation 4-1 based upon the Miner's law. If the damage factor is equal to zero, the element does not have any damage, and a damage factor of one indicates failure of the element.

$$Damage\ Factor = \sum_{i=1}^{T} \frac{N_i}{N_{fi}} \qquad 4\text{-}1$$

where,
T = total number of periods,
N_i = traffic for period i, and
N_{fi} = allowable failure repetitions under the conditions that prevail in period i.

Figure 4.79 shows an example of the damage factor distribution for the thin pavement case for all of the study mixtures after five years. The plots show the cross-section of the pavement with the direction of traffic into the page. It is noted that the fatigue performance predicted from the LVECD program has not been fully calibrated against the field performance data. A preliminary comparison of the LVECD predicted damage and the percent cracking area measured from in-service pavements is presented in Norouzi and Kim (2014). However, transfer functions that convert the damage predicted from the LVECD to the percent cracking area have not been developed yet. Therefore, the LVECD predictions presented in the remaining portion of this paper use the number of fatigue failure points to evaluate the expected relative effects of different RAP mix design factors on the pavement performance with respect to fatigue cracking.

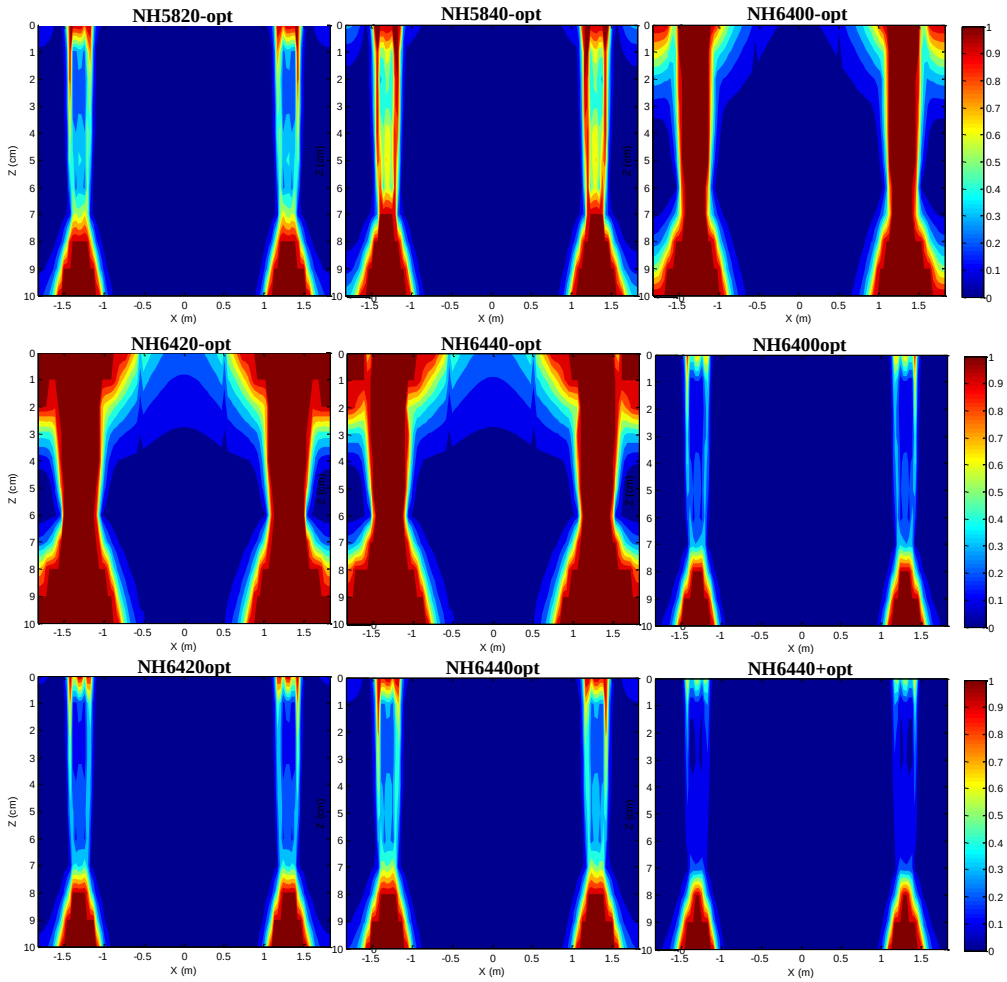

Figure 4.79 Fatigue damage factor contours for all the study mixtures after five years

In order to compare the fatigue resistance of the mixtures, the number of failure points (elements with the damage factor of '1') during the design period is shown for the thin and thick pavements in Figure 4.80 and Figure 4.81, respectively. Comparing these two figures (note different vertical scales) clearly suggests better performance of the thick pavement, as it has fewer failure points during the design period in all the cases. This finding would suggest that incorporating higher RAP contents in thicker pavements is possible. Also, the mixture rankings in terms of fatigue resistance are the same for both the thin and thick pavements. Figure 4.80 (a) and (b) and Figure 4.81 (a) and (b) show the effects of incorporating RAP into the mixture. As expected, by adding more RAP into the mixture, the fatigue resistance decreased in all the cases. Figure 4.80 (c) and (d) and Figure 4.81 (c) and (d) show the effects of binder content at 20% and 40% RAP, respectively. The analysis shows that binder content has an important role in determining the fatigue behavior of the mixtures, because the number of failure points decreased considerably with an increase of the binder content from below the optimum to the optimum binder content in both cases. Increasing the binder content above the optimum binder content (NH6440+opt) still shows some improvements in fatigue resistance, but the impact is smaller. The effects of using softer binder is shown in Figure 4.80 (c) and (d) and Figure 4.81 (e) and (f) for 20% and

40% RAP, respectively. Using the softer binder obviously improved the fatigue resistance of the pavements for both levels of RAP content.

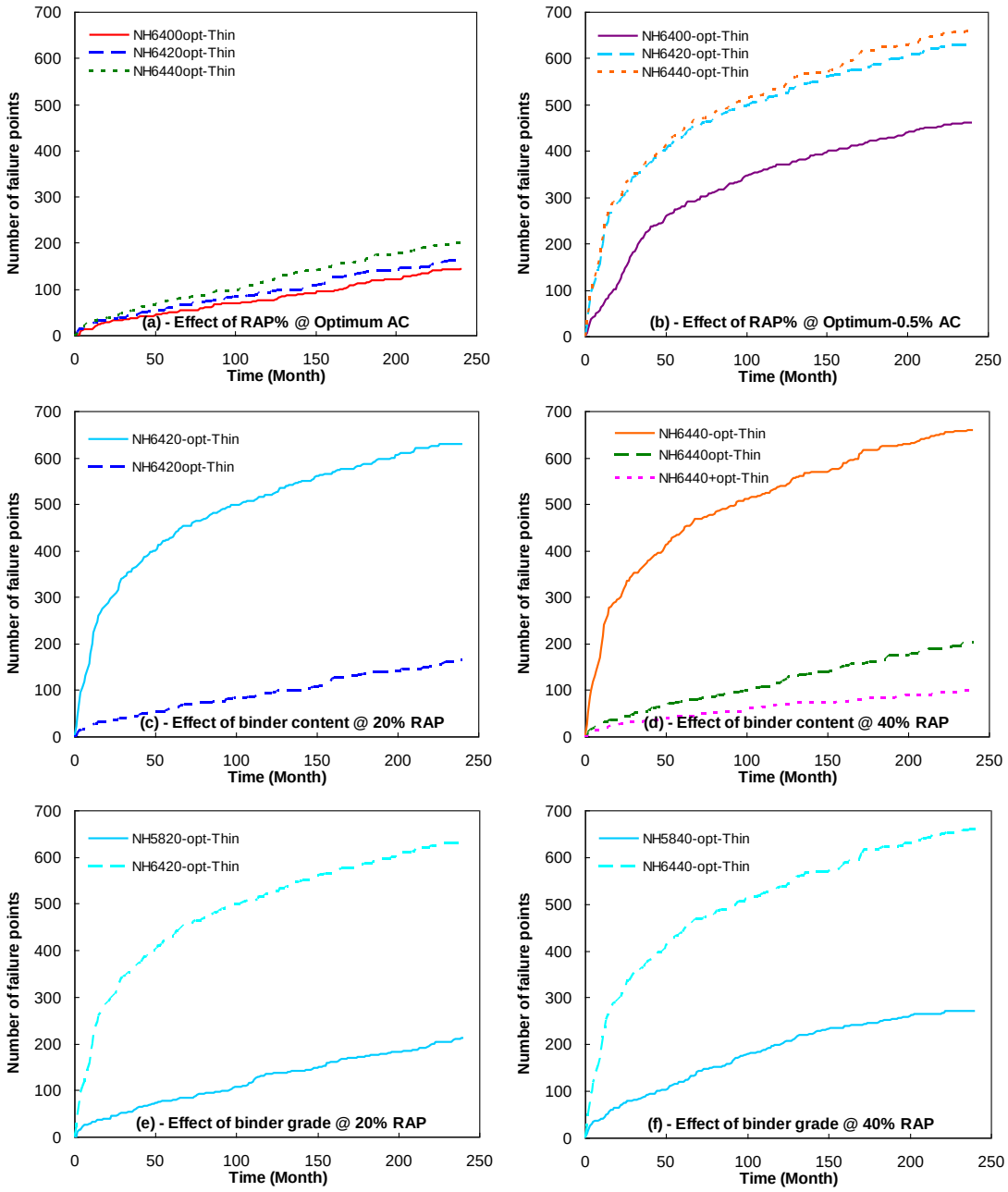

Figure 4.80 Evaluation of the effect of: (a) RAP content at the optimum AC, (b) RAP content at the optimum-0.5% AC, (c) binder content at 20% RAP, (d) binder content at 40% RAP, (e) binder base PG at 20% RAP, and (f) binder base PG at 40% RAP on the thin pavement fatigue life prediction

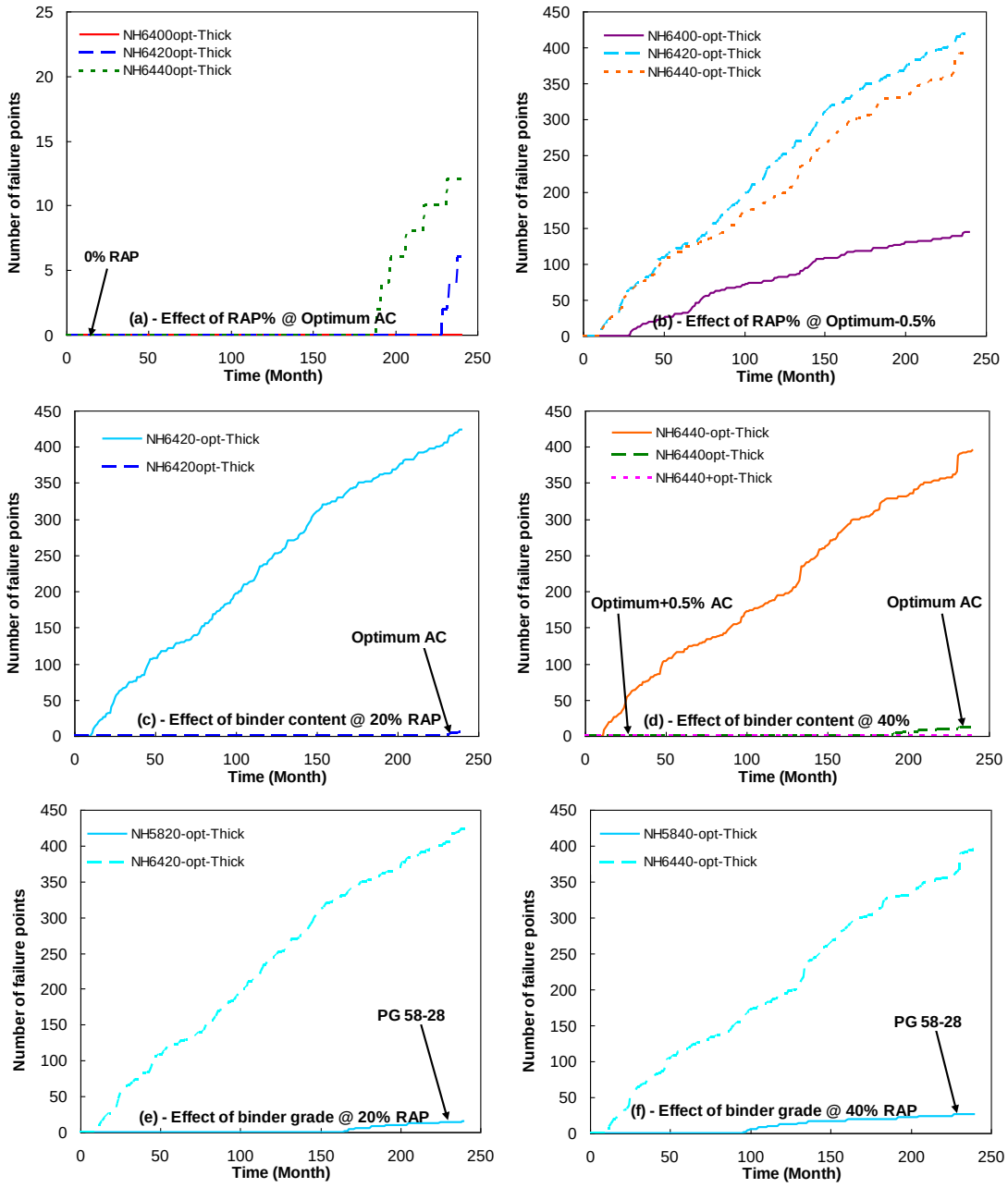

Figure 4.81 Evaluation of the effect of: (a) RAP content at the optimum AC, (b) RAP content at the optimum-0.5% AC, (c) binder content at 20% RAP, (d) binder content at 40% RAP, (e) binder base PG at 20% RAP, and (f) binder base PG at 40% RAP on the thick pavement fatigue life prediction.

It is noted that the current version of the LVECD program does not include an aging model. When the aging model is included in the LVECD program, the damage patterns in Figure 4.80 and Figure 4.81 the trends and the magnitude of differences in the failure points shown in Figure 4.80 and Figure 4.81 may change. For example, the inclusion of the aging model in the LVECD analysis could yield more top-down cracking in the thick pavement than in the thin pavement. Currently, the diffusion-based aging model coupled with the viscoelastic continuum damage model is in development under the auspices of the NCHRP Project 09-54. This aging model will be included in the LVECD program in the future.

CHAPTER 5 OVERALL CONCLUSIONS FROM PHASE III

In Phase III, the performance of nine laboratory-produced RAP mixtures was evaluated in terms of fatigue and rutting. Mixture variables included two virgin PG grades (PG 58-28 and PG 64-28), three RAP contents (0, 20, and 40%), and three asphalt contents (optimum and optimum ± 0.5%). Binders were extracted and recovered from the laboratory produced mixtures for testing. Binder testing included PG grading, G* master curves and analysis of rheological parameters, and MSCR testing. The S-VECD model (dynamic modulus and uniaxial tensile fatigue) was used to evaluate the fatigue properties of the mixtures, which were then input in the LVECD pavement analysis program to predict the long-term fatigue performance of thin and thick asphalt pavements with the study mixtures. Mixtures were also evaluated using the overlay tester and TSRST test. TSS testing was performed to assess the rutting behavior of the mixtures.

The results from both the binder and mixture testing show that, in general, all the factors that improved the fatigue resistance deteriorated the rutting resistance of the asphalt mixture. Nevertheless, the study shows that it is still possible to balance all the different factors to produce a material that performs well and is economical. The use of a soft binder is effective for this set of materials, as the LVECD predictions showed a noticeable improvement in fatigue resistance, whereas the TSS data suggested that rutting resistance would not worsen significantly. The LVECD program's predictions on fatigue cracking performance for thin and thick pavements clearly showed that high percentages of RAP can be tolerated easily once the layer thickness increases. Also, the optimum binder content was, not surprisingly, found to be the best, because increasing the asphalt binder above the optimum level resulted in higher levels of rutting even at a high percentage of RAP, and below the optimum level caused a noticeable decrease in fatigue resistance. The impact of the softer base binder and changing the binder content is greater for the 40% RAP mixtures than the 20% RAP mixtures.

Hence, for the mixtures evaluated in this phase, the best strategies for incorporating high percentages of RAP seems to be using soft base binder and maintaining the optimum asphalt binder content and/or increasing the asphalt layer thickness. However, it is important to note that these conclusions are based on the laboratory mixtures and the relative impact of RAP content, binder grade and binder content could change significantly with plant production, as has been observed in Phase I and II.

CHAPTER 6 REFERENCES

Anderson, M., P. Kriz, G. King, and J.P. Planche (2011). "Evaluation of the Relationship between Asphalt Binder Properties and Non-Load Related Cracking," *Journal of the Association of Asphalt Paving Technologists*, 80, pp. 615-664.

Chehab, G. R., Y. R. Kim, R. A. Schapery, M. Witczack, and R. Bonaquist (2003). Characterization of Asphalt Concrete in Uniaxial Tension Using a Viscoelastoplastic Model. *Asphalt Paving Technology*, AAPT, Vol. 72, pp. 315-355.

Daniel, J. S. and Y. R. Kim (2002). Development of a Simplified Fatigue Test and Analysis Procedure Using a Viscoelastic Continuum Damage Model. *Journal of the Association of Asphalt Paving Technologists*, AAPT, Vol. 71, pp. 619-650.

Hou, T., B. S. Underwood, and Y. R. Kim (2010). Fatigue Performance Prediction of North Carolina Mixtures Using Simplified Viscoelastic Continuum Damage Model. *Journal of the Association of Asphalt Paving Technologists*, AAPT, Vol. 79, pp. 35-80.

Glover, C. R. Davison, C. Domke, Y. Ruan, P. Juristyarini, D. Knorr, and S. Jung, 2005, Development of a New Method for Assessing Asphalt Binder Durability with Field Validation, Report 0-1872-2, FHWA.TX-05/1872-2, 334 pp.

Kim, Y. R. and D. N. Little (1990). One-Dimensional Constitutive Modeling of Asphalt Concrete. *ASCE Journal of Engineering Mechanics*, Vol. 116, No. 4, pp. 751-772.

Kim, Y. R., D. N. Little, and R. L. Lytton (2003). Fatigue and Healing Characterization of Asphalt Mixtures. *Journal of Materials in Civil Engineering*, JMCE, Vol. 15, No. 1, pp. 75-83.

Kim, Y. R., M. N. Guddati, B. S. Underwood, T. Y. Yun, V. Subramanian, S. Savadatti, and S. Thirunavukkarasu (2008). *Development of a Multiaxial VEPCD-FEP++*. Publication FHWA-HRT-08-073, U.S. Department of Transportation, Federal Highway Administration.

Lee, H. J. and Y. R. Kim (1998a). A Uniaxial Viscoelastic Constitutive Model for Asphalt Concrete under Cyclic Loading. *ASCE Journal of Engineering Mechanics*, Vol. 124, No. 1, pp. 32-40.

Lee, H. J. and Y. R. Kim (1998b). A Viscoelastic Continuum Damage Model of Asphalt Concrete with Healing. *ASCE Journal of Engineering Mechanics*, Vol. 124, No. 11, pp. 1224-1232.

Rowe, G.M. (2011) "Prepared Discussion for the AAPT paper by Anderson et al.: Evaluation of the Relationship between Asphalt Binder Properties and Non-Load Related Cracking." Journal of the Association of Asphalt Paving Technologists, 80, pp. 649-662.

Schapery, R. A. (1984). Correspondence Principles and a Generalized J-integral for Large Deformation and Fracture Analysis of Viscoelastic Media. International Journal of Fracture, Vol. 25, pp. 195-223.

Sui, C., M. Farrar, W. Tuminello, and T. Turner, 2011, "New Technique for Measuring Low-Temperature Properties of Asphalt Binders with Small Amounts of Material", Transportation Research Record: Journal of the Transportation Research Board, No. 2179, Transportation Research Board of the National Academies, Washington D.C., pp. 23 – 28.

Underwood, B. S., C. M. Baek, and Y. R. Kim (2012). Use of Simplified Viscoelastic Continuum Damage Model as an Asphalt Concrete Fatigue Analysis Platform. Transportation Research Record: Journal of the Transportation Research Board, TRB, No. 2296, pp. 36-45.

Zhou, F. and Tom Scullion, 2005, "Overlay Tester: A Simple Performance Test for Thermal Reflective Cracking", Journal of the Association of Asphalt Paving Technologists, Vol. 74, pp. 443 – 484.